UNIVERSITY OF NAPLES FEDERICO II

Department of Structures
for Engineering and Architecture

PH.D. PROGRAMME IN
STRUCTURAL GEOTECHNICAL AND SEISMIC ENGINEERING
XXXII CYCLE

ALBERTO COMPAGNONE

PROBABILISTIC APPROACH FOR SIMPLIFIED VERIFICATION METHODS OF RESISTANCE OF STEEL FRAMES IN FIRE

TUTOR:
PROF. EMIDIO NIGRO
CO-TUTORS:
DOTT. ING. ANTONIO BILOTTA
DOTT. ING. MARCO ANDREINI

2020

Abstract

As alternative to formulation provided in Eurocode 3 for analyses on single members, this thesis shows the development of a probabilistic model to estimate critical temperature to take in account the parameters that influence the behaviour of framed steel structure in fire. A new simplified formulation has been developed to estimate the critical temperature of a steel member in the context of FSE. In other words the simplified model allows to use a general fire curve instead of the ISO standard fire also for single members, because takes into account the nonlinearities of the structure and the indirect actions generally considered with structural analysis through nonlinear FEM models.

To develop the probabilistic regression model, results of FEM simulations were used and thirteen parameters were identified to describe the behaviour of the structure in fire, taking in account fluid dynamic aspects. Simple Monte Carlo simulation is not suitable to develop the regression model due to the large variability of the parameters affecting the problem. Therefore, the probabilistic study was conducted using two techniques in order to reduce the size of the sample and to preserve the quality of the results. With the Latin Hypercube Sampling (LHS) we generated a small number of samples with high meaningfulness and with the Simulated Annealing optimization method we achieved diagonal correlation matrix.

The analyses were handled through a in house developed software that, starting from sampling data (i) automatically generates the input files for fluid dynamic, thermal and thermomechanical analysis, (ii) performs all analyses, (iii) stores the results in a database and (iv) generates the report file to analyse the results.

The probabilistic model, created using the Bayesian updating, has been used to estimate collapse temperature of beams and columns, separately. The significant parameters have been defined through a step deletion process in order to simplify the formulation.

Therefore the proposed formulations for the critical temperature take in account the effective stiffness of the structure, the non-linear structural behaviour and indirect actions due to thermal expansions and allow to exploit the resistance reserves due to the internal forces redistribution in steel framed structures. Moreover define the critical temperature as a random variable, to be easily used in reliability analysis and to develop fragility curves.

Acknowledgments

Il Dottorato di Ricerca non si limita alla stesura di una tesi, è un percorso. Come tale, esso mi ha permesso di crescere in maniera molto più rapida di quanto avessi potuto mai fare da solo. Ovviamente tutto ciò è stato possibile solo grazie alle persone che mi hanno accompagnato durante questo viaggio e che meritano tutta la mia gratitudine. Questa pagina della tesi è dedicata a loro.

Innanzi tutto è necessario che io ringrazi tutta la mia famiglia per aver sostenuto finanziariamente, con pazienza e attenzione la mia formazione. Ciò che rende inestimabile il loro contributo è stata la capacità di fare silenziosamente tutto quello che si sarebbe potuto fare molto più facilmente alzando la voce. In particolar modo mio padre, col quale oggi non posso gioire di questo traguardo. Anche se qualche volta non ho compreso i suoi messaggi, di certo ho sempre sentito tutto il suo sostegno.

Ringrazio i miei tutor Emidio Nigro, Antonio Bilotta e Marco Andreini per avermi fatto da guida non solo durante lo sviluppo della tesi ma soprattutto dal punto di vista professionale e culturale.

Ringrazio Sofia, che mi è stata accanto e mi ha sostenuto in ogni momento e per questo a lei devo la mia serenità.

Infine il mio ringraziamento va agli amici sia vicini che lontani: gli ex coinquilini con i quali ho trascorso serate goliardiche, Rosanna con la quale ho condiviso il percorso, compagni di studio degli anni dell'università che ricordo con affetto, i colleghi dell'aula dottorandi e le amicizie di infanzia che durano ancora oggi.

Naples, 2020

Table of Contents

List of Figures

List of Tables

Chapter 1

1 Introduction

1.1 General Overview

Fire is an exothermic oxidation reaction occurring in the gas phase, which results from the mixing of flammable gases with air or other oxidative means. If the concentration of the flammable substance reaches its critical mass for ignition, and a proper ignition source capable of supplying the required power is present, then there will be a fire. Moreover, fires and explosions are the most significant and most common causes of damage to equipment and of injuries and deaths in industry. This is especially true in offshore oil drilling, where there is a high concentration of equipment in very close spaces.

The fire has a double effect on the structure because it causes a burden of stresses due to thermal expansion of the materials and at the same time the temperature increasing cause a worsening of material's mechanical properties. Structures involved in fire can be seriously damaged in terms of residual displacements, partial collapse or total collapse of the building. The damage depends on construction materials, goods stored in buildings and also in depending on the condition of ventilation during fire.

In order to evaluate effects, mitigate and assess the risk or design sturdy structures we can use a performance-based approach (PBA) which allows to model through complex numerical method the evolution of fire and the response of the structure to the thermal input. Fire Safety engineering (FSE) is a set of methodologies and strategies that have the purpose of reduce the risk and the impact of fire on buildings and their occupants.

Fire Safety engineering is the application of science and engineering principles to protect people, property, and their environments from the harmful and destructive effects of fire and smoke. It encompasses engineering which focuses on fire detection, suppression and mitigation, human behavior and maintaining a tenable environment for evacuation from a fire.

In Fire safety engineering, the risk assessment plays a central role because thanks to the risk, defined as well in further chapters, allows designers to estimate design parameters of structure in order to predict the costs of accidents.

In recent times the FSE is focusing on the probabilistic analysis of the structures in fire starting from the study of collected historical data. Several study like the one of the last conducted by Manes et al. 2018 highlights the high quantity of fires and the spreads through the meta-analysis of some fire database of US, New Zeeland etc. One of the most important characteristics of the PBA with a probabilistic approach is the possibility to exploit data of results to do a multi-hazard analysis of natural phenomena (Suwondo et al.). By the fluid dynamic point of view most of researcher focus on the specific fire load that generally is used for risk assessment analysis in all types of building (Mikkola et al.2012) but the fire problem depends from a lot of parameters also using a simplified methodology of resolution like in the two-zone model. By the structural point of view there is a completely different framework. Several studies on thermal and mechanical properties (Stephani et al. 2018, Khorasani et al. 2015, Compagnone et al. 2017) was conducted in order to characterize materials by the probabilistic point of view. Other studies were conducted in order to investigate responses of structural elements in fire (Van Coile et al. 2018) taking in account nominal and parametrical fires.

This work focusing on steel structures behaviour in fire want to provide a method to assess the critical temperature of structure exposed to fire. The critical temperature could be defined as the value of temperature for that the structure collapse. The randomness of the fire phenomena obliges us to model the fire as a random process and as random variables a lot of characteristics of fire and thermo-mechanical problem. The probabilistic study's result is a regression model that assess, in function of structural element's characteristics, the value of the temperature that induces collapse. Starting from consolidated methodologies

(Gardoni et al. 2002a) used to build prediction models the work, new mathematical model was used to improve optimize the process (Vorechovský et al. 2009) of constitution of the regression model. In particular the methodology proposed by Vorechovský is based on the application of the simulated annealing method to LHS sampling in order to reduce the number of samples without sacrifice the precision of the probabilistic study.

1.2 Organization and outline

The dissertation is organized into six chapters. Since there are concepts of the probability theory applied to results obtained through thermomechanical analysis, the work is organized in two part. The first part (Chapter 1, 2 and 3) is dedicated to the theoretical background. In particular there are defined concepts and tools relative to the probability theory and the thermomechanical analysis. The second part (Chapter 4, 5 and 6) is dedicated to the application of concepts introduced in previous chapters to the problem. This chapters are focused on the definition of problem's parameters and to results obtained. Follow the detailed organization.

Chapter 1 contains the introduction to the thesis that was done through a general overview. In previous section there is a very synthetic and fast literature review, whereas this section and further explain the organization of the document and show the objectives of the thesis.

The Chapter 2 summarize concepts relative to the analysis of structure in fire. This chapter is used to introduce the fluid dynamic problem, with its own variables and characteristics and it is focused on the two-zone model analysis of fire. Moreover, in this chapter will be described the thermo-mechanical analysis method used in further chapters looking over the thermomechanical model's hypothesis.

Chapter 3 summarize concepts of the probability theory starting from the definition of the probability concepts, random variables and random variable models used in this study. This chapter introduce also some theorems of the probability theory.

In Chapter 4 there is the formalization of the problem through the definition of random variables that influence the fire process. Variables are divided in two groups: the first concerns the fire modelling problem and the second that concern the thermomechanical problems. After the definition of parameters, it was described the software developed in order to automatically generate input file for thermomechanical analysis starting from the sampling procedure. Follow the single analysis of results analysis in order to understand some aspects relative to the structural response in fire condition. The last part of the chapter shows the development of the probabilistic regression model.

The analysis database was analysed in Chapter 5. Data provided from thermomechanical and fire model analysis was stored in a database with the input data that come from the sampling procedure. These data were analysed in order to do some interesting broadly considerations about the structural response and maximum temperature that could be realised in a compartment exposed to fire.

Finally, in Chapter 6 there are summarized conclusions from the present research along with suggestion for future research.

1.3 Objectives

The scope of this thesis is to provide a simple method to assess the capacity through a simple parameter that allows to assess the capacity of the structure taking in account also cold members not directly exposed to fire.

One of the biggest problems in engineering is related to the definition of the domain that we have to investigate. Due to the numerical complexity of the problem and the fact that the fire generally involves only a part of the structure, analysis domain is generally confined to a part of the structure in fire or adjacent structural members neglecting the influence of remaining part not directly exposed (or in contact) to fire. The aim of this work starts from this consideration about structure in fires, an issue that in research framework is generally neglected or viewed as a side problem.

Due to the low specific heat and the high thermal conductivity of material, steel structure resistance to fire action doesn't tends to depend from the time of exposure. Thanks to this property is possible to the resistance of a structure could be defined through a single scalar value that is the value of the maximum temperature reached in compartment during fire.

The regression model presented in further chapters exploit this characteristic of the steel structure and provide the temperature of collapse in function of several parameters. The formulation in Gardoni et al. (2002a) is used to develop the probabilistic models and determine the unknown parameters. Specifically, a Bayesian approach is used to allow for updating of the models if additional data become available. The posterior statistics of the parameters are determined by a Monte Carlo simulation, implementing the procedure presented by Gardoni et al. (2002b), adaptable to parallel computing programming (Andreini et al., 2016) to reduce the calculus time.

The procedure used to build the regression model needed to perform a lot of analysis. Results of all analysis were stored in the database and were used to understand better the fire phenomena and to provide some rules that could be used to do right assumption when we approach the detailed study of structure involved in fire. For instance, thanks to the results stored in the database is possible to do a rapid assessment of the maximum temperature induced by a fire or assessment of the order of magnitude of the collapse temperature.

Chapter 2

2 Structural analysis in fire condition

In order to describes the structural behavior in fire, two type of analysis are needed to calculate temperatures and displacements of the structure. As usual, the research of solutions can be carried out in several ways which differ from one another by the level of accuracy and by the computational costs.

In order to gain a precise and punctual estimation of temperature distribution in compartments during fire a Thermo-Fluid-Dynamic Analysis with the Computational Fluid Dynamics (CFD) technique is needed. Unfortunately, CFD Analysis requires a large amount of resources and time to give a solution, moreover results of CFD Analysis needs to be validated. The structural behavior could be investigated with several approach but all of these passes through a Finite element analysis (FEA). There are several types of Finite Element Models which allows to investigate the thermomechanical problem, which differ from input parameters and results gettable.

Since several analysis types are needed, they can be combined in various form:

- Fluid Structure Interaction (FSI) Analysis: the most accurate approach, for each step the solver uses the CFD results in terms of heat flow and use it in order to compute first temperature in the structural elements, then the displacements and use the results to change the domain of the CFD problem;

- Fully coupled temperature displacement (CTD) analysis: starting from the results of a Fluid Dynamic Analysis, for each step of thermomechanical analysis, the solver uses the temperature distribution in the room to compute temperature in the elements and at the same time the displacements. Using this approach, we're able to study behavior of porous material because results of each step change the thermal analysis domain
- Uncoupled Temperature Displacement (UTD) analysis: The uncoupled thermomechanical approach is very similar to the coupled temperature-displacement analysis excepts for the calculation protocol. Indeed, with this approach the solver starting from compartment's temperature perform a thermal analysis first, then a structural analysis is conducted without take into account the displacements effect on thermal domain.

Analysis types are listed in order of accuracy and therefore computational costs. Note that if the deformation of fluid dynamic analysis doesn't depend form displacements (i.e. a fuel tank in fire which can change Fluid Dynamic domain if break up) the FSI Analysis return the same results of a CTD Analysis. We can say the same if temperature's distribution doesn't depend from displacements, in this case CTD is tantamount to UTD. In this work was assumed that the fluid dynamic domain does not change during fire and the displacements of structure doesn't influence temperature evolution and distribution for these reasons only UTD analysis was performed.

In this chapter will be shown some methods and techniques available in literature which could be used to get structural behavior in fire condition. Since this work is focused on the stochastic approach to fire condition, in order to obtain a large number of numerical results in a little time, a nearly simplified methods have been used in order to conjugate the accuracy of solution with the need of a small computational costs and time.

2.1 Thermo-Fluid-Dynamic Analysis

The first task to be performed in structural analysis in fire condition regard temperature assessment. In order to do this, we have to simulate fire process and

starting from quantities of fuel and oxygen we're able, through a Thermo-Fluid-Dynamic Analysis (TFDA), to do a prediction heat fluxes which allows to compute temperature in compartments. There are many ways to compute temperatures in compartments, in literature are available some simplified methods that bypass the TFDA and give us function that express the evolution of gas temperature in time but also these methods require to know fuel and ventilation.

Damages are a direct consequence of the generated heat flux. To a first approximation for the calculation of the heat flux, q' (W/m2), in the flame surface, the Stefan-Boltzmann equation can be employed:

$$q' = \varepsilon \sigma (T_f^4 - T_a^4) \quad 2.1$$

where ε denotes the grey-body emissivity (-) and σ the Stefan-Boltzmann constant (= $5.6703 \cdot 10^{-8}\ W \cdot m^{-2} \cdot K^{-4}$). The temperatures, T_f and T_a (K), refer to the temperature at the flame surface and the ambient temperature, respectively. In fact, however, this equation cannot be employed, since the temperature differs all over the flame and hence it is not a unique temperature that can be determined. Furthermore, the flame does not radiate from its whole surface, since a part of it is covered by soot, and a large part of the heat flux is absorbed by the carbon dioxide and the humidity in the atmosphere. As a consequence of these, the heat flux calculated by the Stefan-Boltzmann equation is significantly larger than the actual heat flux. In an effort to estimate the heat flux, and its effects, many models appear in the literature. The most important groups of such models are the following:

a) **Point-Source Models**: The point-source models do not consider the shape of the flame, but assume that the heat-flux originates from a point source. The heat flux, q' (W/m²), in a distance, X (m), from the center of the fire, can be expressed as:

$$q' = \frac{1}{4 \pi X^2} \eta m_k \Delta H_c \quad 2.2$$

where, m_k (kg/s) denotes the burning rate with which the flammable material is burnt, ΔH_c (J/kg) the heat of combustion, and η the combustion

efficiency. While the above relation has the advantage of simplicity, the analogy of the heat flux with the square of the distance has not been experimentally observed. These models usually overestimate the heat flux, but produce good results in a distance of about 10 radii from the center of the fire.

b) **Solid-Flame Models**: The solid-flame models assume that the flame is of a solid shape that radiates heat only from its surface. Models take into consideration the shape of the flame and calculate the heat flux as a function of the Surface Emitting Power, the Shape Factor and the Atmospheric Transmissivity. These models are simple in their application, easy to program and produce relatively good results.

c) **Field Models**: The field models, or computational fluid dynamics models (CFDs), are based upon the numerical solution of the partial differential Navier-Stokes equations. These models require careful validation against real or experimental data. Their main disadvantage is the large requirements in computing time, the difficulty in programming and the inflexibility in compatibility with many applications.

d) **Integral Models**: The integral models constitute a compromise between the semi-empirical models and the CFD models. They are based upon the solution of differential equations for the conservation of mass, momentum and energy, but their mathematical approach is more simplified and refers to the specific case to be examined. In this way, a significant reduction in computing time is achieved.

e) **Zone Models**: According to the zone models, space is separated into homogeneous space zones of unified approach, which are connected through empirical equations and mass and energy balances. These models are employed in structural areas, but not in open spaces.

2.1.1 ZONE MODELS, CFAST

Zone models rely on the assumption that a compartment can be vertically subdivided into zones, perfectly mixed and with homogeneous properties in terms of temperature and composition: a hot layer with combustion products, located near the ceiling, and a cold layer with fresh clean air at the bottom, separated by

a moving interface. The properties (and the layer height) can vary over time and are identified when solving global conservation equations (Tavelli et al, 2014).

CFAST is a two-zone fire model used to calculate the smoke dispersion, the fire gases dynamics and the temperature throughout compartments of a constructed facility over time; each compartment is divided into two gas layers. The fundamental equations (conservation of mass and energy over the layers, ideal gas law and relations for density and internal energy) are implemented as system of ordinary differential equations (ODEs), which are solved to give the values of pressure, layer heights and temperatures over time. A series of algorithms allow to compute the mass and enthalpy source terms required by the ODEs.

The equations used in CFAST take the form of an initial value problem for a system of ordinary differential equations. These equations are derived from the conservation laws of mass and energy (equivalently the first law of thermodynamics) and the ideal gas law. These equations predict the evolution in time of the compartment pressure, layer height, and layer temperatures due to the gains and losses of mass and energy. The assumption of a zone model is that properties such as temperature can be approximated throughout a control volume by a representative average value. Though equivalent mathe-matically, these formulations differ in their numerical solution. The exchange of mass and enthalpy between zones is due to physical phenomena such as fire plumes, natural and forced ventilation, convective and radiative heat transfer, and so on. For example, a vent exchanges mass and enthalpy between zones in connected rooms, a fire plume typically adds heat to the upper layer and transfers entrained mass and enthalpy from the lower to the upper layer, and convection transfers enthalpy from the gas layers to the surrounding walls. The momentum equation is explicitly included since conditions within a control volume are assumed to be uniform. Of course, included plume entrainment, ceiling jet, and vent flow correlations are applications of momentum principles used for specific purposes within the model.

It is assumed that each compartment is divided into two control volumes, a relatively hot upper layer and a relatively cool lower layer, as illustrated in Figure 1. The gas temperature and density are assumed constant in each layer. The compartment as a whole is assumed to have a single value of pressure, P. It is also assumed that all thermodynamic parameters are constant. The specific heat

at constant volume and at constant pressure, c_v and c_p, the specific1 gas constant, R, and the ratio of specific heats, γ, are related by $\gamma=c_p/c_v$ and $R=c_p-c_v$. Regardless of the composition of the gas mixture, c_p =1012 J/(kg·K) and γ=1.4; thus

$$R=\frac{\gamma-1}{\gamma}c_p\approx 289.14\,J/kgK \qquad 2.3$$

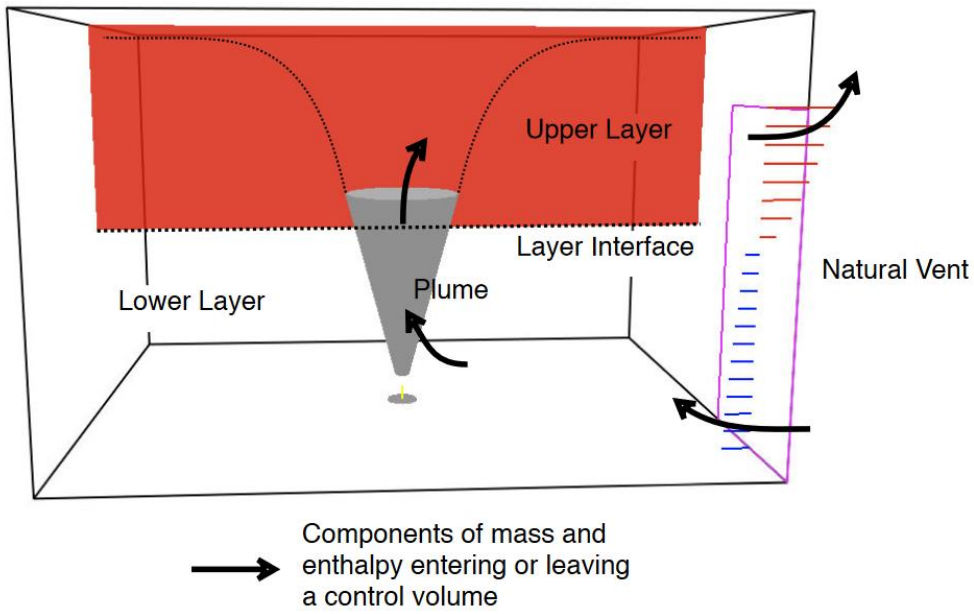

Figure 1 Two zone model.

The set of governing equations start with the conservation of mass. The change of mass in each layer, i, is expressed as:

$$\frac{dm_i}{dt}=\dot{m}_\iota \qquad 2.4$$

Where $\dot{m}_\iota$ represents the sum of all mass flow terms, such as plume mass entrainment and ventilation, entering and leaving layer i. Conservation of energy

takes the form of the first law of thermodynamics, which states that the rate of increase of internal energy plus the rate at which the layer does work by expansion is equal to the rate at which enthalpy is added to the gas:

$$\frac{d(c_v m_i T_i)}{dt} + \frac{PdV}{dt} = \dot{h_i} \qquad 2.5$$

The enthalpy source term, $\dot{h_i}$, consists of the fire's heat release rate, conduction losses to walls, and radiation exchange. The layer temperature and mass are related to the layer volume and compartment pressure via the ideal gas law:

$$PV_i = m_i R T_i \qquad 2.6$$

Combining equations 2.4, 2.5 and 2.6 we obtain a system, function of state's properties:

$$\frac{dP}{dt} = \frac{\gamma - 1}{V}\left(\dot{h_1} + \dot{h_u}\right) \qquad 2.7$$

$$\frac{dV_u}{dt} = \frac{1}{P\gamma}\left((\gamma - 1)\dot{h_u} - V_u \frac{dP}{dt}\right) \qquad 2.8$$

$$\frac{dT_u}{dt} = \frac{1}{c_p m_u}\left(\dot{h_u} - c_p \dot{m_u} T_u + V_u \frac{dP}{dt}\right) \qquad 2.9$$

$$\frac{dT_1}{dt} = \frac{1}{c_p m_1}\left(\dot{h_1} - c_p \dot{m_1} T_1 + V_1 \frac{dP}{dt}\right) \qquad 2.10$$

Best way to solve this system is with methods that calculate/estimate Jacobian because the state's variable Pressure tends to change very fast then another variable.

2.1.2 FIRE DYNAMICS IN ZONE MODELS

Heat release rate (RHR) from a fire is the most important parameter to describe the potential hazards posed from a fire. Indeed, the environmental consequences of a fire in a confined space depend in large measure on the HRR. Typically, the HRR curves of combustible items are determined in laboratory experiments but when we have to simulate fires in which the quantity of fuel and its characteristics are not known in advance, we have to estimate the fire curve in order to characterize phenomenon.

By a physic-analytic point of view when fuel and oxygen are consumed, heat is released and various products of combustion are formed. The heat is released as radiation and convection enthalpy:

$$\dot{Q}_r = \chi_r \dot{Q} \quad 2.11$$

$$\dot{Q}_c = (1 - \chi_r)\dot{Q} \quad 2.12$$

Where $\dot{Q}$ is the total heat released by the fire, $\dot{Q}_r$ and $\dot{Q}_c$ are the heat released by radiation and convection, and χ_r is the fraction of the fire's heat release rate emitted as radiation.

When we model fire event, we specify the heat release rate, $\dot{Q}$, as the actual heat released accounting for combustion efficiency, along with a characteristic base diameter, D, which is used in the plume temperature and mass entrainment correlations. The combustion efficiency , is a fraction of the theoretical energy released during combustion. This is a function of fuel type, scale, and vitiation. In CFAST, user can specify a radiative fraction which takes a default value of 0.35.

Using the RHR $\dot{Q}$ of the fire and the Heat of Combustion ΔH, the solver determines the pyrolysis rate of fuel $\dot{m}_f$

$$\dot{m}_f = \frac{\dot{Q}}{\Delta H} \quad 2.13$$

In the event that the HRR is constrained by the availability of oxygen, it is assumed that the pyrolysis rate does not change. However, only part of the pyrolyzed fuel burns and the HRR becomes:

$$\dot{Q} = \min\left(\dot{m}_f \Delta H;\ \dot{m}_e Y_{O_2} C_{LOL} \Delta H_{O_2}\right) \qquad 2.14$$

where $\dot{m}_e$ is the entrainment rate, Y_{O_2} is the mass fraction of oxygen in the layer containing the fire, ΔH_{O_2} is the heat of combustion based on oxygen consumption1, and C_{LOL} (Lower Oxygen Limit) is the smoothing function ranging from 0 to 1:

$$C_{LOL} \approx \frac{\tanh\left(800\left(Y_{O_2} - Y_{O_2,1}\right) - 4\right) + 1}{2} \qquad 2.15$$

The limiting oxygen mass fraction $Y_{O_2,1}$, is assumed equal to 0.15 and isn't a function of temperature.

Any unburned fuel is tracked by the model, and transported to the upper layer via entrainment in the fire plume or to other compartments through any vents. Unburned fuel may burn in the upper layer or at vents if sufficiently hot and if additional oxygen is available.

Once the heating is defined, we can focus on how the heat pass from the fuel to the hot layer. A fire pumps mass and energy (see Figure 1) from the lower layer into the upper layer. The vertical flow of mass through a horizontal plane at height z above the base of the fire is called the mass entrainment rate,$\dot{m}_e(z)$. The vertical flow of energy through this horizontal plane is given by $\dot{Q}_c + \dot{m}_e(z) c_p T_1$. The empirical correlation for the mass entrainment rate depends on whether the plume is unobstructed, against a wall, or in a corner.

In schematic representation of a turbulent fire plume originating at a flaming source (Figure 2), which may be solid or liquid. Smoke driven off from the combustible, pushed away from the fire by heat and mix with the surrounding air and form a diffusion flame. Laboratory simulations often employ controlled release of flammable gas through a horizontal, porous surface. The mean height of the flame is L. Surrounding the flame and extending upward is a boundary

(broken lines) that confines the entire buoyant flow of combustion products and entrained air. The air is entrained across this boundary, which instantaneously is very sharp, highly convoluted, and easily discernible in smoky fires. The flow profile could be the time-averaged temperature rise above the ambient temperature, or of the concentration of a gas (such as CO_2) generated by the fire, or of the axial velocity in the fire plume.

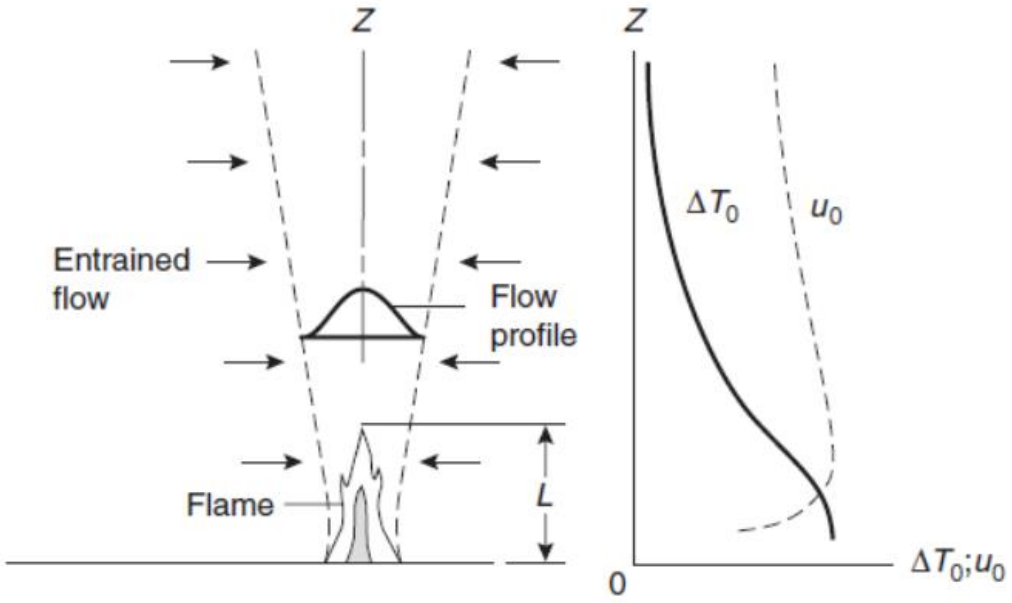

Figure 2 Fire Plume.

Still in Figure 2 we can see the qualitative temperature ΔT_0 and velocity u_0 evolution along the plume axis of the fire, based on experimental results. In this figure is shown a relatively tall flame, the temperatures are nearly constant in the lower portion of the flame. Temperatures begin to decay in the intermittent, upper portion of the flame as the combustion reactions trail off and air entrained from the surroundings cools the flow. The centerline velocities, u_0 , tend to have their maxima slightly below the mean flame height and always decay toward higher elevations. If the combustible is porous and supports internal combustion, there may not be as pronounced a falloff in the gas velocity toward the top of the combustible, the total heat release rate of a fire source, $\dot{Q}$, is either convected or

radiated away from the combustion region. In a fire deep in a porous combustible pile (i.e.: a stack of wood pallets), some of the total heat generated is trapped by and stored in the not yet burning material; the rest escapes from the combustible array as either convective or radiative energy flux. If most of the volatiles released undergo combustion above the fuel array, as in pool fires of liquids and other horizontal-surface fires, and even in well-developed porous pile fires, then the convective fraction of the total heat release rate is rarely measured at less than 60 to 70 percent of the total heat release rate. The convective flux, $\dot{Q}_c$, is carried away by the plume above the flames, while the remainder of the total heat liberated, $\dot{Q}_r$, is radiated away in all directions.

The total heat release rate, $\dot{Q}$, is often assumed to be equal to the theoretical heat release rate, which is based on complete combustion of the burning material. The theoretical heat release rate in kW is evaluated as the mass burning rate in kg/s multiplied by the lower heat of complete combustion in kJ/kg. The ratio of the total heat release rate to the theoretical heat release rate, which is the combustion efficiency, is indeed close to unity for some fire sources.

Heskestad, 1984 proposes a method to estimate geometry and characteristics of the plume, and the same methods is implemented in Cfast.

Using RHR functions suggested by the Eurocode it can happens that temperatures have a peak at the end of the RHR cure.

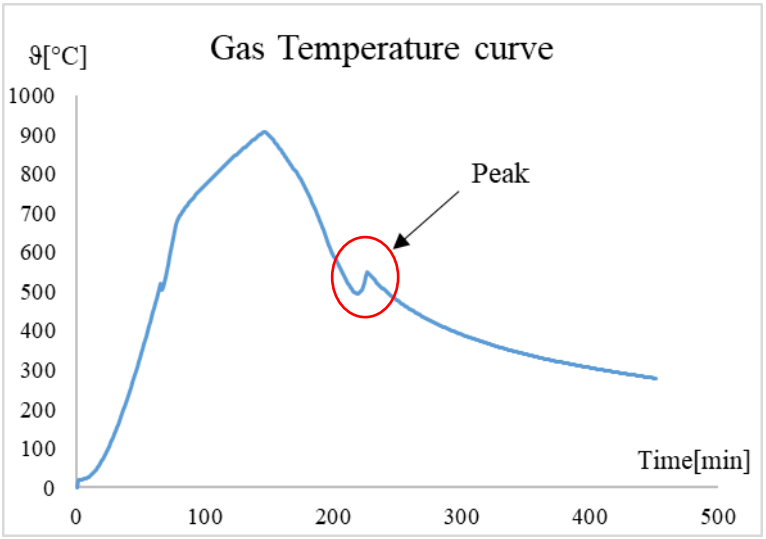

Figure 3 Temperature Peak.

This effect is due to the two-zone model analysis and even if the peak of temperature in numerical analysis. In further chapter temperature peaks have no influence on the structural behaviour it could cause considerable errors in some cases.

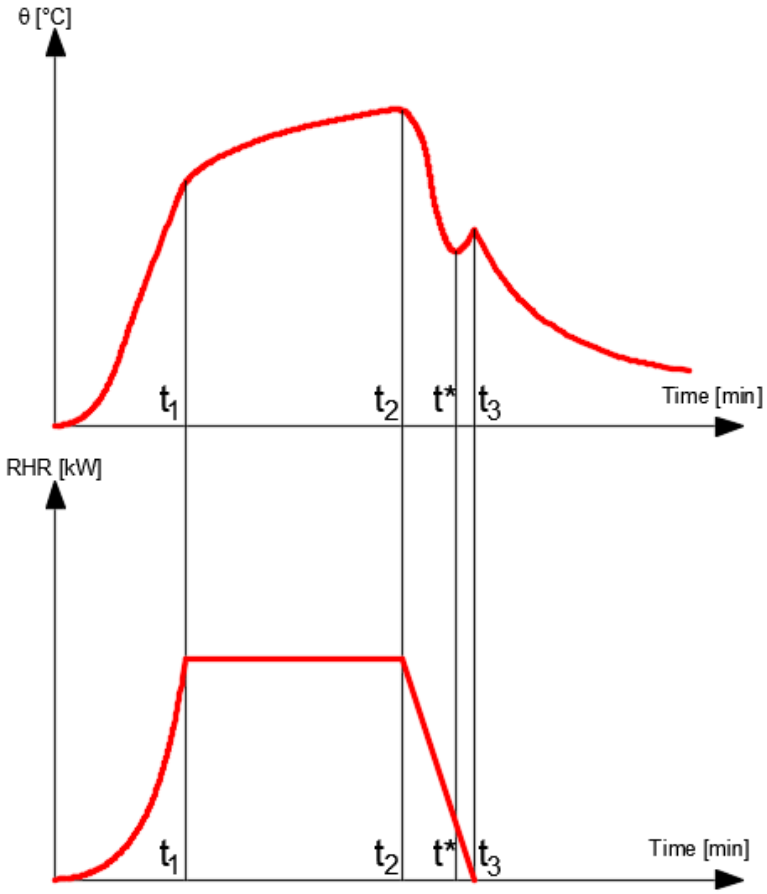

Figure 4 $RHR(t)$ vs $\vartheta(t)$.

The Gas temperature curve reach its peak when the RHR curve end, but temperature begins to increase just before the time t_3. If we compare the Gas temperature curve, the RHR curve (Figure 4) and the height of hot layer Figure 5,

during the analysis we can see that, as the RHR reduces, the gas temperature reduces itself, but with a varying slope. In particular, the slope of the gas temperature rapidly changes determining the reaching of a local minimum at t^*, after which the slope sign changes and determines a further increase of the gas temperature up to a local peak (at the time t_3). The slope change begins at t^* because the hot zone layer climb the limit of the window's soffit (Figure 5) so there is a change of the mass equilibrium because the hot zone no longer communicates with the outside(or other compartment). Temperature increasing stops when the RHR reach the time t_3 and the heat fluxes through the plume end. After t_3 the temperature has a monotonic decrease up to ambient temperature.

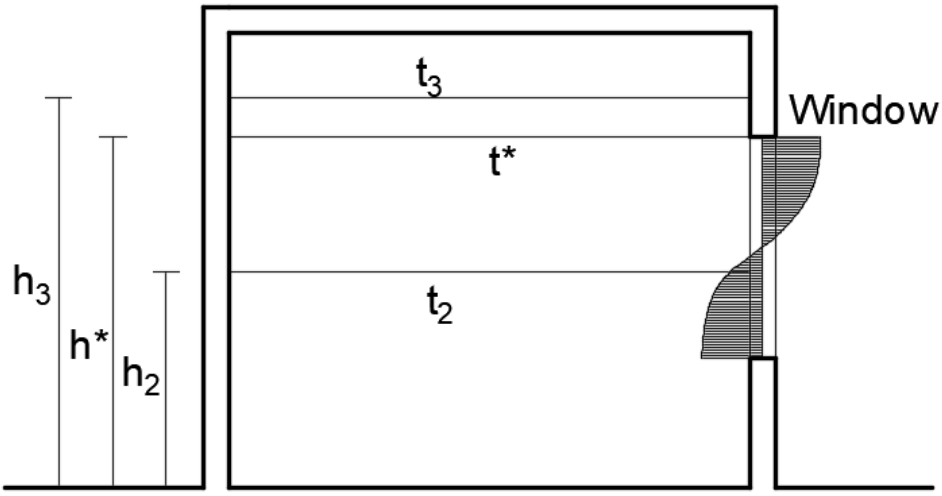

Figure 5 Hot zone layer height.

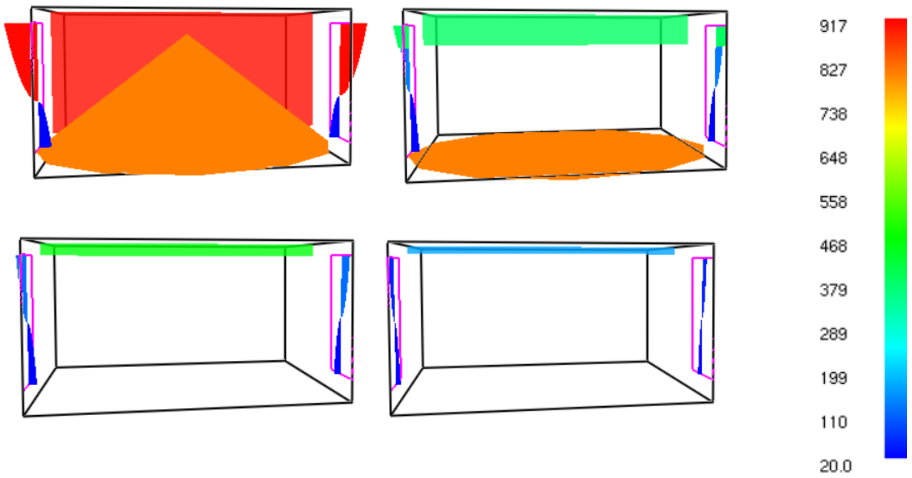

Figure 6 Hot zone layer height.

2.2 Thermal Problems

Once gas temperatures are known, a procedure is needed to analyze the effects on structural elements. This procedure is called Thermal analysis and in this work it was conducted under simplifying hypotheses. In fire problems, temperatures in structural elements needs to be calculated with high accuracy and since temperature could variate in an interval of several hundreds of Celsius degrees the variation of thermal properties of materials cannot be neglected.

In thermal analysis there are two entities which we have to investigate: temperatures and heat fluxes. While firsts are scalar quantities, and actually are results of analysis, the seconds are vectorial quantities and tells us how the energy flows in elements.

There are three different types of heat transfer: conduction, convection, and radiation. A temperature difference must exist for heat transfer to occur. Heat is always transferred in the direction of decreasing temperature.

Conduction takes place within the boundaries of a body by the diffusion of its internal energy. The temperature within the body, ϑ, is given in units of degrees Celsius[C], Fahrenheit [F], Kelvin [K], or Rankin [R]. Its variation in space

defines the temperature gradient vector, $\nabla\vartheta$, with units of [K/m] say. The heat flux vector, q, is defined by Fourier's Conduction Law, as the thermal conductivity, k, times the negative of the temperature gradient, $q = -\lambda\,\nabla\vartheta$. Thermal conductivity has the units of [W/mK] while the heat flux has units of [W/m²]. The conductivity, k (or λ), is usually only known to two or three significant figures. For solids it ranges from about 417 W/mK for silver down to 0.76 W/mK for glass. A perfect insulator material ($\lambda \equiv 0$) will not conduct heat; therefore, the heat flux vector must be parallel to the insulator surface. A plane of symmetry act as a perfect insulator, but in order that the plane is considered of symmetry it must have same not only geometry thermal conductivity but temperature and heat sources must be mirror images. In finite element analysis, all surfaces default to perfect insulators unless you give a specified temperature, a known heat influx, a convection condition, or a radiation condition.

Convection occurs in a fluid by mixing. Here we will consider only free convection from the surface of a body to the surrounding fluid. Forced convection, which requires a coupled mass transfer, will not be considered. The magnitude of the heat flux normal to a solid surface by free convection is:

$$q = h\,A_h\,(T_h - T_f) \qquad 2.16$$

Where h [W/m²K] is the convection coefficient A_h is the surface area contacting the fluid, T_h is the convecting surface temperature, and T_f is the surrounding fluid temperature. Values of convection coefficient h range in the interval [5-35] (for natural convection without temperature gradients and for convection with high temperature gradients respectively.

Radiation heat transfer occurs by electromagnetic radiation between the surfaces of a body and the surrounding medium. It is a highly nonlinear function of the absolute temperatures of the body and medium. The magnitude of the heat flux normal to a solid surface by radiation is

$$q = \varepsilon\,\sigma\,A_r\,(T_r^4 - T_m^4) \qquad 2.17$$

Where T_r is the absolute temperature of the body surface, T_m is the absolute temperature of the surrounding medium, A_r is the body surface area subjected to radiation, $\sigma = 5.67 \cdot 10^8\ W/m^2K^4$ is the Stefan-Boltzmann constant, and ε is the emissivity of the body (assumed in calculation as 0.7).

Transient, or unsteady in time also requires the material properties of specific heat at constant pressure, $c_p\ \left[\frac{kJ}{kgK}\right]$ and the mass density $\rho\ [\frac{kg}{m^3}]$. These properties, plus the conductivity λ regarding the structural analysis in fire condition are considered as variable in function of temperature.

Eurocodes provide thermal and mechanical properties about several material. Regarding steel, the specific heat should be determined from the following ($\vartheta[°C]$):

$$\begin{aligned} c_p &= 425 + 0.773\,\vartheta - 1.69 \cdot 10^{-3}\,\vartheta^2 + 2.22 \cdot 10^{-6}\,\vartheta^3 && 20 \le \vartheta \le 600 \\ c_p &= 666 - \left(\frac{13002}{\vartheta - 738}\right) && 600 \le \vartheta \le 735 \\ c_p &= 545 - \left(\frac{17820}{\vartheta - 731}\right) && 735 \le \vartheta \le 900 \\ c_p &= 650 && 900 \le \vartheta \le 1200 \end{aligned} \qquad 2.18$$

As concern the thermal conductivity of steel, it's expressed in a bilinear form:

$$\begin{aligned} \lambda &= 54 - 3.33 \cdot 10^{-2}\,\vartheta && 20 \le \vartheta \le 800 \\ \lambda &= 27.3 && 800 \le \vartheta \le 1200 \end{aligned} \qquad 2.19$$

From Figure 7 we can observe that the thermal conductivity decreases when temperature grows up. This is a common trend of the law of conductivity of most solid materials. Moreover, from the same figure we can see that specific heat has a peak between 700 °C and 800 °C. The peak is due to the phase change of the steel: in this temperature interval the steel change its chemical structure rearranging the disposition of molecules.

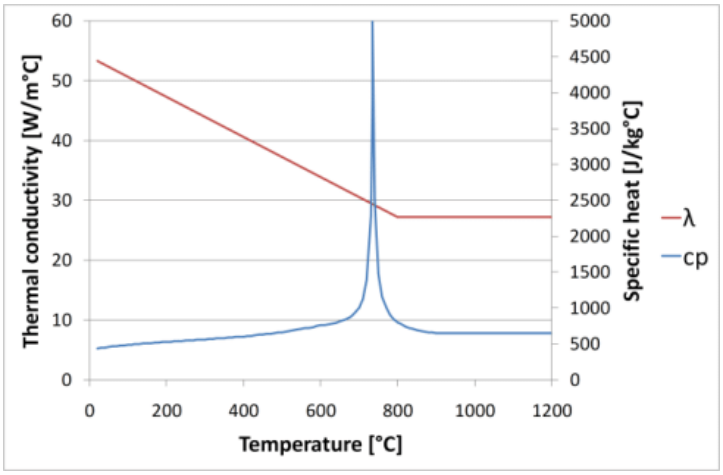

Figure 7 Thermal properties of steel.

2.2.1 FEM THERMAL ANALYSIS

Thermal analysis of structural elements consists in an unsteady state analysis with nonlinear thermal properties of structural elements. In this framework the problem could be formalized in the determination by integration of a function that describe temperature distribution in the space and time $\vartheta(x, y, z, t)$. In order to determine temperature, the integration of Fourier Law of conduction is needed.

$$\frac{d\left(\rho(\vartheta)\cdot c_p(\vartheta)\cdot\vartheta(x,y,z,t)\right)}{dt} = -\lambda\,\nabla\vartheta(x,y,z,t) \qquad 2.20$$

This equation is based on the differential equilibrium the elementary volume. The first member of 2.20 means the energy stored in the unit volume of material, and it depends from the specific heat, density and temperature. The second member of the equation symbolize net heat fluxes that pass through the unit volume so it can assume also the expression of the 2.16 or 2.17 at the borders of the integration domain.

Since the 2.20 represent a differential equation with partial derivates, it cannot be integrated but for special cases. For this reason, we need to solve the problem

through a numerical integration that means the application of numerical methods like the finite difference method (FDM) or the finite element method (FEM).

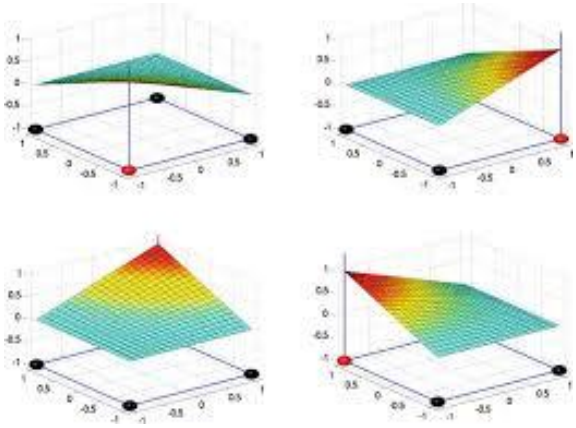

Figure 8 Quadrangle Shape Function.

The thing that makes the FEM the most powerful method to resolve this problem is its high flexibility. Starting from characterization of a finite Element through a series of shape function and the discretization of the domain the method let us to know the best numerical solution compatible with form function.

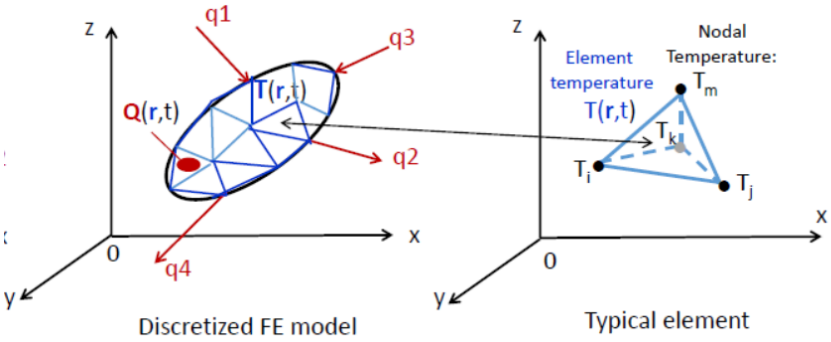

Figure 9 Discretization of domain and tetrahedron element characterization.

The same definition of interpolation function for stress analysis is used for the heat conduction analysis. There are several interpolation functions, that differ by several parameters, including dimension (1D,2D,3D), shape (line, quad, triangle, tetrahedron, etc.) and sophistication (linear or quadratic).

$$Element\ Temperature = form\ function \times Nodal\ Temperature \tag{2.21}$$

Referring to Figure 9, the form function and nodal temperature is assumed as

$$[N(x,y,z)] = \{N_i \quad N_j \quad N_k \quad N_m\}$$
$$[T] = \{T_i \quad T_j \quad T_k \quad T_m\}^T \tag{2.22}$$

The temperature gradients in the element may be obtained in terms of nodal temperature by differentiate the 2.21:

$$\begin{bmatrix} \frac{\partial T(x,y,z)}{\partial x} \\ \frac{\partial T(x,y,z)}{\partial y} \\ \frac{\partial T(x,y,z)}{\partial z} \end{bmatrix} = \begin{bmatrix} \frac{\partial N_i}{\partial x} & \frac{\partial N_j}{\partial x} & \frac{\partial N_k}{\partial x} & \frac{\partial N_m}{\partial x} \\ \frac{\partial N_i}{\partial y} & \frac{\partial N_j}{\partial y} & \frac{\partial N_k}{\partial y} & \frac{\partial N_m}{\partial y} \\ \frac{\partial N_i}{\partial z} & \frac{\partial N_j}{\partial z} & \frac{\partial N_k}{\partial z} & \frac{\partial N_m}{\partial z} \end{bmatrix} [T] = [B][T] \tag{2.23}$$

Because the conduction of heat in solids can be completely described by the 2.20, we can rewrite it as

$$\begin{aligned} &\frac{\partial}{\partial x}\left(\lambda \frac{\partial \vartheta(x,y,z,t)}{\partial x}\right) + \frac{\partial}{\partial y}\left(\lambda \frac{\partial \vartheta(x,y,z,t)}{\partial y}\right) \\ &\quad + \frac{\partial}{\partial z}\left(\lambda \frac{\partial \vartheta(x,y,z,t)}{\partial z}\right) + Q(x,y,z,t) \\ &\quad = \frac{d\left(\rho(\vartheta) \cdot c_p(\vartheta) \cdot \vartheta(x,y,z,t)\right)}{dt} \end{aligned} \tag{2.24}$$

In order to solve this equation through algebraic way, the Galerkin method needs to be implemented. In contrast to the Rayleigh-Ritz method, this method is used to derive the element equations for the cases in which specific differential equations with appropriate mathematical expressions for the boundary conditions

available for the analytical problems, such as heat conduction and fluid dynamic analyses.

We must think that the problem which we want to solve through FEM can be schematized as a domain where is valid a differential equation or a system of differential equations $D(\Phi)$ and sufficiently boundaries condition $B(\Phi)$ are defined. Thus, the mathematical model is

$$\int_{\Omega} W\, D(\phi)\, d\Omega + \int_{\partial\Omega} \overline{W}\, B(\phi)\, ds = 0 \qquad 2.25$$

Where $\overline{W}$ and W are arbitrary weighting functions. After the approximation due to discretization of the domain, the differential equation and boundaries become function of the form function, function of position vector $\boldsymbol{r}$:

$$\int_{\Omega} W_j\, D\left(\sum N_i(\boldsymbol{r})\, \phi_i\right)\, d\Omega + \int_{\partial\Omega} \overline{W_j}\, B\left(\sum N_i(\boldsymbol{r})\, \phi_i\right)\, ds = R \qquad 2.26$$

Where $\overline{W_j}$ and W_j are discretized weighting functions and R is the residual. The Galerkin method lets $\overline{W_j}$ and W_j equal to $N(r)$ and let R to be minimum. Through this procedure is we can rewrite the basic heat conduction equation in the following form:

$$\int_{\Omega} \left(\frac{\partial q_x}{\partial x} + \frac{\partial q_y}{\partial y} + \frac{\partial q_z}{\partial z} - Q + \rho c_p \frac{\partial T}{\partial t}\right) N_i\, d\Omega = 0 \qquad 2.27$$

By incorporate the boundary conditions in the above equation will result in the element equation with the balanced of heat flus across the boundary and the induced temperature in the element in the following equation:

$$\begin{aligned} \int_{\Omega} \rho c \frac{\partial T}{\partial t}\, N_i\, d\Omega - \int_{\Omega} \left[\frac{\partial N_i}{\partial x} \;\; \frac{\partial N_i}{\partial y} \;\; \frac{\partial N_i}{\partial x}\right] [q]\, d\Omega = \\ = \int_{\Omega} Q N_i d\Omega - \int_{\partial\Omega} [q]^T [n] N_i ds - \int_{\partial\Omega} q_s N_i ds \\ - \int_{\partial\Omega} h\big(T - T_f\big) N_i ds \end{aligned} \qquad 2.28$$

With the heat flux across boundaries $[q]^T = \begin{bmatrix} q_x & q_y & q_z \end{bmatrix}$ and the direction cosine to outward normal $[n]^T = \begin{bmatrix} n_x & n_y & n_z \end{bmatrix}$.

The heat balance in above equation may be lumped to the following element equation:

$$[C]\left[\dot{T}\right] + ([K_c] + [K_h])[T] = [R_I] + [R_T] + \left[R_q\right] + [R_h] \qquad 2.29$$

Where:

The heat capacitance matrix: $[C] = \int_\Omega \rho c\, [N]^T [N]\, d\Omega$;

The conductivity matrix: $[K_c] = \int_\Omega \lambda\, [B]^T [B]\, d\Omega$;

The convective matrix $[K_h] = \int_{\partial\Omega} h\, [N]^T [N]\, ds$;

$[R_T]$, $\left[R_q\right]$ and $[R_h]$ are the heat flux across boundaries;

The internal heat generation $[R_I] = \int_\Omega Q [N]^T d\Omega$.

The thermal conditions in one dimensional problem are related to the displacements and stress in an axial bar as summarized in Table 1.

	Thermal Analysis	**Structural Analysis**
Results	Temperature	Displacements
Gradient	Temperature Gradient	Strains
Flux	Heat	Stresses
Source	Heat Sources	Loads
Restraint	Prescribed Temperature	Prescribed Displacements
Reaction	Heat Flow resultant	Force Component
Mat. prop.	Conductivity	Elastic Modulus
Mat. law	Fourier Law	Hooke's Law

Table 1 Structural analogy to thermal problem.

2.3 Structural Analysis in fire condition

The main objective of a fire-structure analysis is to predict the effects of fires in buildings, e.g. the fire resistance and the structure's performance under heating and cooling caused by fire. The results of such analysis can be applied in the design of fire protection systems, in the evaluation of fire safety and as an addendum of experiments. Advanced calculation techniques can be helpful in the areas where experiments encounter difficulties such as testing large specimens, implementation of loading and boundary condition, measurements and interpretation of specimen's behaviour. A computational model used for fire-structural (member or global) analysis should properly represent the considered problem in terms of type of analysis and solution methods, geometry, temperature dependent material properties, mechanical boundary conditions and loading, thermal conditions. From the constructional point of view, buildings and structures at fire have to carry mechanical loadings and thus provide safe people evacuation and safe firemen work. High temperatures have a very significant adverse effect on thermo-mechanical properties of steel members. High temperatures substantially reduce strength of concrete and steel, and causes significant increase in cracking, strains and deflections. Load bearing capacity of structure decreases and may fail at critical points.

Also, in this case, the best way to solve the analytical problem is through a Finite element analysis. In order to reduce costs of calculations the Thermomechanical analysis was conducted using a beam finite element characterized on a thermomechanical analysis of the sections. Also, this type of analysis was carried out with the software SAFIR.

The Safir solver perform a Finite element analysis taking in account the temperature variation of the structural elements. In this section the material properties will be introduced and a brief description of the solver will be done. Other information about Safir are be available at Frannsen et al, 2000, Frannsen et al, 2017 and Frannsen et al, 2019.

2.3.1 MATERIAL'S MECHANICAL PROPERTIES

In order to determine the structural response subjected to fire, it is necessary to formulate constitutive laws for steel at elevated temperatures. A complete formulation is required only where a full analysis is undertaken.

The mechanical property test is usually carried out by using a steady-state testing regime and the structural component fire test is usually carried out by using a transient-state testing regime. In the steady state test, the specimen is heated to a pre-determined temperature before the test and kept constant during the test. The stress-strain relationship of steel at a specific temperature can be obtained directly. Usually, in a building fire the temperature keeps changing. The steady state test is not representative of the actual fire scenario.

In the transient state test, the specimen is loaded to a pre-determined stress level before test, then it is heated to failure at a specific heating rate. Usually, the heating rate is in a range of 5–50 °C/min, according to International Organization for Standardization, 19990. The thermal expansion should be obtained first and subtracted from the total strain to determine the strain caused by stress. The transient state test represents the real situation of a structure in a fire. However, the test result includes the creep strain and relaxation of steel.

Kay et al,1996 compared steady state test results and transient state test results and found that strength of steel obtained by the steady state test was higher than the transient state test.

Owing to large strains exhibited at elevated temperatures in fire affected members, it is more usual to quote the 1.0% or 2.0% proof stress rather than the conventional ambient value of 0.2% proof stress. As reported by G. Li et al, 2013 there are a lot of constitutive law available for steel elements.

Performed analysis showed in further chapters, needs only the uniaxial material law to describe the behaviour of the beam elements.

High temperatures distribution induced in structural elements by fires depends from the heat transmission problem formalized in previous sections. Temperatures induces the mechanical properties variation and the dilatation of elements that influences stress entities, deformations and resistance of structural elements. As reported in the Eurocode 3 (EN 1993-1-2, 2005) the constitutive law

of steel in fire condition is the same in compression and tension and it is showed in Figure 10.

This constitutive law is characterized by a first perfect elastic branch up to a traction called traction of proportional limit, then an elliptic branch that connect the first perfect elastic branch with the plastic branch that start at a deformation $\varepsilon = 2\%$. The final part of the $\sigma - \varepsilon$ function, is characterized by a linear softening branch that reach the point $\sigma = 0$ at $\varepsilon = 20\%$

So, the characterization of the mechanical properties of the steel depends from:

- $E_{a,\vartheta}(\vartheta)$ elastic modulus of steel that depends from temperature ϑ;
- $f_{a,p,\vartheta}(\vartheta)$ proportional limit that depends from ϑ;
- $f_{a,y,\vartheta}(\vartheta)$ the yielding stress of steel, that depends from ϑ;
- $\varepsilon_{ap} = f_{a,p}(\vartheta)/E_a(\vartheta)$ the strain relative to proportional limit;
- $\varepsilon_{ay} = 0.02$ the strain relative to yielding stress;
- $\varepsilon_{au} = 0.15$ the strain at the end of the perfect plastic branch;
- $\varepsilon_{ae} = 0.2$ the strain at the end of the linear softening branch.

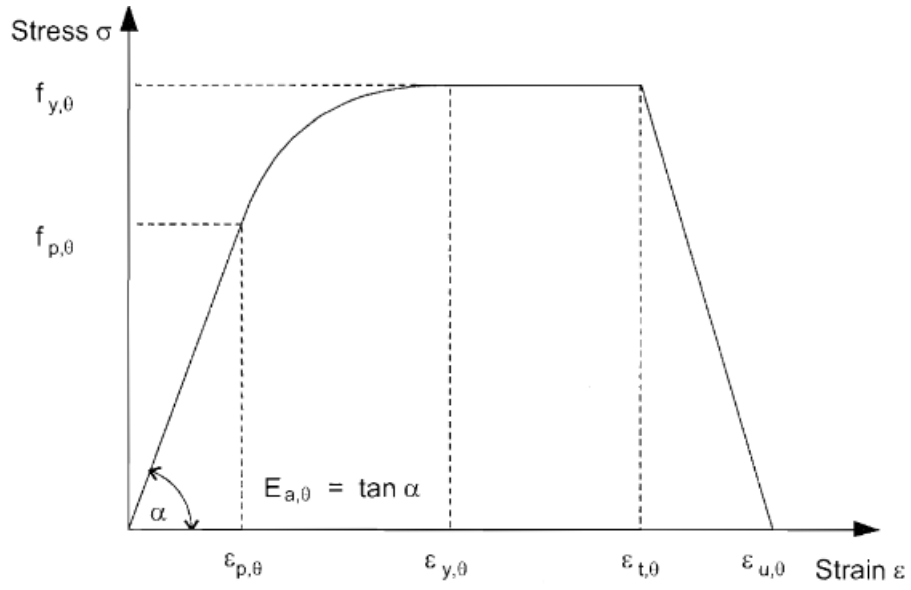

Figure 10 Constitutive Law of steel at elevated temperatures.

The equation that gives the $\sigma(\varepsilon, \vartheta)$ in the first branch is:

$$\sigma(\varepsilon,\vartheta) = E_{a,\vartheta}\cdot\varepsilon \qquad for \quad \varepsilon < \varepsilon_{a,p} \tag{2.30}$$

The elliptic branch is characterized by the equation:

$$\sigma(\varepsilon,\vartheta) = \left(f_{a,p,\vartheta} - c\right) + \frac{b}{a}\sqrt{a^2 - \left(\varepsilon_{ay} - \varepsilon\right)^2} \quad for\ \varepsilon_{a,p} < \varepsilon < \varepsilon_{ay} \tag{2.31}$$

Where the coefficients a, b and c could be calculated as:

$$\begin{aligned} a &= \sqrt{\left(\varepsilon_{ay} - \varepsilon_{ap}\right)\left(\varepsilon_{ay} - \varepsilon_{ap} + c/E_{a,\vartheta}\right)} \\ b &= \sqrt{E_{a,\vartheta}\left(\varepsilon_{ay} - \varepsilon_{ap}\right)c + c^2} \\ c &= \frac{\left(f_{a,y,\vartheta} - f_{a,p,\vartheta}\right)^2}{E_a(\vartheta)\left(\varepsilon_{ay} - \varepsilon_{ap}\right) - 2\left(f_{a,y,\vartheta} - f_{a,p,\vartheta}\right)} \end{aligned} \tag{2.32}$$

And finally, the stress in the plastic branch is:

$$\sigma(\varepsilon,\vartheta) = f_{a,y,,\vartheta} \quad for\ \ \varepsilon_{a,y} < \varepsilon < \varepsilon_{au} \tag{2.33}$$

Values of $E_a(\vartheta)$, $f_{a,p}(\vartheta)$ and $f_{a,y}(\vartheta)$ must be calculated through the application of reduction factors named k_E , k_p and k_y respectively. We can observe that reduction factors, reported in Table 2 and displayed in Figure 11, are always ≤ 1 and regarding to stiffness and proportional limit traction, they have a faster reduction respect the reduction of the yielding stress. Moreover, if we observe the $k_{a,y\vartheta}$values there is no reduction of strength up to 400°C but the reduction of strength is faster than stiffness: at 593°C steel strength is reduced of 50%. Anyway, even if material's strength doesn't reduce itself due to temperature there is always a burden of stresses in the structure already from when it reaches 100°C due to the stiffness reduction and birth of thermal strains.

ϑ [°C]	$k_{E,\vartheta} = E_{a,\vartheta}/E_a$	$k_{p,\vartheta} = f_{a,p,\vartheta}/f_{a,p}$	$k_{y,\vartheta} = f_{a,y,\vartheta}/f_{a,y}$
20	1.00	1.00	1.00
100	1.00	1.00	1.00
200	0.90	0.807	1.00
300	0.80	0.613	1.00
400	0.70	0.420	1.00
500	0.60	0.360	0.78
600	0.31	0.180	0.47
700	0.13	0.075	0.23
800	0.09	0.050	0.11
900	0.0675	0.0375	0.06
1000	0.0450	0.0250	0.04
1100	0.0225	0.0125	0.02
1200	0	0	0

Table 2 Reduction factors.

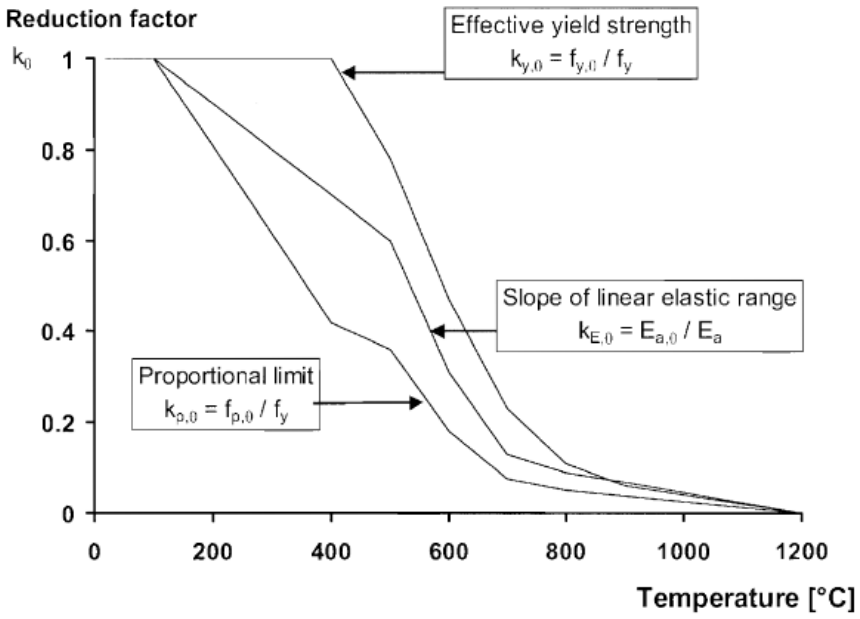

Figure 11 Reduction factors.

In Figure 12 we can see the representation of the stress strain diagram at various elevated temperatures. Note that the elliptical branch takes more space when temperatures increase, this involves stress burden due to II order effects. In Figure 13 we can see the diagram of thermal elongation $\varepsilon_\vartheta = \Delta l/l$ in function of temperatures. Plateau coincides with the specific heat peak.

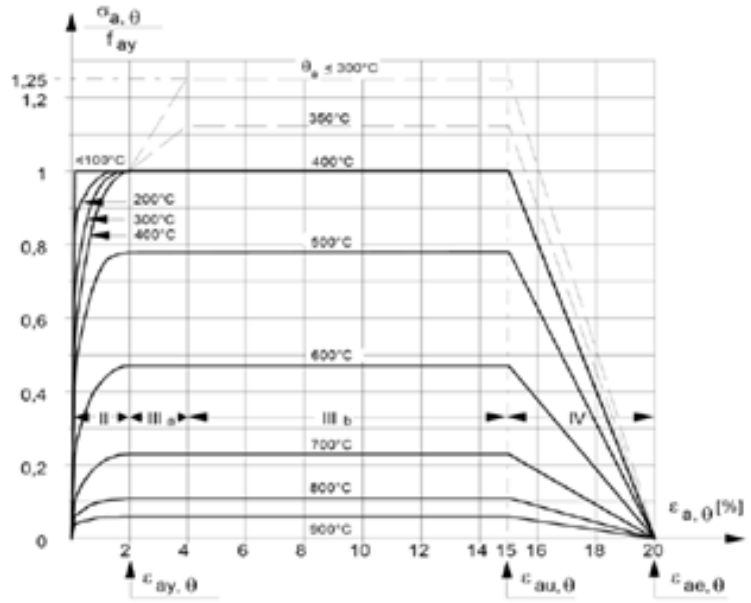

Figure 12 $\sigma - \varepsilon$ diagram at various temperatures.

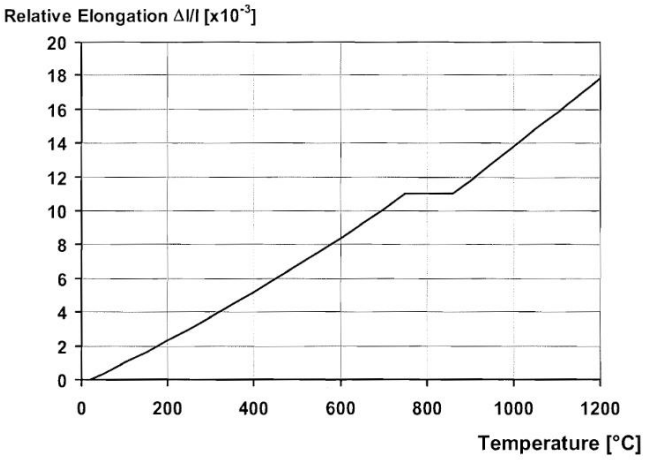

Figure 13 Thermal strain.

2.3.2 THERMOMECHANICAL ANALYSIS

The section's thermal analysis is performed before the structural analysis and independently from the structural context. After meshing procedure, that is needed to define material's thermal properties, thermal input on section and section geometry, a FEM analysis of the structure is performed (Franssen et al 2000). SAFIR User Manual. University of Liege, Belgium.]. The FEM analysis is conducted taking in account large displacements and thermal effects. In particular, since thermal actions are punctual computed on the nonlinear gradient in sections, for each fibre of the section mesh it was calculated the associated deformation.

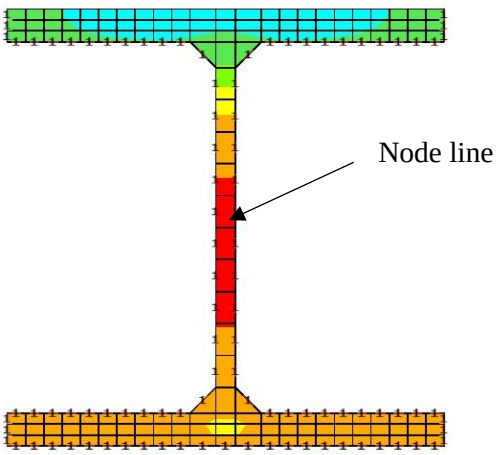

Figure 14 Section's Thermal Analysis result.

The FEM model is based on the plane section conservation hypothesis, indeed during the phase of model definition, we have to define the point of application of internal stresses. This phase is crucial because thanks to the identification of

this point (called node line) the software evaluate the stress distribution without taking in account the strain field of the near sections. The equilibrium in this framework could be achieved through:

$$N_{int} = \int_A \sigma_z \, dA = N_{NL} \qquad 2.34$$

Where N_{NL} is the Axial Force applied on the node line and N_{Int} is the sum of the internal stresses of the section. The field of σ_z is calculated by the deformation of the section taking in account the compatibility of the constitutive law. The curvature and neutral axis are computed so that:

$$\begin{aligned} M_{x,int} &= \int_A \sigma_z \, y \, dA = M_{x,NL} \\ M_{y,int} &= -\int_A \sigma_z \, x \, dA = M_{y,NL} \end{aligned} \qquad 2.35$$

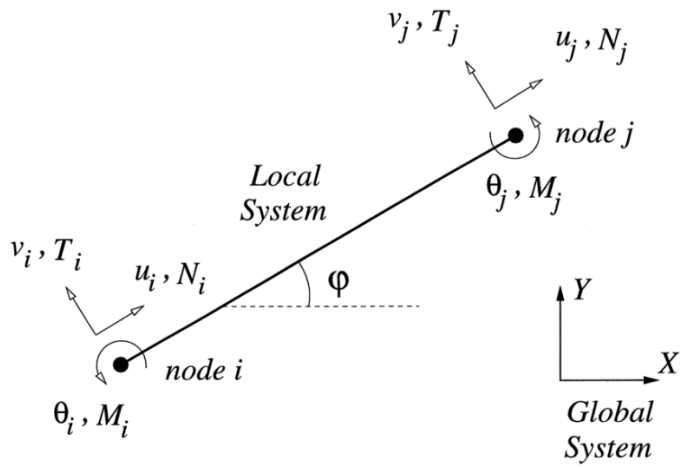

Figure 15 Beam Finite element

Where $M_{x,int}$ and $M_{y,int}$ are bending moments in direction x and y, x and y are the position of the fibre respect to local coordinate system, and $M_{x,NL}$ and $M_{y,NL}$ are bending moments applied on the node line. If we focus only on the y direction,

deformation of the i-th fibre $\varepsilon_{i,Tot}$ is evaluated thanks to the following relationship:

$$\varepsilon_{i,Tot} = \varepsilon_{G,Tot} + \chi y \qquad 2.36$$

Where $\varepsilon_{G,Tot}$ is the barycentre strain, χ [1/m] is the curvature of the section and y is the position of the fibre. Since the deformation evaluated is the *total* strain, in order to evaluate stresses, we have to take into account the thermal strain $\varepsilon_\vartheta(\vartheta)$,

$$\varepsilon_{Tot} = \varepsilon_\sigma(\sigma, \vartheta) + \varepsilon_\vartheta(\vartheta) \qquad 2.37$$

So, the mechanical strain, is calculated as:

$$\varepsilon_\sigma(\sigma, \vartheta) = \varepsilon_{Tot} - \varepsilon_\vartheta(\vartheta) \qquad 2.38$$

Once the mechanical strain is known, we can calculate stresses by taking in account the compatibility with the constitutive law for each fibre of the section.

$$\sigma = \sigma(\varepsilon_\sigma) \qquad 2.39$$

Concepts introduced in this paragraph have been treated by simplified way, to implement them in numerical solver of computer program a formalization of a finite element method is needed. More information are available in bibliography at and Frannsen et al, 2019, Compagnone et al, 2018.

Chapter 3

3 Probability application in structural framework

In this section several probability concepts will be introduced in order to uniquely define the terms that will be used in the further sections and chapters. In particular, in this section will be introduced the basic probability concepts, the Baesyan theorem, Random Variables, the Central Limit Theorem the Monte Carlo Simulation and the Latin Hypercube Sampling procedure.

3.1 Basic Probability Concepts

Many processes in nature have uncertain outcomes. This means that their result cannot be predicted before the process occurs. A random process is a process that can be reproduced, to some extent, within some given boundary and initial conditions, but whose outcome is uncertain. This situation may be due to insufficient information about the process intrinsic dynamics which prevents to predict its outcome, or lack of sufficient accuracy in reproducing the initial conditions in order to ensure its exact reproducibility. This will lead to possibly different outcomes if the experiment is repeated several times, even if each time the initial conditions are exactly reproduced, within the possibility of control of the experimenter. Probability is a measurement of how favored one of the possible outcomes of such a random process is compared with any of the other possible outcomes. There are two main different approaches to the concept of probability

which result in two different meanings of probability. These are referred to as frequentist and Bayesian probabilities.

Frequentist probability is defined as the fraction of the number of occurrences of an event of interest over the total number of possible events in a repeatable experiment, in the limit of very large number of experiments. This concept can only be applied to processes that can be repeated over a reasonably long range of time. It is meaningless to apply the frequentist concept of probability to an unknown event, like the possible values of an unknown parameter.

Bayesian probability measures how much anyone can believe a statement is true. The quantitative definition of Bayesian probability makes use of an extension of the Bayes theorem. Bayesian probability can be applied wherever the frequentist probability is meaningful, as well as on a wider variety of cases in which one wants to determine a probability of unknown events or of unknown quantities.

The probability could be defined in several ways, next paragraphs will show two different definition of probability which can be used in order to treat data.

3.1.1 CLASSIC DEFINITION OF PROBABILITY

If under certain experimental conditions N results may occur, independent each other and equally possible, and if N_A of them are favorable to the occurrence of an event A, the probability of A is the ratio between the number of favorable cases N_A over the number of possible cases:

$$P(A) = \frac{N_A}{N} \tag{3.1}$$

This definition of probability is the first in chronological order for this it is called classical, but even if founded on a valid criterion it cannot be accepted as a definition because it is circular. Indeed, when we say “equally possible” we indirectly use the concept of probability. Moreover, this definition is incomplete

because doesn't take into account the possibility that events aren't equiprobable and the possibility that results of the statistical process are infinite.

3.1.2 FREQUENTIST DEFINITION OF PROBABILITY

In order to extend the classical probability definition a new definition was introduced. It's also known as statistical definition of probability and allows to circumvent the limits of the first.

If repeating an experiment N times the event A occur N_A times the frequency of occurrence of A tends to the probability of A assuming that N is sufficiently large:

$$P(A) = \frac{N_A}{N} \qquad 3.2$$

Just written expression is the same of the previous paragraph but it has a different meaning. In this definition the probability as the result's frequency of occurrence, so it can be used even if there is non-numerable possible cases N because to evaluate it we need only to repeat an experiment enough times.

Even in this case there is a critical aspect that makes it impossible to accept this definition as the general one, indeed this definition assumes that the experiment is repeatable and this is not always true.

3.1.3 AXIOMATIC DEFINITION OF PROBABILITY

An axiomatic definition of probability as a theory of measurement that is valid either in the discrete and the continuous case is due to A. Kolmogorov, 1956. Let's consider a measure space, $(\Omega, F \subseteq 2^{\Omega}, P)$, where P is a function that maps elements of F, a subset of the power set 2^{Ω} of Ω, to real numbers. The entity Ω is

called sample space and F is called event space. P is a probability measure if the following properties are satisfied:

$$P(E) \geq 0\,, \qquad \forall\, E \in F \tag{3.3}$$

$$P(\Omega) = 1 \tag{3.4}$$

$$\forall(\, E_1, \dots, E_n) \in F^n \;:\; E_i \cup E_j = 0, P(\cup_{I=1}^{n}\; E_i) = \sum_{i=1}^{n} P(E_i) \tag{3.5}$$

This definition allows to generalize the classical probability to the case of continuous variables.

3.2 Conditional probability

Given an event A and an event B, the conditional probability, $P(A|B)$, is defined as the probability of A given the condition that the event B has occurred, and is given by:

$$P(A|B) = \frac{P(A \cap B)}{P(B)} \tag{3.6}$$

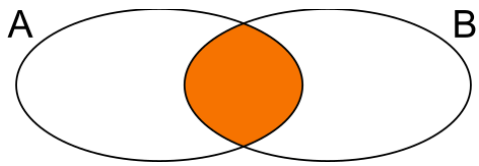

Figure 16 Conditional Probability

The conditional probability can be visualized in Figure 16. While the probability of A, $P(A)$, corresponds to the area of the set A, relative to the area of the whole sample space Ω, which is equal to one, the conditional probability, $P(A|B)$, corresponds to the area of the intersection of A and B, relative to the area of the set B.

An event A is independent on event B if the conditional probability of A, given B, is equal to the probability of A, i.e.: the occurrence of B does not change the probability of A:

$$P(A|B) = \frac{P(A \cap B)}{P(B)} \tag{3.7}$$

Two events are independent if, and only if, the probability of their simultaneous occurrence is equal to the product of their probabilities, i.e.:

$$P(A \cap B) = P(A) \cdot P(B) \tag{3.8}$$

3.3 Law of Total Probability

Let's consider a number of sets (events) $\{E_1, \dots, E_n\}$, subsets of another set E_0 included in the sample space Ω, such that the set of the E_i is a partition of E_0, i.e.: $E_i \cap E_j = 0$ for all i and j, and:

$$\bigcup_{i=1}^{n} E_i = E_0 \tag{3.9}$$

This can be clarified by looking at the Figure 17: considering only grey area, it result immediately that the probability corresponding to E_0 is equal to the sum of the probabilities of E_i:

$$P(E_0) = \sum_{i=1}^{n} P(E_i) \tag{3.10}$$

For a partition $\{A_1, \dots, A_n\}$ of the sample space Ω of disjoint sets ($A_i \cap A_j = 0$ and $\sum_{i=1}^{n} P(A_i) = 1$)we can build the sets:

$$E_i = E_0 \cap A_i \tag{3.11}$$

Seeing the Figure 17, considering the yellow part, the probability can be calculated as:

$$P(E_i) = P(E_0 \cap A_i) = P(E_0|A_i)P(A_i) \tag{3.12}$$

In this case we can rewrite $P(E_0)$ as:

$$P(E_0) = \sum_{i=1}^{n} P(E_0|A_i)P(A_i) \tag{3.13}$$

This decomposition can be interpreted as weighted average of probabilities $P(A_i)$ with weights $w_i = P(E_0|A_i)$.

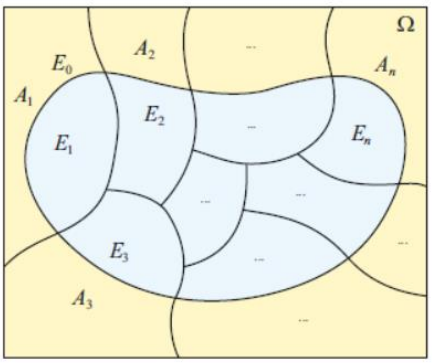

Figure 17 Law of total probability

3.4 Bayes theorem

According to the definition of conditional probability in Eq. (1.4), the probability of

an event A given the condition that the event B has occurred is given by:

$$P(A|B) = \frac{P(A \cap B)}{P(B)} \tag{3.14}$$

We can conversely write the probability of the event B given A as:

$$P(B|A) = \frac{P(A \cap B)}{P(A)} \tag{3.15}$$

Using equations 3.14 and 3.15 we can write:

$$P(A|B)P(B) = P(B|A)P(A) \tag{3.16}$$

From this we can derive the Bayes' theorem in the notorious form:

$$P(A|B) = \frac{P(B|A)P(A)}{P(B)} \tag{3.17}$$

The probabilities P(A) and P(A|B) can be interpreted as probability of event A before the knowledge that the event B has occurred (prior probability) and as the probability of the same event A having as further information the knowledge that the event B has occurred (**posterior** probability).

3.5 Random Variables: Definition and models

A Random Variable (RV), aleatory variable, or stochastic variable is described informally as a variable whose values depend on outcomes of a random phenomenon. In that context, a random variable is understood as a measurable function defined on a probability space whose outcomes are typically real numbers.

A random variable's possible values might represent the possible outcomes of a yet-to-be-performed experiment, or the possible outcomes of a past experiment whose already-existing value is uncertain. They may also conceptually represent either the results of an "objectively" random process (such as rolling a die) or the "subjective" randomness that results from incomplete knowledge of a quantity.

The meaning of the probabilities assigned to the potential values of a random variable is not part of probability theory itself but is instead related to philosophical arguments over the interpretation of probability. The mathematics works the same regardless of the particular interpretation in use.

As a function, a RV is required to be measurable, which allows for probabilities to be assigned to sets of its potential values. It is common that the outcomes depend on some physical variables that are not predictable.

The domain of a RV is a sample space, which is interpreted as the set of possible outcomes of a random phenomenon.

A RV has a probability distribution, which specifies the probability of its values. Random variables can be discrete, that is, taking any of a specified finite or countable list of values, endowed with a probability mass function characteristic of the random variable's probability distribution; or continuous, taking any numerical value in an interval or collection of intervals, via a probability density function that is characteristic of the random variable's probability distribution; or a mixture of both types.

If a RV named $X: \Omega \to \mathbb{R}$ defined on the probability space $(\Omega, F, P)$is given, we can define a function of a value x such that the same function calculated in x give us the probability that the occurrence of X is minus or equal to the value of x:

$$F_X(x) = P(X \leq x) \tag{3.18}$$

Or a function like:

$$f_X(x) = P(X = x) \tag{3.19}$$

These two functions describe also taken one at a time the random variable X and are called Cumulative Distribution Function (CDF) and Probability Density Function (pdf) respectively. These two functions are related to each other and have some constant characteristics:

$$f_X(x) = \lim_{\Delta x \to 0} \frac{F_X(x + \Delta x) - F_X(x)}{\Delta x} = \frac{\partial F_X(x)}{\partial x} \tag{3.20}$$

$$\int_{\Omega} f_X(x)\, dx = 1 \tag{3.21}$$

There are a lot of RV models in literature and they are frequently used to describe random processes. Generally, pdf and CDF functions of a RV model are characterized by some quantities that have to be evaluated, they are called distribution parameters and they often coincide with special quantities like mean and average. In next paragraph they will be quickly recalled.

3.5.1 CHARACTERISTIC QUANTITIES IN DISTRIBUTION FUNCTIONS

In this section they will be introduced some quantities used in further chapters for applications. To make the text simpler and more streamlined in this paragraph we will refer only to a continuous random variable defined in the domain $[-\infty, +\infty]$ but all quantities can also refer to discrete variables. These quantities are generally calculated using the operator $E[\cdot]$, which is defined as:

$$E[\varphi(X)] = \int_{-\infty}^{+\infty} \varphi(x)\, f_X(x)\ dx \tag{3.22}$$

Where $\varphi(x)$ is a real function. If $\varphi(x)$ is the identity function $E[X]$ return the mean of the distribution. it could be demonstrated that $E[\cdot]$ is a linear operator, so:

$$E[aX + b] = a\, E[X] + b \tag{3.23}$$

$$E[X + Y] = E[X] + E[Y] \tag{3.24}$$

3.5.1.1 AVERAGE, VARIANCE AND OTHER USEFUL QUANTITIES

Mean and variance provide us with brief information on the distribution functions. Mean (also known as expected value) provide us the "center of gravity" of the RV. It is defined as:

$$\mu_X = E[X] = \int_{-\infty}^{+\infty} x\, f_X(x)\, dx \tag{3.25}$$

while the variance provides us the "moment of inertia" of the RV:

$$Var[x] = \sigma_X^2 = E\left[\left[X - E[X]\right]^2\right] = \int_{-\infty}^{+\infty} \left[x - E[X]\right]^2 f_X(x)\, dx \tag{3.26}$$

There are some properties that good to remember:

$$Var[x] = E\left[\left[X - E[X]\right]^2\right] = E[X^2] - \left[E[X]\right]^2 \tag{3.27}$$

$$Var[a\,X + b] = a^2 Var[X] \tag{3.28}$$

$$Var[X + Y] = Var[X] + Var[Y] + 2E[(X - \mu_X)(Y - \mu_Y)] \tag{3.29}$$

The last Addendum of the 2.29 is called Covariance. Covariance (Cov[X,Y]) quantify the trend of two RV to assume simultaneously higher or lower than the respective averages. The covariance of two independent variable is null.

The covariance is used also to calculate the *correlation coefficient*:

$$\rho_{XY} = \frac{Cov[X,Y]}{\sigma_X \sigma_Y} \tag{3.30}$$

Median $x_{0.5}$ is defined starting from the CDF:

$$P[X \leq x_{0.5}] \geq 0.5 \qquad P[X \geq x_{0.5}] \geq 0.5 \tag{3.31}$$

The Mode is a value (if exist) for that is maximum the pdf.

$$mode[X] = \zeta : f_X(\zeta) = \max [f_X(x)] \tag{3.32}$$

Average and variance expressed in 3.25 and 3.26 are referred to a RV model, but actually never know the real distribution of a RV in application. Generally, mean and variance needs to be calculated through the study of samples and are referred to statistics.

In application we do some implicit operations that allows us to use the probability concept extrapolating some data from samples and extending it to population.

Population generally can't be studied because is constituted N (too large) number elements, this means that we aren't able to know μ and σ. We extrapolate a representative sample (n<N) from population and evaluate statistics. Even if the average $(\bar{x})$ and variance (s^2) that we calculate are referred to sample we can say that if the sample is representative:

$$\begin{cases} \mu \cong \bar{x} \\ \sigma^2 \cong s^2 \end{cases} \qquad if \quad n \to N \tag{3.33}$$

In this sense $\bar{x}$ and s^2 assume the meaning of estimators of the RV's parameters. Since we can only estimate parameters of a RV, there are many ways to do that, but the best way to estimate parameters is

$$\bar{x} = \frac{\sum_{i=1}^{n}(x_i)}{n} \tag{3.34}$$

$$s^2 = \frac{\sum_{i=1}^{n}(x_i - \bar{x})^2}{n-1} \tag{3.35}$$

3.5.1.2 STATISTICAL MOMENTS

Moment of a distribution is defined as:

$$E[(X - E[X])^n] \tag{3.36}$$

Where n is the order of the moment. As already said, the mean and the variance provide information on the location and variability (spread, dispersion) of a set of numbers, and by doing so, provide some information on the appearance of the distribution of the numbers. The mean and variance are the first two statistical moments, and the third and fourth moments also provide information on the shape of the distribution. For comparison, the

$$First\ Moment = E\big[X - E[X]\big] \tag{3.37}$$

is by definition is equal to zero. One might think of the mean as being that value of x that makes the above statement true, and consequently indicates where the individual numbers generally lie.

$$Second\ Moment = E[(X - E[X])^2] \tag{3.38}$$

The third and fourth moment is used to define the skewness and kurtosis of a distribution.

$$\gamma = \frac{E[(X - E[X])^3]}{\sigma^3} \tag{3.39}$$

Skewness is a measure of the symmetry of the shape of a distribution. If a distribution is symmetric, the skewness will be zero. If there is a long tail in the positive direction, skewness will be positive, while if there is a long tail in the negative direction, skewness will be negative.

$$\eta = \frac{E[(X - E[X])^4]}{\sigma^4} \qquad 3.40$$

Kurtosis is a measure of the flatness or peakedness of a distribution. Flat-looking distributions are referred to as "platykurtic," while peaked distributions are referred to as "leptokurtic."

3.5.2 RANDOM VARIABLE MODELS

In this section will be introduced some random variable models that will be used in further chapters. RV models meaning there is a functional form that describe the distribution of a random variable. As already said in previous paragraph each RV model needs to be characterized by some parameters that depend from the model adopted. Since the RV model is predefined, also statistics of the distribution could be calculated a priori.

3.5.3 UNIFORM DISTRIBUTION (CONTINUOUS)

The uniform distribution (continuous) is one of the simplest probability distributions in statistics. Itis a continuous distribution, this means that it takes values within a specified range.

The probability density function for a uniform distribution taking values in the range a to b is:

$$f(x) = \begin{cases} \frac{1}{b-a} & if \quad a \le x \le b \\ 0 & otherwise \end{cases} \qquad 3.41$$

By integration of pdf we can evaluate the CDF as:

$$f(x) = \begin{cases} 0 & if \quad x < a \\ \dfrac{x-a}{b-a} & if \quad a \le x \le b \\ 1 & if \; x > b \end{cases} \tag{3.42}$$

Expected value of a uniform distribution is:

$$E[X] = \mu = \int_a^b x \, f_X(x) \, dx = \frac{b-a}{2} \tag{3.43}$$

Variance could be calculated using 3.27:

$$\sigma^2 = \frac{(b-a)^2}{12} \tag{3.44}$$

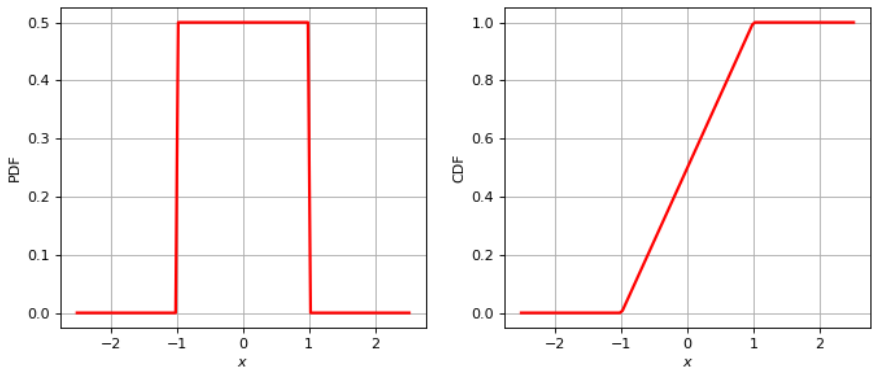

(a) (b)

Figure 18 Uniform distribution (a) pdf (b) CDF

3.5.4 UNIFORM DISTRIBUTION (DISCRETE)

The uniform distribution (discrete) is one of the simplest probability distributions in statistics. It is a discrete distribution, this means that it takes a finite set of possibilities.

The probability mass function for a uniform distribution taking one of n possible values from the set $A = \{x_1, \dots, x_n\}$ is:

$$f(x) = \begin{cases} \frac{1}{n} & if \quad x \in A \\ 0 & otherwise \end{cases} \tag{3.45}$$

The expected value in this case is calculated as:

$$E[X] = \sum_{i=1}^{n} x_i f(x_i) = \sum_{i=1}^{n} \frac{x_i}{n} = \frac{x1 + x_n}{2} \tag{3.46}$$

Variance of the distribution is:

$$\sigma^2 = \frac{(b - a + 1)^2 - 1}{12} \tag{3.47}$$

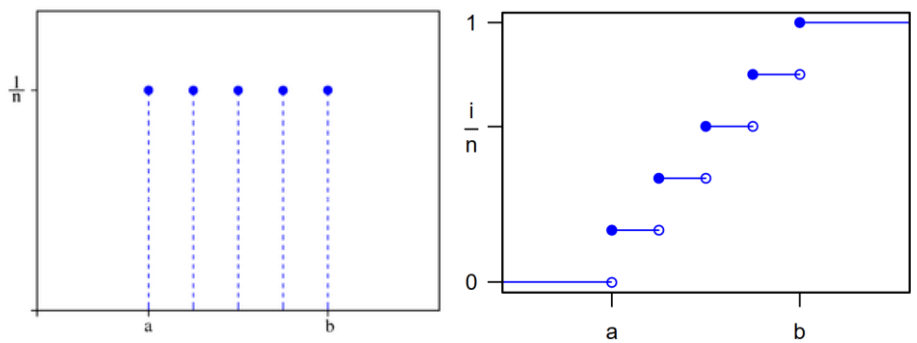

(a) (b)

Figure 19 Uniform distribution (a) pdf (b) CDF

3.5.5 NORMAL DISTRIBUTION

The normal distribution is the most widely known and used of all distributions. Because the normal distribution approximates many natural phenomena so well, it has developed into a standard of reference for many probability problems.

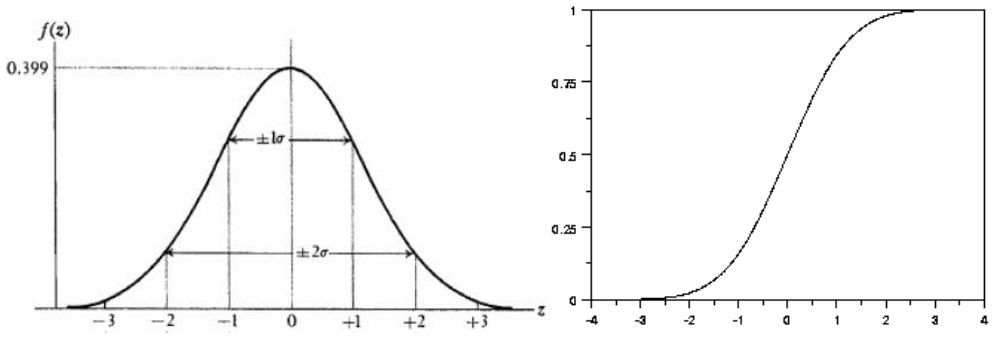

Figure 20 Normal distribution

The normal distribution is characterized by a symmetric bell-shaped pdf, it's a continuous distribution of probability and it's defined in $\mathbb{R}$. The distribution has two parameters μ and σ which determine the position respect to $x = 0$ and the "opening of the bell" respectively.

The pdf equation is:

$$f(x) = \frac{1}{\sqrt{2\pi\sigma^2}} e^{-\left(\frac{(x-\mu)^2}{2\,\sigma^2}\right)} \qquad 3.48$$

Regarding to cumulative distribution function (CDF) it is named with the notation:

$$\Phi(\mu, \sigma) = \int_{-\infty}^{+\infty} \frac{1}{\sqrt{2\pi\sigma^2}} e^{-\left(\frac{(x-\mu)^2}{2\,\sigma^2}\right)} dx \qquad 3.49$$

The integral 3.49 has not solution but it could be evaluated in numerical way.

The normal distribution is characterized by the equality through mean, median and mode coincident. The expected value and variance of Normal distribution are:

$$E[X] = \mu \tag{3.50}$$

$$Var[X] = \sigma^2 \tag{3.51}$$

About 2/3 of all cases fall within one standard deviation of the mean, that is

$$P(\mu - \sigma \leq X \leq \mu + \sigma) = 0.6826 \tag{3.52}$$

About 95% of cases lie within 2 standard deviations of the mean, that is

$$P(\mu - 2\sigma \leq X \leq \mu + 2\sigma) = 0.9544 \tag{3.53}$$

Many things actually are normally distributed, or very close to it. For instance, height and intelligence are approximately normally distributed; measurement errors also often have a normal distribution. The normal distribution is easy to work with mathematically. In many practical cases, the methods developed using normal theory work quite well even when the distribution is not normal. There is a very strong connection between the size of a sample N and the extent to which a sampling distribution approaches the normal form. Many sampling distributions based on large N can be approximated by the normal distribution even though the population distribution itself is definitely not normal.

3.5.6 LOG-NORMAL DISTRIBUTION

A random variable X is said to have the lognormal distribution with parameters $\mu \in \mathbb{R}$ and $\sigma > 0$ if ln(X) has the normal distribution with mean μ and standard deviation σ. Equivalently, $X = e^Y$ where Y is normally distributed withmean μ and standard deviation σ. The lognormal distribution is used to model continuous random quantities when the distribution is believed to be skewed, such as certain income and lifetime variables.

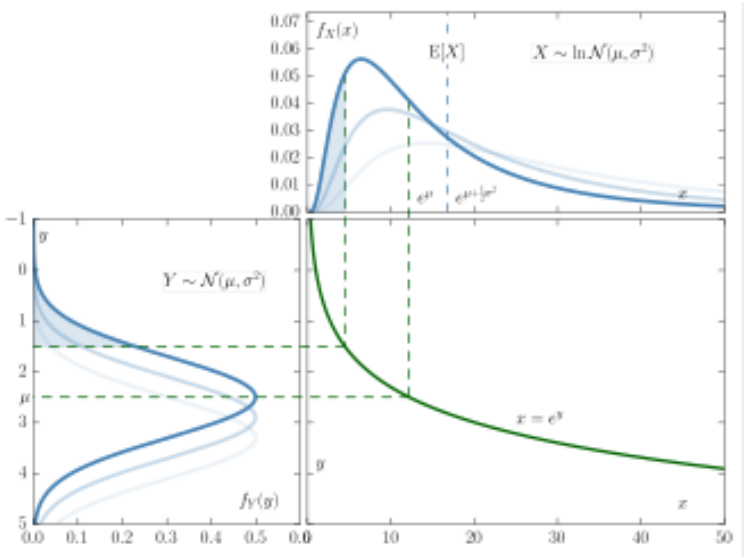

Figure 21 Transformation from Normal to Log-Normal distribution

Using the change of variables theorem to show that the probability density function of the lognormal distribution with parameters μ and σ is given by:

$$f(x) = \frac{1}{\sqrt{2\pi}\,\sigma\,x}\exp\left(-\frac{(\ln(x)-\mu)^2}{2\sigma^2}\right) \qquad 3.54$$

The lognormal distribution is defined in the domain in the domain $\mathbb{R}^+$ and in this case mean, median and mode aren't coincident. The expected value is:

$$E[X] = \exp(\mu + \frac{1}{2}\sigma^2) \qquad 3.55$$

$$Var[X] = \exp(\,2\,(\mu+\sigma^2)\,) - \exp\,(2\,\mu+\sigma^2) \qquad 3.56$$

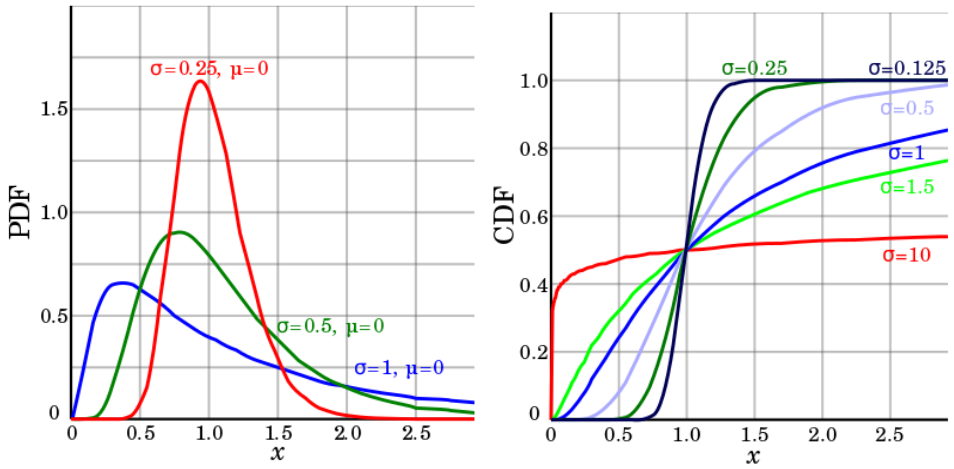

Figure 22 Lognormal pdf and CDF

3.5.7 BOLTZMANN DISTRIBUTION

The Boltzmann distribution law says that if the energy associated with some state or condition of a system is ε then the frequency with which that state or condition occurs, or the probability of its occurrence, is proportional to

$$e^{-\varepsilon/k\vartheta} \tag{3.57}$$

Where ϑ is the system's absolute temperature and k is the Boltzmann constant.

This distribution is used to evaluate the confidence in step solutions of the simulated annealing method, introduced in further chapters.

$$F(x) = e^{-\Delta E/k\vartheta} \tag{3.58}$$

3.6 Central Limit Theorem

n probability theory, the central limit theorem (CLT) establishes that, in some situations, when independent random variables are added, their properly normalized sum tends toward a normal distribution even if the original variables themselves are not normally distributed. The theorem is a key concept in probability theory because it implies that probabilistic and statistical methods that work for normal distributions can be applicable to many problems involving other types of distributions.

The central limit theorem has a simple proof using characteristic functions (D. S. Lemons, 2002). It is similar to the proof of the (weak) law of large numbers.

Assume $\{X_1, \ldots, X_n\}$ are independent and identically distributed random variables, each with mean μ and finite variance σ². The sum $X_1 + \ldots + X_n$ has mean nμ and variance nσ². Consider the random variable

$$Z_n = \frac{X_1 + \cdots + X_n - n\mu}{\sqrt{n\sigma^2}} = \sum_{i=1}^{n} \frac{X_i - \mu}{\sqrt{n\sigma^2}} = \sum_{i=1}^{n} \frac{Y_i}{\sqrt{n}} \qquad 3.59$$

where in the last step we defined the new random variables $Y_i = X_i - \mu/\sigma$, each with zero mean and unit variance (var(Y) = 1). The characteristic function of Z_n is given by

$$\varphi_{Z_n}(t) = \varphi_{Y_1}\left(\frac{t}{\sqrt{n}}\right)\varphi_{Y_2}\left(\frac{t}{\sqrt{n}}\right)\ldots\varphi_{Y_n}\left(\frac{t}{\sqrt{n}}\right) = \left[\varphi_{Y_1}\left(\frac{t}{\sqrt{n}}\right)\right]^n \qquad 3.60$$

where in the last step we used the fact that all of the Y_i are identically distributed. The characteristic function of Y_1 is, by Taylor's theorem,

$$\varphi_{Y_1}\left(\frac{t}{\sqrt{n}}\right) = 1 - \frac{t^2}{2n} + o\left(\frac{t^2}{n}\right), \qquad \frac{t}{\sqrt{n}} \to 0 \qquad 3.61$$

where $o\left(\frac{t^2}{n}\right)$ is "little o notation" for some function of t that goes to zero more rapidly than $\frac{t^2}{n}$. By the limit of the exponential function ($e^x = lim\left(1 + \frac{x}{n}\right)^n$), the characteristic function of Z_n equals

$$\varphi_{Y_1}\left(\frac{t}{\sqrt{n}}\right) = \left(1 - \frac{t^2}{2n} + o\left(\frac{t^2}{n}\right)\right)^n \quad \rightarrow \quad e^{-\frac{t^2}{2}}, \quad if \quad n \rightarrow \infty \qquad 3.62$$

All of the higher order terms vanish in the limit n → ∞. The right hand side equals the characteristic function of a standard normal distribution N(0,1), which implies through Lévy's continuity theorem that the distribution of Z_n will approach N(0,1) as n → ∞. Therefore, the sum $X_1 + \ ... + \ X_n$ will approach that of the normal distribution N(nμ,nσ²), and the sample average

$$S_n = \frac{X_1 + \ ... \ + \ X_n}{n} \qquad 3.63$$

converges to the normal distribution N(μ,σ²/n), from which the central limit theorem follows.

3.7 Monte Carlo Simulations

In case we want to study very complicated process or problem we can proceed through a statistical approach. If we generate suitable random numbers, thanks to law of large numbers, the sample tends to be distributed as the random variable. Numerical methods involving the repeated use of computer-generated pseudorandom numbers are often referred to as Monte Carlo methods, from the name of the city hosting the famous casino, which exploits the properties of random numbers to generate profit.

Monte Carlo method can be defined as a method that allows to estimating the value of an unknown quantity using the principles of inferential statistics.

Inferential statistics use a random sample of data taken from a population to describe and make inferences about the population. Inferential statistics are

valuable when examination of each member of an entire population is not convenient or possible.

The method is based on the idea that a random sample tends to exhibit the same properties as the population from which is drawn. For this reason, the sample procedure plays a central role in method's applications because if it isn't representative of the population method provide bad results. In further paragraphs will focus on the sampling procedure. A rather general-purpose and simple to implement method to generate random numbers according to a given PDF is the hit-or-miss Monte Carlo. It assumes we have a PDF defined in an interval $x \in [a, b[$, that is known as a function $f(x)$. We also assume that we know the maximum value m of f, or at least a value m that is greater or equal to the maximum of f (as you can see in Figure 23.

The method consists of first extracting a uniform random number x in the interval $[a, b[$, and then computing $f(x)$. Then, a random number r is extracted

uniformly in $[0, m[$. If $r > f$ ("miss") we repeat the extraction of x, until $r < f$ ("hit").

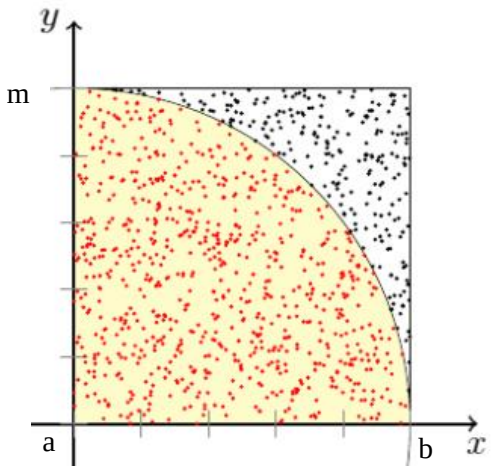

Figure 23 Hit-or-miss

In this case, we accept x as the desired extracted value. In this way, the probability distribution of the accepted x is our initial (normalized) PDF by construction. A possible inconvenient of this method is that it rejects a fraction of extractions equal to the ratio of area under the curve $f(x)$, and the area of the

rectangle that contains f. The method has an efficiency (i.e.: the fraction of accepted values of x) equal to:

$$\varepsilon = \frac{\int_a^b f(x)dx}{(b-a) \times m} \qquad 3.64$$

which may lead to a suboptimal use of the computing power, in particular if the shape of $f(x)$ is very peaked. Hit-or-miss Monte Carlo can also be applied to multi-dimensional cases. In those cases, one first extracts a multi-dimensional point $\vec{x} = (x_1, \dots, x_n)$, then accepts or rejects $\vec{x}$ according to a random extraction $r \in [0, m[$, compared with $f(x_1, \dots, x_n)$.

Different from a physical experiment, Monte Carlo simulation performs random sampling and conducts a large number of experiments on computer. Then the statistical characteristics of the experiments (model outputs) are observed, and conclusions on the model outputs are drawn based on the statistical experiments. In each experiment, the possible values of the input random variables $X = (X_1, \dots, X_n)$ are sampled according to their distributions. Then the values of the output variable Y are calculated through the performance function $Y = g(X)$ at the samples of input random variables. With a number of experiments carried out in this manner, a set of samples of output variable Y are available for the statistical analysis, which estimates the characteristics of the output variable Y.

The outline of Monte Carlo simulation is depicted in Figure 24. Three steps are required in the simulation process:

1. Step 1 – sampling on random input variables X;
2. Step 2 – evaluating model output Y;
3. Step 3 – statistical analysis on model output.

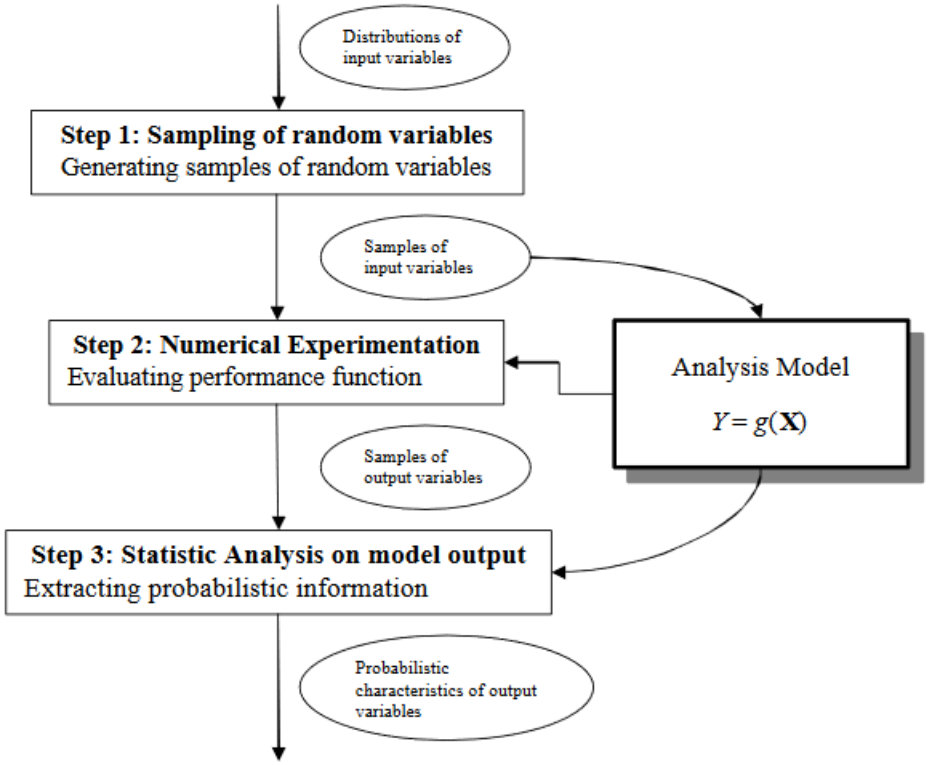

Figure 24 Monte Carlo Simulation

3.7.1 SAMPLING

Many computer applications, ranging from simulations to video games and 3Dgraphics application, take advantage of computer-generated numeric sequences having properties very similar to truly random variables. Sequences generated by computer algorithms through mathematical operations are not really random, having no intrinsic unpredictability, and are necessarily deterministic and reproducible. Indeed, it is often a good feature for many applications the possibility to reproduce exactly the same sequence of computer-generated

numbers given by a computer algorithm. Good algorithms that generate "random" numbers (pseudorandom numbers),

Monte Carlo simulation could be adopted to study also multivariate problems.

The purpose of sampling of input random variables $X = (X_1, \dots, X_n)$ is to generate samples that represent distributions of the input variable from CDF$F_{X_i}(x_i)$. The samples of the random variables will then be used as inputs to the simulation experiments. The generation of sample is composed by two steps: the first generate a uniform distributed sample and the second transform the generated numbers in the objective RV.

The importance of uniform numbers over the continuous range [0, 1] is that they can be transformed into real values that follow any distributions of interest. In the early times of simulation, random numbers were generated by mechanical ways, such as drawing balls, throwing dice, as the same way as many of today's lottery drawings. Now any modern computers have the capability to generate uniformly distributed random variables. Random variables generated this way are called pseudo random numbers.

To transform the samples of a uniform variable $Z = (z_1, \dots, z_n)$ into values of random variable $X = (x_1, \dots, x_n)$ follows a given distribution $F_X(x_i)$ there are several methods for such a transformation.

The simple and direct transformation is the inverse transformation method. By this method, the random variable is given by $x_i = F_{x_i}^{-1}(z_i)$.

3.7.2 LATIN HYPERCUBE SAMPLING

Sampling procedure is a fundamental part of the Monte Carlo Simulation. Unfortunately, the MC simulation has some contraindications. It could happen, especially in problems where a lot of RV are involved in the problem, that the number of sample's element need to be high, so much that have a representative sample requires resources not available. Moreover, if the sample isn't sufficiently representative unwanted correlations may arise between RV realization of the sample, in this case some strategies can be adopted like the Latin Hypercube Sampling (LHS) and the Simulated Annealing method (SA).

The LHS Sampling procedure could be used in MC simulation in order to obtain small number of realizations but preserving the quality of the samples.

Latin Hypercube Sampling is a form of simultaneous stratification for all variables. There are several alternative forms of LHS. In the Lattice Sampling (Patterson, 1954) the jth realization (of total N_{sim}) of i-th random variable X_i of the set of N_{var} variables is denoted $x_{i,j}$ and generated as:

$$x_{i,j} = F^{-1}\left(\frac{\pi_i(j) - 0.5}{N_{sim}}\right) \qquad 3.65$$

Where: $\pi_i(j)$ is a random permutation of jth realization and F_i^{-1} is the inverse of cumulative distribution function of the ith random variable.

If F_i is continuous, then each of the Nsim equiprobable subintervals j for X_i is represented by one value $x_{i,j}$. In the unbiased version, from McKay et al. ,the Latin Hypercube Sample is generated by replacing the number 0.5 in Eq. 3.65 by U_j^i, a standard uniformly distributed random variable, independent of the permutations π_i. This last technique in this document will be called LHS-random while that one used in 3.65 will be called LHS-mean.

This objection deals mainly with samples of the tails of PDF, which mostly influence the sample variance, skewness and kurtosis. This elementary simple approach has already been overcome by the sampling of interval mean values

$$x_{i,j} = N_{sim} \int_{\xi_{i,j-1}}^{\xi_{i,j}} x f_i(x) dx \qquad 3.66$$

Where f_i is the pdf of X_i, and $\xi_{i,j}$ are given by the equiprobable segmentation of $F^{-1}(j/N_{sim})$. With LHS-mean samples represent one dimensional marginal pdf better in terms of the distance of the point estimators from the exact statistics. By this way the mean value is evaluated exactly and estimated variance is much closer to that of the target. However, such an increase in computational effort is definitely worthwhile especially when N_{sim} is very small. Samples selected by both 3.65 3.66 are almost identical except for the values in the tails of pdf.

Therefore, one can use the more advanced scheme 3.66 only for the tails, considering the fact that tail samples mostly influence the estimated variance of the sample set. Generally, in all three cases, regularity of sampling (the range of distribution function is stratified) ensures good sampling and consequently good estimation of statistical parameters of response using a small number of simulations. In LHS stratification with proportional allocation never increases variance compared to crude Monte Carlo sampling, and can reduce it. The amount of variance reduction increases with the degree of additivity in the random quantities on which the function $g(X)$ depends.

The sampling scheme of any Monte Carlo type technique is represented by Table 3Table 3 LHS Sampling., where simulation numbers are in columns while rows are related to random variables (N_{var} is the number of input variables). Note that Table 1 can be obtained either by sampling from a parametric distribution or from a set of raw data, bounded or unbounded, continuous or discrete, empirical histogram, etc. The only requirement is that the sample size N_{sim} is identical for all sampled variables. From here on, we assume that the values representing each variable from Table 3 have already been selected, and that we want to pay attention to the correlation structure among the variables.

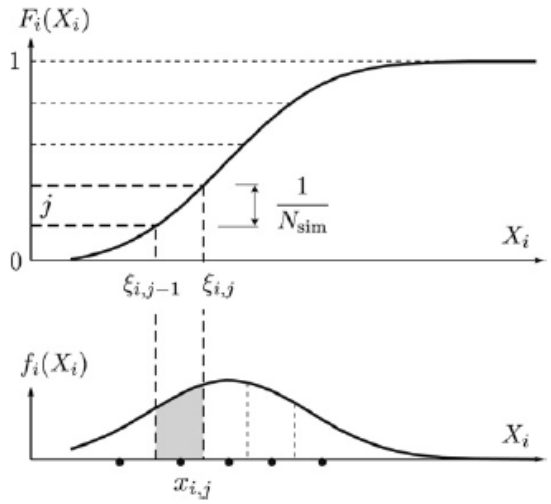

Figure 25 Sampling protocol LHS-mean

Sampling return as result a “table of values” that corresponds to the list of realizations of each variable X_i.

Var	Simulations			
	1	2		N_{Sim}
$\boldsymbol{X}_1$	$x_{1,1}$	$x_{1,2}$	…	$x_{1,N_{sim}}$
$\boldsymbol{X}_2$	$x_{2,1}$	$x_{2,2}$	…	…
…	…	…	…	…
…	…	…	…	…
$\boldsymbol{X}_{N_{var}}$	$x_{N_{var},1}$	…	…	$x_{N_{var},N_{Sim}}$

Table 3 LHS Sampling.

3.7.2.1 STATISTICAL CORRELATION

There are generally two problems related to LHS concerning statistical correlation: First, during sampling an undesired correlation can be introduced between random variables (rows of Table 3). It can be significant, especially in the case of a very small number of simulations, where the number of interval combinations is rather limited. The second task is to determine how to introduce prescribed statistical correlations between pairs of random variables defined by the target correlation matrix $\boldsymbol{C_X} \equiv \boldsymbol{T}$. The samples in each row of Table 3 should be rearranged in such a way as to fulfill the following two requirements: to diminish spurious random correlation, and to introduce the prescribed correlation given by T. Two widely used possibilities exist for the point estimation of correlation between two variables: the Pearson correlation coefficient (PCC) and the Spearman rank order correlation coefficient (SRCC). The PCC takes values between -1 and 1 and provides a measure of the strength of the linear relationship between two variables. For samples in the form of rows of Table 3, the sample PCC A_{ij} between two variables, say x_i and x_j, is defined by:

$$A_{ij} = \frac{\sum_{k=1}^{N_{sim}}(x_{i,k} - \overline{x_i})(x_{j,k} - \overline{x_j})}{\sqrt{\sum_{k=1}^{N_{sim}}\left(x_{i,k} - \overline{x_i}\right)^2 \sum_{k=1}^{N_{sim}}\left(x_{i,k} - \overline{x_i}\right)^2}} \qquad 3.67$$

Where $\bar{x}_i$ and $\bar{x}_j$ are the estimation of mean calculated from the realization of X_i and X_j respectively. The SRCC is defined similarly to the PCC but with rank-transformed data. Let us define a matrix $\boldsymbol{r}$ in which each row/column is filled with rank numbers corresponding to a matrix $\boldsymbol{x}$. Specifically, the smallest value $x_{i,j}$ of a variable i is given a rank $r_{i,j} = 1$; the next largest value is given a rank of 2; and so on up to the largest value, which is given a rank equal to sample size N_{sim}. In the event of ties, average ranks are assigned. Note that when LHS is applied to continuous parametric distributions no ties can occur in the generated data. The SRCC is then calculated in the same manner as the PCC except in the use of rank-transformed data. Specifically, $x_{i,j}$ must be replaced by rank number $r_{i,j}$ in 3.67. In the formula $\bar{x}_i$ simplifies to the average rank of $(N_{sim} + 1)/2$.

3.7.3 SIMULATED ANNEALING

In order to resolve the two problems introduced in the previous paragraph, we need to optimize the correlation matrix calculated as 3.67. Optimization means that we have to find a global minimum of a function. This particular problem of optimization could be very hard to resolve when there are a lot of variables that we have to take into account because a lot of algorithm of optimization tends to require much time or much resource, moreover a complex function could have several local minimum that it's like a trap for the algorithm.

The algorithm implemented in this document is named Simulated Annealing (SA) as it's implemented by Vorechovský et al, 2009.

The most widespread applications of the SA are on combinatorial problems, in particular on scheduling problems. All SA applications in the context of combinatorial problems show a remarkable efficiency of the method together with a robustness with respect to the type of problem, confirmed also in other mixed-whole combinatorial applications.

Simulated annealing (SA) is a random-search technique which exploits an analogy between the way in which a metal cools and freezes into a minimum energy crystalline structure (the annealing process) and the search for a minimum in a more general system; it forms the basis of an optimization technique for

combinatorial and other problems. Simulated annealing was developed in 1983 to deal with highly nonlinear problems 0. SA approaches the global maximization problem similarly to using a bouncing ball that can bounce over mountains from valley to valley. It begins at a high "temperature" which enables the ball to make very high bounces, which enables it to bounce over any mountain to access any valley, given enough bounces. As the temperature declines the ball cannot bounce so high, and it can also settle to become trapped in relatively small ranges of valleys. A generating distribution generates possible valleys or states to be explored. An acceptance distribution is also defined, which depends on the difference between the function value of the present generated valley to be explored and the last saved lowest valley. The acceptance distribution decides probabilistically whether to stay in a new lower valley or to bounce out of it. All the generating and acceptance distributions depend on the temperature. It has been proved that by carefully controlling the rate of cooling of the temperature, SA can find the global optimum. However, this requires infinite time. Fast annealing and very fast simulated re-annealing (VFSR) or adaptive simulated annealing (ASA) are each in turn exponentially faster and overcome this problem.

SA's major advantage over other methods is an ability to avoid becoming trapped in local minima. The algorithm employs a random search which not only accepts changes that decrease the objective function f (assuming a minimization problem), but also some changes that increase it. The latter are accepted with a probability

$$P(\Delta F) = e^{-\frac{\Delta F}{T}} \tag{3.68}$$

where ΔF is the increase in F and T is a control parameter, which by analogy with the original application is known as the system "temperature" irrespective of the objective function involved.

Referring to a system characterized by its energy E and its temperature T, SA algorithm can be schematized in following steps:

1. Given the initial configuration or the solution x^0 or the value of the objective function E_0, we calculate the initial temperature T_0.
2. For each temperature we need to repeat these steps:
    a. Generate an allowable candidate configuration through little random perturbation of the current configuration and evaluate the difference of energy ΔE between the two configurations;

b. If $\Delta E \leq 0$ the candidate configuration has a value of the objective function smaller then the current. In this case the candidate configuration become the new current configuration.

   If $\Delta E > 0$, the candidate configuration has higher energy than the current configuration. In this case the algorithm accepts the solution with a probability

$$P(\Delta \mathrm{E}) = e^{-\frac{\Delta \mathrm{E}}{k_B T}} \qquad 3.69$$

   Where k_B is the Boltzmann's constant; refresh the current configuration if it is necessary

c. If thermal equilibrium isn't achieved repeat go to 2.a else go to step 3;

3. If the annealing process is not complete reduce temperature and go to step 2.

Figure 26 show the procedure in a graphical way.

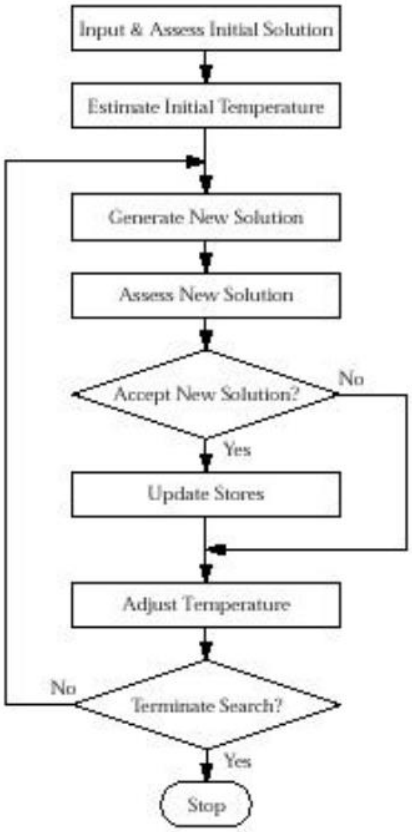

Figure 26 Simulated Annealing Algorithm

Initially, when the annealing temperature is high, some large increases in f are accepted and some areas far from the optimum are explored. As execution continues and T falls, fewer uphill excursions are tolerated (and those that are tolerated are of smaller magnitude). The last 40% of the run is spent searching around the optimum. This performance is typical of the SA algorithm.

Simulated annealing can deal with highly nonlinear models, chaotic and noisy data and many constraints. It is a robust and general technique. Its main advantages over other local search methods are its flexibility and its ability to approach global optimality. The algorithm is quite versatile since it does not rely on any restrictive properties of the model. For any reasonably difficult nonlinear or stochastic system, a given optimization algorithm can be tuned to enhance its performance and since it takes time and effort to become familiar with a given

code, the ability to tune a given algorithm for use in more than one problem should be considered an important feature of an algorithm.

Since SA is a metaheuristic, a lot of choices are required to turn it into an actual algorithm. There is a clear tradeoff between the quality of the solutions and the time required to compute them. The tailoring work required to account for different classes of constraints and to fine-tune the parameters of the algorithm can be rather delicate. The precision of the numbers used in implementation is of SA can have a significant effect upon the quality of the outcome.

3.8 Regression Models

In science and engineering, the data obtained from experiments usually contain a significant amount of random noise due to measurement errors. The purpose of curve fitting is to find a smooth curve that one average, fits data points. This curve should have a simple form with a low-order polynomial, so it does not reproduce the random errors.

Abstracting the reasoning curve fitting could be applied to data that contain noise and, in any cases, where there is a high non linearity of results and a simplified model is needed to predict results. Curve fitting methods in this work will be used to do regression on dataset, in order to build a regression model. Regression is a measure of the relation between the mean value of one variable (e.g. output) and corresponding values of other variables.

3.8.1 LEAST SQUARES FIT

The most popular curve fitting technique is the least squares method, which is usually used to solve overdetermined systems. It is often applied in statistics, particularly in regression analysis. The best fit, in the least squares sense, is the instance of the model in which the sum of squared residuals has the least value.

Suppose that a given data set consists of n data points (x_i, y_i) ,where the i vary in the interval $0, .., n-1$ and x_i and y_i are the independent variable and the dependent variable respectively. The model function can be defined as

$$f(x; \alpha) = f(x; a_0, \dots, a_m) \qquad 3.70$$

This function is to be fitted to the data set with $n + 1$ data points. The above model function contains $m + 1$ variable parameters $a_0, \dots, a_m$ where $m < n$. The purpose is to find the value of $a_0, \dots, a_m$ such that the model (determined beforehand) best fits data.

The last squares method minimizes the sum of squared residuals. Residuals are the difference between the value of y_i and the value obtained by calculating the model function in the point x_i:

$$r_i = y_i - f(x_i; \alpha) \tag{3.71}$$

Sum of squared residuals is:

$$S(\alpha) = \sum_{i=0}^{n} r_i^2 \tag{3.72}$$

Therefore, the optimal values of the parameters are obtained by the condition of minimum:

$$\frac{\partial S(\alpha)}{\partial a_i} = 2 \sum_{i=0}^{n} r_i \frac{\partial r_i}{\partial a_i} = -2 \sum_{i=0}^{n} r_i \frac{\partial f(x_i; \alpha)}{\partial a_i} = 0 \tag{3.73}$$

These gradient equations are generally nonlinear in a_i and may be difficult to solve. These gradient equations could be applied to all least square problems.

3.8.2 LINEAR REGRESSION

Considering the least squares fit 3.72 of the linear form, sum of residuals is given by:

$$S(\alpha) = \sum_{i=0}^{n} \left[y_i - \sum_{j=0}^{m} a_j f_j(x_i) \right] \qquad 3.74$$

The corresponding gradient equation 3.73 can be reduced to:

$$\sum_{j=0}^{m} \sum_{i=0}^{n} f_j(x_i) f_k(x_i) a_j = \sum_{i=0}^{n} f_k(x_i) y_i \qquad 3.75$$

With $k = 0, \dots, m$. The equation 3.75 can be written in a matrix form:

$$A\alpha = \beta \qquad 3.76$$

$$A_{jk} = \sum_{i=0}^{n} f_j(x_i) f_k(x_i), \qquad \beta = \sum_{i=0}^{n} f_k(x_i) y_i \qquad 3.77$$

Resolving the system 3.76 the coefficients of regression could be obtained.

3.8.3 ADVANCED REGRESSION MODEL

In further chapter, data which come from numerical experimentation exploited to build a regression model with Bayesian updating as proposed by Gardoni et al., 2002. In this section the background framework is explained.

The main purpose of a model is to predict results given deterministic or random values of the variables $\boldsymbol{x}$ and it is said "univariate" when the quantity that the model predict is one. The univariate capacity model has the general form:

$$C = C(\boldsymbol{x}, \boldsymbol{\Theta}) \qquad 3.78$$

where **x** is a vector of material and geometric properties, $\boldsymbol{\Theta} = (\boldsymbol{\theta}, \boldsymbol{\lambda}, \sigma)$ is the set of unknown model parameters to fit data with the C model. In this work the function $C(\boldsymbol{x}, \boldsymbol{\Theta})$ has an algebraic form but it can be also a differential or integral form. Adopting the general univariate model form:

$$C(\boldsymbol{x}, \boldsymbol{\Theta}) = \hat{c}(\boldsymbol{x}) + \gamma(\boldsymbol{x}, \boldsymbol{\Theta}) + \sigma\varepsilon \qquad 3.79$$

Where $\boldsymbol{\Theta} = (\boldsymbol{\theta}, \sigma)$, $\boldsymbol{\theta} = (\theta_1, \theta_2, \dots)$, denotes the set of unknow model parameters, $\hat{c}(\boldsymbol{x})$ is the deterministic model, $\gamma(\boldsymbol{x}, \boldsymbol{\Theta})$ is the correction term for the bias inherent in the deterministic model that is expressed as a function of the variables $\boldsymbol{x}$ and parameters $\boldsymbol{\theta}$, ε is the random variable with zero mean and unit variance, and σ represents the standard deviation of the model error. With this assumption for a given $\boldsymbol{x}$, $\boldsymbol{\theta}$ and σ the variance of the model has the value $Var[\, C(\boldsymbol{x}, \boldsymbol{\Theta})] = \sigma^2$. Regarding the correction term, since deterministic model involves approximations, the true form of $\gamma(\boldsymbol{x}, \boldsymbol{\Theta})$ is unknown. In order to explore the source of bias in the deterministic model, a suitable set of "explanatory functions" $h_i(\boldsymbol{x})$ was selected, so the bias correction term has the form:

$$\gamma(\boldsymbol{x}, \boldsymbol{\Theta}) = \sum_{i=1}^{p} h_i(\boldsymbol{x}) \qquad 3.80$$

By examining the posterior statistics of the unknown parameters θ_i , we are able to identify those explanatory functions that are significant in describing the bias in the deterministic model. Note that, while the bias correction term is linear in the parameters θ_i , it is not necessarily linear in the basic variables $\boldsymbol{x}$.

The models are formulated and calibrated under three assumptions: 1) σ is independent of **x** (homoskedasticity assumption), 2) ε follows the normal distribution (normality assumption), and 3) the model error can be added to the model (additive assumption.) Since generally these three assumptions are not satisfied, we use a variance stabilizing transformation to approximately satisfy these assumptions within the range of the data. The vector of parameter **λ** is used to define the variance stabilizing transformation within a family of possible

transformations. For example, one can use the family of dual power transformation proposed by Yang, 2006:

$$f_\lambda(\cdot) = \begin{cases} \dfrac{(\cdot)^\lambda - (\cdot)^{-\lambda}}{2\lambda} & if \quad \lambda \neq 0 \\ ln(\cdot) & if \quad \lambda = 0 \end{cases} \tag{3.81}$$

whose inverse is

$$f_\lambda^{-1}(\cdot) = \begin{cases} \left(\lambda(\cdot) + \sqrt{1 + \lambda^2(\cdot)^2}\right)^{\frac{1}{\lambda}} & if \quad \lambda \neq 0 \\ e^{(\cdot)} & if \quad \lambda = 0 \end{cases} \tag{3.82}$$

Such functions show properties similar to the well-known Box and Cox (1964) power transformation, but without the long-standing truncation problem. In this paper it is used $\boldsymbol{\lambda} = \lambda = 0$.

In assessing a model, or in using a model for prediction purposes, one has to deal with two broad types of uncertainties: aleatory uncertainties (also known as inherent variability or randomness) and epistemic uncertainties. The former is those that are inherent in nature; they cannot be influenced by the observer. The epistemic uncertainties arise from lack of knowledge, the deliberate choice to simplify matters, from errors in measuring observations, and from the finite size of observation samples. This kind of uncertainty is present in the model parameters $\boldsymbol{\Theta}$ and in the error term ε. The fundamental difference between the two types of uncertainties is that, whereas aleatory uncertainties are irreducible, epistemic uncertainties are reducible.

There are three specific types of uncertainties that affects capacity models:

- **Model Inexactness**: This type of uncertainty arises when approximations are introduced in the derivation of the deterministic model. It has two essential components: not sufficiently refined model (i.e. Linear model in high non-linear problem), and missing variables. While the correction term $\gamma(\boldsymbol{x}, \boldsymbol{\Theta})$ provides a correction to the form of the deterministic model, the error term $\sigma\varepsilon$ represents the influence of the missing variables as well as that of the remaining error due to the inexact model form. However, after correction of the model form with the term $\gamma(\boldsymbol{x}, \boldsymbol{\Theta})$, one can usually

assume that most of the uncertainty inherent in ε is of aleatory nature. The coefficient σ represents the standard deviation of the model error arising from model inexactness.

- **Measurement Error**: In next chapter, model's parameters are assessed by use of a sample of observations C_i of the dependent variable for observed values x_i of the independent variables. Observed values, could be inexact due to errors in the measurement devices or procedures. To model these errors, it was assumed that $C_i = \hat{C}_i + e_{C_i}$ and $x_i = \hat{x}_i + e_{x_i}$ be the true values for the i-th observation, where $\hat{C}_i$ and $\hat{x}_i$ are the measured values and e_{C_i} and e_{x_i} are the respective measurement errors. The statistics of the measurement errors are usually obtained through calibration of measurement devices and procedures. The mean values of these errors coincide with the systematic error, and the variances represent the uncertainties inherent in the measurements. Due to central limit theorem, in most cases the random variables e_{C_i} and e_{x_i} can be assumed to be statistically independent and normally distributed. The uncertainty arising from measurement errors is epistemic in nature, since improving the measurement devices or procedures can reduce it.
- **Statistical Uncertainty**: The accuracy of estimation of the model parameters $\boldsymbol{\Theta}$ depends on the observation sample size n. The smaller the sample size, the larger the uncertainty in the estimated values of the parameters. This uncertainty can be measured in terms of the estimated variances of the parameter. Statistical uncertainty is epistemic in nature, as it can be reduced by further collection of data.

3.8.3.1 BAYESIAN UPDATING

In a Bayesian approach, the unknown model parameters are estimated through the following the updating rule:

$$p(\boldsymbol{\Theta}|\boldsymbol{y}) = \kappa L(\boldsymbol{\Theta}|\boldsymbol{y}) p(\boldsymbol{\Theta}) \qquad 3.83$$

where $p(\boldsymbol{\Theta}|\boldsymbol{y})$ is the posterior distribution that reflects the updated state of information about Θ, $L(\boldsymbol{\Theta}|\boldsymbol{y})$ is the likelihood function which captures the

information from the data vector of n observations $\boldsymbol{y}' = (y_1, y_2, \ldots, y_n)$, $p(\boldsymbol{\Theta})$ is the prior distribution which represents the information available before collecting the data, and $\kappa = [\int L(\boldsymbol{\Theta}|\boldsymbol{y})p(\boldsymbol{\Theta})d\boldsymbol{\Theta}]^{-1}$ is the normalizing factor. More specifically, the likelihood function is proportional to the probability of seeing the data. Gardoni et al. (2002a) gives a general formulation of the likelihood function that considers different types of data (i.e., equality data - when the quantity of interest is measured, and lower-/upper- bound data - when a smaller or larger value is measured).

Computation of these posterior statistics can be challenging, especially when a large number of parameters is to be determined. Following Gardoni et al. (2002b), an importance sampling algorithm can be successfully used to compute a common integral I which provides the desired posterior statistics. Such integral can be expressed in the general form

$$I = \int B(\boldsymbol{\Theta}) d\,\boldsymbol{\Theta} \tag{3.84}$$

where the integrand is $B(\boldsymbol{\Theta}) = w(\boldsymbol{\Theta})L(\boldsymbol{\Theta})p(\boldsymbol{\Theta})$. If $w(\boldsymbol{\Theta}) = 1$ is selected we obtain $I = 1/\kappa$. If $w(\boldsymbol{\Theta}) = \kappa\boldsymbol{\Theta}$ is selected we have the mean $I = \boldsymbol{M_\Theta}$, and finally if $w(\boldsymbol{\Theta}) = \kappa\boldsymbol{\Theta}\boldsymbol{\Theta}'$, then $I = E[\boldsymbol{\Theta}\boldsymbol{\Theta}']$, from which we can determine the covariance matrix $\boldsymbol{\Sigma_{\Theta\Theta}} = E[\boldsymbol{\Theta}\boldsymbol{\Theta}'] - \boldsymbol{M_\Theta}\boldsymbol{M_\Theta'}$. By using an importance sampling density $S(\boldsymbol{\Theta})$, the Bayesian integrand can be modified as

$$I = \int \left[\frac{B(\boldsymbol{\Theta})}{S(\boldsymbol{\Theta})}\right] S(\boldsymbol{\Theta}) d\,\boldsymbol{\Theta} \tag{3.85}$$

Considering N total random realizations, we have the estimation

$$\bar{I} = \frac{1}{N}\sum_{i=1}^{N} \frac{B(\boldsymbol{\Theta}_i)}{S(\boldsymbol{\Theta}_i)} \tag{3.86}$$

As a termination criterion, we set that the maximum coefficient of variation (COV), given by

$$\mathrm{COV}\left(\frac{\boldsymbol{\Theta}}{\kappa}\right) = \\ = \frac{\sqrt{\frac{1}{N}\sum_{i=1}^{N}[\boldsymbol{\Theta}_i L(\boldsymbol{\Theta}_i)p(\boldsymbol{\Theta}_i)/S(\boldsymbol{\Theta}_i)]^2 - \left\{\frac{1}{N}\sum_{i=1}^{N}[\boldsymbol{\Theta}_i L(\boldsymbol{\Theta}_i)p(\boldsymbol{\Theta}_i)/S(\boldsymbol{\Theta}_i)]\right\}^2}}{\frac{1}{N}\sum_{i=1}^{N}[\boldsymbol{\Theta}_i L(\boldsymbol{\Theta}_i)p(\boldsymbol{\Theta}_i)/S(\boldsymbol{\Theta}_i)]} \tag{3.87}$$

be sufficiently small (e.g., less than 0.05).

3.8.3.2 MULTIPLE BAYESIAN UPDATING

In addition, the updating rule can be used to continuously update the current knowledge every time new data become available. For example, if an initial sample of observations $\boldsymbol{y}_1$ is originally available, a first application of the updating rule gives

$$p(\boldsymbol{\Theta}|\boldsymbol{y}_1) = \kappa_1 L(\boldsymbol{\Theta}|\boldsymbol{y}_1)p(\boldsymbol{\Theta}) \tag{3.88}$$

where κ_1 is the normalizing factor for the first updating. If a second sample of observations $\mathbf{y}_2$, distributed independently from the first one, becomes available, $p(\boldsymbol{\Theta}|\mathbf{y}_1)$ can be updated to account for the new information obtaining

$$\begin{aligned} p(\boldsymbol{\Theta}|\boldsymbol{y}_1, \boldsymbol{y}_2) &= \kappa_2 L(\boldsymbol{\Theta}|\boldsymbol{y}_2)p(\boldsymbol{\Theta}|\boldsymbol{y}_1) \\ &= \kappa_2 L(\boldsymbol{\Theta}|\boldsymbol{y}_1)L(\boldsymbol{\Theta}|\boldsymbol{y}_2)p(\boldsymbol{\Theta}) \end{aligned} \tag{3.89}$$

in which κ_2 is the normalizing factor for the second updating.

Eq. 3.84 is of the same form as Eq. 3.85(i.e., the posterior distribution of Θ given $\mathbf{y}_1$ works as the prior distribution for the second sample). Such updating process can be carried out any number of times, obtaining the following general form for n_q sets of samples

$$p\left(\boldsymbol{\Theta}|\boldsymbol{y}_1,\ldots,\boldsymbol{y}_{n_q}\right)=\kappa_{n_q}\left[\prod_{q=1}^{n_q}L\left(\boldsymbol{\Theta}|\boldsymbol{y}_q\right)\right]p(\boldsymbol{\Theta})$$
$$=\kappa_{n_q}L\left(\boldsymbol{\Theta}|\boldsymbol{y}_{n_q}\right)p\left(\boldsymbol{\Theta}|\boldsymbol{y}_1,\ldots,\boldsymbol{y}_{n_q-1}\right), \quad 3.90$$

where $\kappa_{n_q}=\left\{\int\left[\prod_{q=1}^{n_q}L\left(\boldsymbol{\Theta}|\mathbf{y}_q\right)\right]p(\boldsymbol{\Theta})d\boldsymbol{\Theta}\right\}^{-1}$ is the normalizing factor associated to the nq−th updating.

Chapter 4

4 Probabilistic study

As described in the previous chapters, to investigate the behaviour of the structure in fire a fire analysis and a thermo mechanical analysis are needed. In order to analyse the structural behaviour by a stochastic point of view It has been chosen to use a two-zone model for the Gas Temperature analysis and a modified Timoshenko's model characterized with a thermo-mechanical analysis of beam and column's cross-section.

In order to perform a large number of analysis a computer program was developed. The software accepts in input the results of sampling procedure and for each sample it makes up three models: one for fire analysis, one fore thermal analysis and one for structural analysis in fire condition.

In this chapter it will be shown the methodology implemented to build the model generated automatically starting from the Latin Hypercube Sampling in the Monte Carlo simulation and general assumptions at the base of the study.

In the modelling phase was assumed that the resistance of whole structure depends only from phenomena that happens on the floor involved in fire.

Eurocode suggest a simplified safety check to verify global instability of the frame. Safety check is based on the calculation of the factor α_{cr} for each floor of the structure. Factor α_{cr} is defined as the multiplier of loads for which the structure fail due to floor instability. As Reported in Eurocode 3:

$$\alpha_{cr} = \frac{H_{ed}}{V_{ed}} \cdot \frac{h}{\delta_{H\,ed}}$$

where: H_{ed} and V_{ed} are the horizontal load and the vertical load respectively, h is the storey height and $\delta_{H_{ed}}$is the horizontal displacement at the top of the storey, relative to the bottom of the storey, when the frame is loaded with horizontal loads . Note that in this formula all quantities are relative to only the floor object of the analysis.

In proposed approach, the modelled substructures take into account the axial loads induced from the superior part of the frame and the boundary condition at the top of the columns allows only the vertical displacements, so the floor can be affected by instability. In fire condition, α_{cr} at the floor involved in fire reduces more than at the other floors. Therefore, the model used for the regression model takes into account global instability of the frame, even if not explicitly.

Finally, as reported in bibliography (Franssen et al. 2005), structural analysis conducted on substructures gives result not much different from analysis of entire structure.

For these reason we can say that regression model that will be developed takes into account global instability of the frame.

Note that since the substructure considered take into account only one floor, upper levels of structure are modelled replacing the equivalent load transmitted by columns. A study on the structural robustness conducted by Gernay et al. 2018 highlight the possibility of structure to redistribute the load through other structural members in some cases. In other words in case of collapse of a columns the structure can redistribute loads like an arc. Modelled substructures aren't able to show this behaviour because upper level's structural elements didn't taken into account, so we aren't able to consider the redistribution of stresses through the remaining part of the structure.

This study is focused on the structural behaviour in fire intended as behaviour of the structural system exposed to several fire scenarios, mechanical and thermal properties of steel was assumed as a deterministic function of temperature, so statistical fluctuation of the value associated to the specific heat, conductivity, and mechanical properties weren't investigated (see 4.2).

Uncoupled thermomechanical analysis was performed using the beam finite element implemented in Safir with no geometrical imperfections. Due to this type of analysis, results are reliable only for section of class 1 and 2.

Moreover, It was decided to model structure as unprotected, in order to study the behaviour of the naked structure. It should be said that protection to thermal action shouldn't have an high influence on the value of critical temperature because the protective layer (i.e. intumescent coating) reduces drastically heat fluxes that enter in steel member. Protection layer influence the critical temperature regarding to the thermal distortions. Due to low modulus of the heat fluxes that enters in steel members, temperature is generally more uniform than the case of the unprotected structures, this means that in a protected structure we should have a lower thermal bending action so a less stressed structure, but this gain in terms of bending moment tends to be recovered from the increasing of axial force. For this reason we can estimate that critical temperature is generally higher than critical temperature in the unprotected structure, or at least similar. This assumption should be verified in further developments.

Finally it is very relevant to highlight that the joint and boundaries of the considered substructures are assumed as perfect. This means that the connection between beams and columns needs to be checked a posteriori in order to guarantee connection resistance, that heavy influences the growing of catenary actions.

4.1 Analysis Generator and Analysis Launcher

An in-house software was developed using C# programming language to handle all that concern the analysis management. The software named AGL manages manage principally the phase of generation of input file to be analysed and run automatically analysis in order to exploit all computing resources. In following image there is reported the flow chard elaborated during the design phase of the software used to store data and organize analyses.

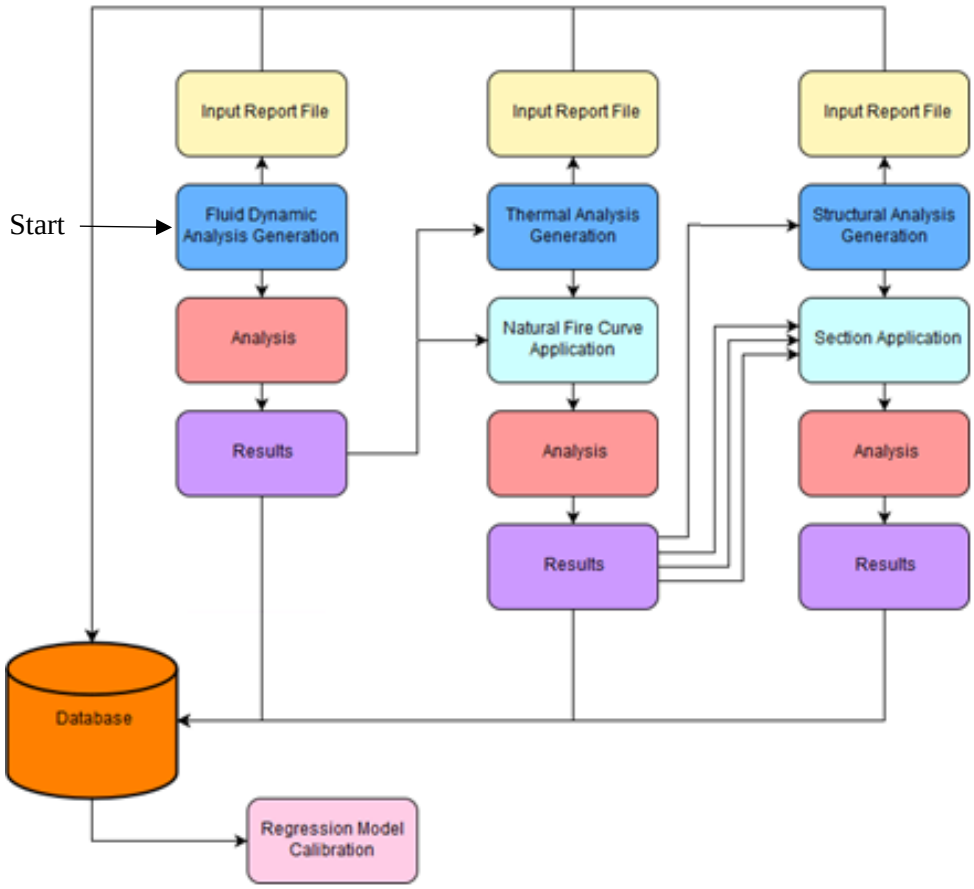

Figure 27 Flow chart.

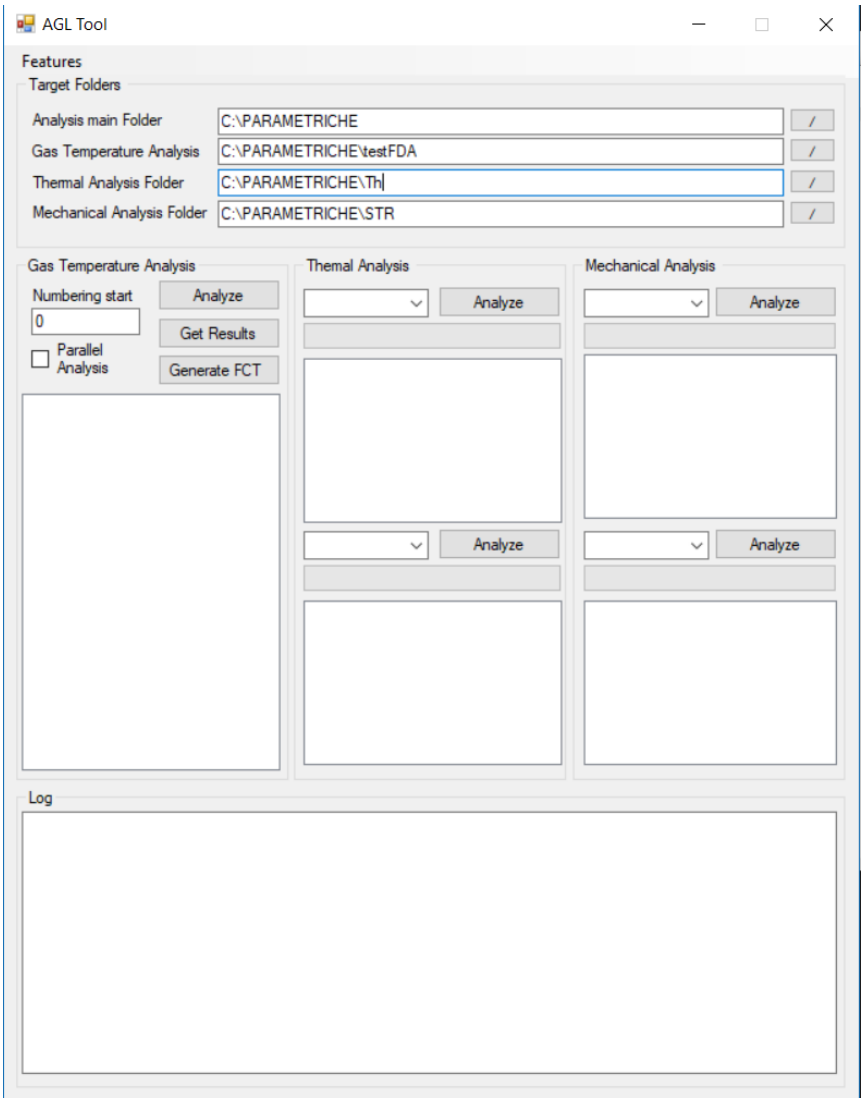

Figure 28 AGL start screen.

In Figure 28 you can see the start screen of AGL. Software has a User Interface (UI) is very simple because it is divided in zones. Start Screen is characterized by four blocks, one dedicated to folder management and the other three are dedicated to analysis management. The folders block Manage the destination folder of analyses; Safir Software (Frannsen et al, 2000) work through a series of input files related to a task of analysis, indeed for a 2D analysis of structures subjected to natural fire it was needed an input file for structural analysis, an input file for thermal analysis and the file that contains the gas temperature data. In order to

organize input and output files, the user must choose the principal folder, fluid dynamic analysis folder (FDA Folder), the thermal analysis folder (TA folder) and the mechanical analysis folder (MA folder).

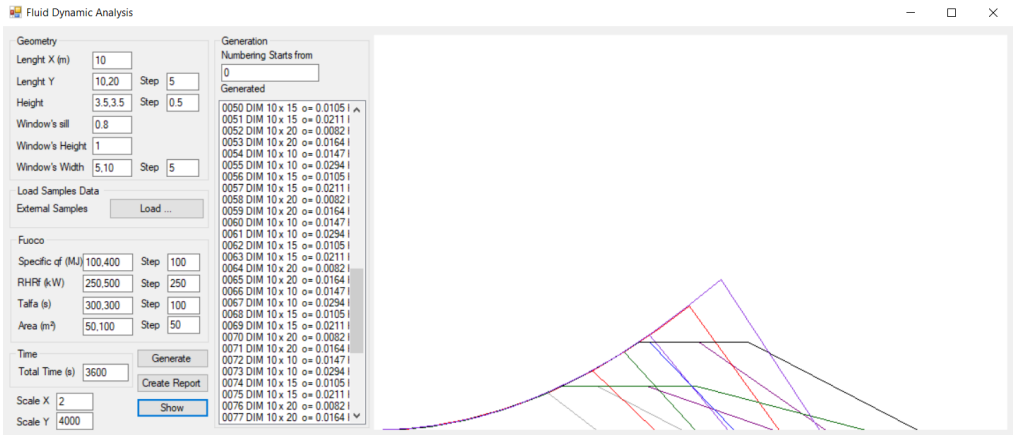

Figure 29 Fluid Dynamic Analysis Form.

Once the organization of folders is defined from a menu the user can start to build input files of FDA (Figure 29 and Figure 30). The user can parametrically build the input files of FDA, varying with a predefined step the characteristic of analysis or use data that come from an external numerical experimentation (simple MCS, LHS-MCS, etc.). In this form the user allows a fast checking of input files through the report file generation and the drawing feature that print input RHR curves on the screen.

After the definition of input files, the FDA can be performed in order to evaluate the gas temperature data. It can be done in the principal form (Figure 28) in two ways: a single thread analysis, where the software perform one by one the FDA, or a multiple thread analysis where the software exploit al computing resource and manage the queue of analysis in automatic. In the same place the user can extract the gas temperature data from output file of each analysis and record results in a report file. In this phase it can be written the files that contains gas temperature data used in thermal analysis (named FCT Files).

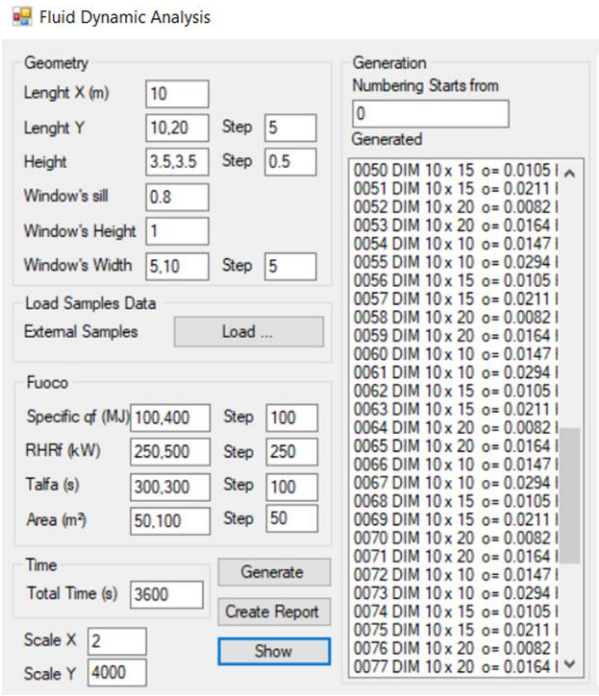

Figure 30 Fluid Dynamic Analysis Parameters.

Thermal analysis input file contains geometry of the cross section, the exposure mode the possible reference to the and thermal properties of materials. Also in this case, with the Thermal Analysis Form (Figure 31), the input file can be generated in a parametric way thanks to the mesher module included in AGL or it can be generated starting from external data. The mesher included in the TA form allows to define a group of section to mesh starting from data of section lists memorized in the program. Once the user chooses the time Domain and the exposure condition of the section, it is possible to add this to the mesh queue. The second part of the TA form is dedicated to the analysis option. After the first step that consist in the mesh mesh of the section the user can choose to perform thermal analysis with the standard ISO-834 curve or replace it with natural fire curves generated in the FDA. The section mesher can be used also to create input file needed for 3D Analysis in Safir (TOR files). The thermal analysis model allows to build a report file with section properties.

As concern the external data loading, if the user uses this function the program asks to select a file that contains all results of the sampling. In this case

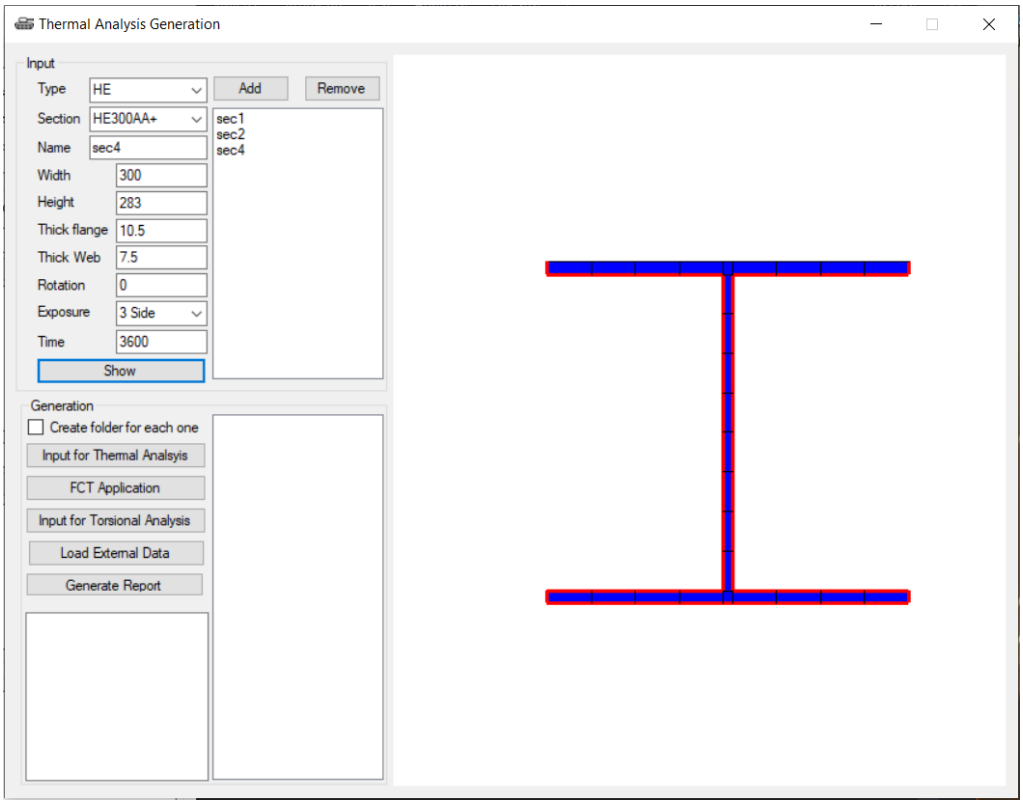

Figure 31 Thermal Analysis Form.

Once thermal analysis input files are defined, thermal analysis can be performed in the principal form (Figure 28), using the TA block. In this case TA can be performed in single thread or in double thread. TA results should be copied in the MA folder.

AGL has a built-in automatic mesher for MA analysis which allows to make input files for mechanical analysis of a single beam or portals in parametric way. Using this tool (Figure 32) the user could characterize behavior of a single beam with yielding constraints, portals and create report files.

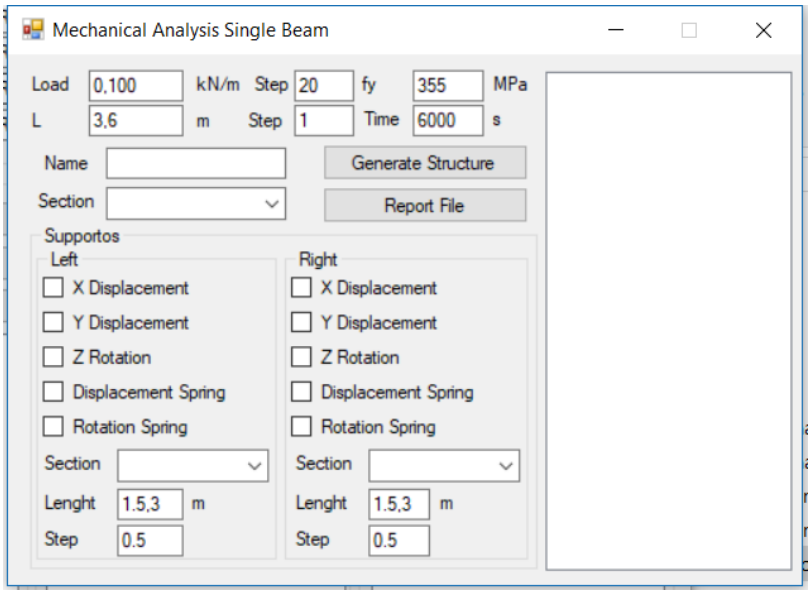

Figure 32 Structural Analysis Form.

Even for MA analysis the user can import external data to characterize more complex structures, but in this case the structures are automatically created when the user import external data for thermal analysis. When the user imports external data the mesher build structures meshes a report file which contain four principal nodes (recorders) that will be used to monitor stresses and displacements. Structural analysis can be managed in the main form in single or double thread like thermal analysis.

Finally, the user can read results and build the database of results through the data mining form. In this section of the program the user can choose data to extract from the output files of MA. The function Get Results automatically compute the section temperatures and identifies, if they exist, the collapse temperature, the collapse time and seek the section collapsed. Moreover, this function merges up all report files written in previous phases. Time History function read all output files and extract results of analysis for each timestep using the recorders saved during the structural mesh phase. Using the Time history function the software create a group of report files that contains internal stresses vs time in points of structure defined in recorder file. It is possible to extract The Axial force, the bending moment and the shear within column and beams.

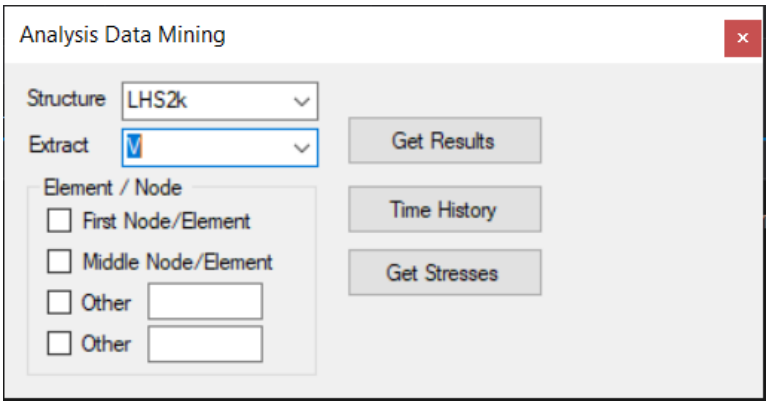

Figure 33 Data Mining Form.

All structures and sections was meshed automatically through the AGL meshing tool. As concern cross sections, meshes was created by dividing in 9 elements the flange and 8 elements the wick of the section. Even meshes of substructures was created automatically using an approximative size of 40 centimetres.

4.2 Parameter's definition

A lot of parameters could have influence on behaviour of structures in fire because the structural response is influenced by temperature dependent mechanical parameters which in turn vary in function of fluid-dynamic parameters. In this section will be presented the parameters taken into account to generate samples.

In order to build the model used in MC Simulation a set of thirteen parameters have been taken into account in LHS Sampling. It was identified four groups: Fluid dynamic, Geometric, mechanics and fire scenarios.

- Fluid Dynamic Parameters (five):
    - A_f Floor's Area of the compartment;
    - A_v/A_f Ratio between Vent's area and floor's area;
    - RHR_f the maximum heat release rate per unit area;
    - q_f the specific fire load;

    - t_α the growth rate parameter of the fire;
- Geometrical Parameters (four):
    - h the height of columns;
    - L the length of beams;
    - n_b a parameter that indicate the size of beam's section;
    - I_c/I_b the ratio between the Column's Inertia and the beam's inertia.
- Mechanical Parameters (three):
    - f_y the tensile strength of the steel (S235, S275, S355);
    - μ_L a parameter that indicates the load level of the beam;
    - μ_N a parameter that indicates the load level of the column.
- Fire Scenario (one):
    - IB index of building, univocally determinate the number of bays of the substructure, number of bays exposed and place of fire.

The set of variables used to describe the problem was selected thinking at the principal factors that influences the fire model, fire scenarios, geometry of the structure and load conditions.

Since the work is focused on the investigation of fire's effects in complex structures through a probabilistic approach, steel's thermomechanical properties have been considerd as fixed in the experimental design. For future application of the probabilistic regressive model in reliability problems (e.g. determination of fragility curves), thermo-mechanical properties of steel, such as the functional shapes of Conductivity, specific heat, mechanical decay and stiffness decay functions, might be assumed as random variables ("Fire fragility curves for steel buildings in a community context: A methodology" T. Gernay et al. Engineering Structures 113 (2016) 259–276 . "Probabilistic fire analysis: material models and evaluation of steel structural members." N Elhami Khorasani et al. J Struct Eng ASCE 2015).

Regarding fire model, they was selected the parameters that influence the RHR. As concern the structural geometry and fire scenarios, since the work is focused on the behaviour of steel structures in fire condition they were selected as parameters the length of beam and columns and other two parameters that

allows to design the structure: I_c/I_b, and n_b. Indeed while the parameter n_b identify the beam's cross section the other one (I_c/I_b,)allows to design a compatible column in order to assess a structural geometry representative of real cases. Moreover, the fire scenario's index (IB) define two characteristics of the building: the size of structure in terms of number of bays and the number of bays exposed to fire. Finally, once the structure was built, and the f_y was defined the procedure exposed in further section automatically compute a load compatible with the sampled geometry through the fictitious load levels μ_L and μ_N.

The sampling process return to us a series of numbers and in function of these a model can be univocally defined. In order to obtain a sufficiently sophisticated model but simple, a standard substructure was adopted. In this section will be shown and discussed, starting from the fire analysis up to thermomechanical analysis.

By a Fluid Dynamic point of view, compatibly with analysis hypotheses, the fire can be depending from fuel quantity, fuel characteristics geometry of compartment and ventilation. Fires are generally expressed through a function of time RHR(t) which express the rate of heat released in compartment during fire. This curve can be defined starting from mentioned parameters. The fuel's quantity influences the duration of fire and it can be represented by the specific fire load (qf [MJ/m²]) which is defined as the total energy released in case of fire divided by compartment's area. The fuel characteristics are synthetized in the parameter RHRf ([kW/m²]) which represents the quantity of heat power released per unit area during the stationary phase of the generalized fire. Moreover fire behaviour needs to be represented by a grow up factor tα (s) defined as the time required for a MW of the RHR curve to be released. Since the two-zone model analysis is based on mass and energy equilibrium equation and neglect the momentum equation, results depend from fewer shape parameters. In this type of analysis, the main dependencies come from the compartment's floor area Af, compartment's height h [m] and openings. This last in the stochastic study is expressed as the opening percentage referred to the floor area Av/Af.

By a structural point of view parameters taken into account are the steel strength fy [MPa], the Section factor Am/V [m-1] the length of beams L[m], the height of column h [m] (assumed equal to compartment height). Moreover, other two parameters have been taken into account in order to define substructures and

these are the ratio between inertia's momentum of column and beam I_c/I_b and the building index (IB) which take into account geometry of substructures. Building index is needed in order to identifies the standard substructures. Standard substructures taken into account are characterized by a variable number of total span and a variable number of spans exposed to fire. Regarding to total number of spans it is assumed as variable number that varies from one to five, instead with regards to the number of spans exposed to fire it was assumed a number that varies from one to three. There is a total of 31 cases if symmetry is exploited.

IB	Exposed	Total
0	1	1
1	1	2
2	1	2
3	2	2
4	1	3
5	1	3
6	1	3
7	2	3
8	2	3
9	3	3
10	1	4
11	1	4
12	1	4
13	1	4
14	2	4
15	2	4

IB	Exposed	Total
16	2	4
17	3	4
18	3	4
19	1	5
20	1	5
21	1	5
22	1	5
23	1	5
24	2	5
25	2	5
26	2	5
27	2	5
28	3	5
29	3	5
30	3	5

These numbers are correlated to the hypothesis of generalized fire. By this way, statistical results allow us to study both internal stresses generated due to thermal effects and redistribution of stresses due to the unexposed zones of substructures.

Finally, the last two parameters which influence the structural behavior are the load levels. Since this study is focused frame's structural typology, they were defined two parameters to well represent the load level: one relative to columns

μ_N and one relative to beams μ_L. the load level is defined as the ratio between the actions and resistances:

$$\mu_N = \frac{N}{N_{pl}} \qquad \mu_L = \frac{M}{M_{pl}} \qquad 4.1$$

Just discussed parameters are summarized in table below:

Variable	**Distribution**	**Min**	**Max**
Af	Uniform	50	200
Av/Af	Uniform	0.01	0.5
h	Uniform	3	6
t_α	Uniform	150	600
RHR_f	Uniform	250	500
qf	Uniform	100	800
fy	Discr. Unif.	235, 275, 355	
μ_L	Uniform	0.2	0.7
μ_N	Uniform	0	0.3
IB	Discr. Unif.	0	30
L	Uniform	3	6
n_b	Discr. Unif.	0	184
I_c/I_b	Uniform	0.9	1.5

Table 4 LHS Sampling Parameters

Uniform distribution was adopted for all parameters except for IB, f_y and Am/V for which a discrete uniform distribution was assumed.

Regarding to the range of variation of these parameters there are a few hypotheses to do. Regarding the compartment's floor area A_f, it was considered as variable through 50m² and 200 m². Bounds was defined in order to neglect very small and very large fires, moreover note that if the compartment's area is too high fires tends to be of a localized type because in this case the hypothesis of uniform distribution of the fire loads in the compartments tends to be strong and

also if it's true we cannot neglect the fire travelling. The hypotheses on the compartment and the generalized fire influences the IB parameter also.

The opening percentage was delimited in the interval 1%-50% in order to take into account the major part of possible cases.

The range of variation of Am/V depends from the number of sections could be adopted as beam (IPE and HEA profiles).

As concern the RHR parameters, they have been considered uniform distributed through the limits prescribed by the Eurocode EN1991-1-2, 2002.

Load level values was assumed as uniform distributed through 0.2 - 0.7 regarding to μ_L and variable in the range 0 - 0.4 as concern columns μ_N (lower upper bound value take into account the buckling check by simplified way).

Regarding to the geometry of structures, the limits for the length of beams are 3m-6m, the same of column's height directly bounded to the height of compartment.

4.3 Experimental Design

In this section it will be shown how the analysed models were built starting from the LHS sampling. The sampling procedure returns an array of numbers which is converted in input model of fire analysis and thermomechanical analysis through an assembling protocol.

4.3.1 LHS Sampling and Simulated Annealing

An experimental design based on a sampling method is used, to provide a pre-set number of samples representing different realizations of the variables x, which represents the input parameters both for the CFAST simulations and for the thermomechanical analyses with SAFIR. It is worth noting that the repetition of the thermomechanical analyses for each sample can be highly expensive in terms of computation resources and time. The selection of the experimental design methodology shall guarantee limited variability of the results in function of the sample set size. The methodology presented by Vořechovský and Novák (2009) matches this requirement. They proposed a Latin Hypercube Sampling (LHS) technique for the efficient Monte Carlo type simulation of samples of random vectors with prescribed marginal distributions and a correlation structure. It has been shown that, if such a technique is applied for small sample simulation, the outcome is a set of samples that matches user-defined marginal distributions and covariance values. The correlation control problem is treated as a combinatorial optimization problem, based on an evolution strategy improved by the Simulated Annealing approach (Kirkpatrick et al., 1983).

Results of the optimization through Simulated Annealing technique is reported in Figure 34. As already said, the SA optimization process in the in the initial phases show a behaviour similar to a random search technique, so the error norm varies in a quasi-constant interval. After $1.5 \cdot 10^7$ iteration the error norm tends to decrease, in this phase the SA algorithm reject solution with lower associated probability. Moreover in Figure 34 we can see the blue line that represent the "temperature" control parameter. As said in section 3.7.3 the temperature parameter should be distributed as the Boltzmann distribution:

$$P(\Delta E) = e^{-\frac{\Delta E}{k_B T}} \qquad 4.2$$

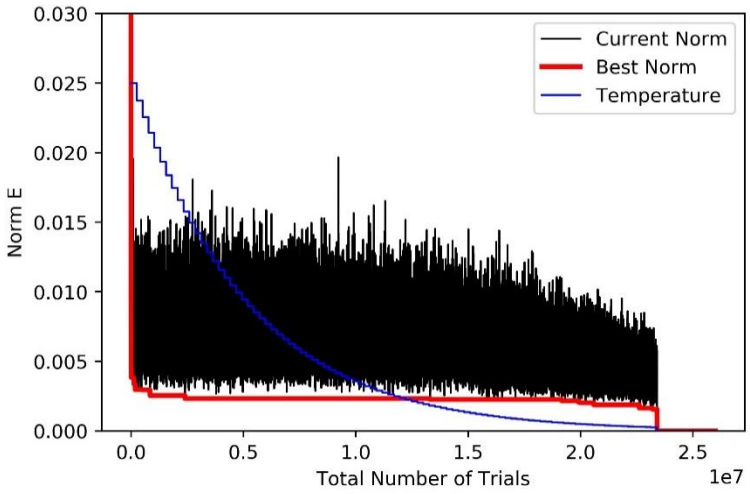

Figure 34 Error Norm variation during the Simulated Annealing process.

4.3.2 FIRE PROBLEM DEFINITION

Since the input parameter are defined, the assembling protocol starts from the building of the Heat Release Rate Curve as reported in Eurocode EN1991-1-2, 2002.

The RHR curve is assumed as a function divided in three branches: the first branch is assumed as parabolic, the second assumed as constant and the third is assumed as linear:

$$\begin{aligned} RHR(t) &= \left(\frac{t}{t_\alpha}\right)^2 && 0 < t < t_1 \\ RHR(t) &= RHR_f \cdot A_f && t_1 < t < t_2 \\ RHR(t) &= \frac{Q_{max}}{t_2 - t_3}(t - t_3) && t_2 < t < t_3 \end{aligned} \qquad 4.3$$

The RHR's parameters are evaluated using expression starting from total thermal power released in compartment defined as the sum of thermal powers in each phase of fire (grow, steady, extinction):

$$W_{Tot} = W_1 + W_2 + W_3 = q_f \cdot A_f \tag{4.4}$$

Assuming that:

$$\begin{gathered} W_1 + W_2 = 70\%\, W_{tot}\,, \qquad W_2 \geq 0 \\ Q_{max} = RHR_f \cdot A_f \\ W_1 = \frac{Q_{max} \cdot t_1}{3} \\ W_2 = (t_2 - t_1) \cdot Q_{max} \\ W_3 = \frac{(t_3 - t_2) \cdot Q_{max}}{2} \end{gathered} \tag{4.5}$$

the times when fire switch its phases t_1, t_2, t_3 are calculated as:

$$t_1 = \sqrt{\frac{Q_{max} \cdot t_\alpha}{10^6}} \tag{4.6}$$

$$t_2 = \frac{W_2 + t_1 Q_{max}}{Q_{max}} \tag{4.7}$$

$$t_3 = \frac{W_3 + 0.5 \cdot t_2 \cdot Q_{max}}{0.5 \cdot Q_{max}} \tag{4.8}$$

Using 4.5 4.6 4.7 and 4.8 RHR curve can be computed and if we represent the heat released in function of time we would get a curve like the one shown in Figure 35. Note that for high values of RHR_f, high values of t_α or small value of the specific fire load q_f the Energy W_1 could exceeds the 70% of the total energy released in the compartment. When this situation occurs, if we use the first equation of 4.5 we get a negative value of W_2. In this case the RHR assumes a form different from the one reported in Figure 35, indeed fire is characterized only by the growing phase and the cooling phase, without the steady fire.

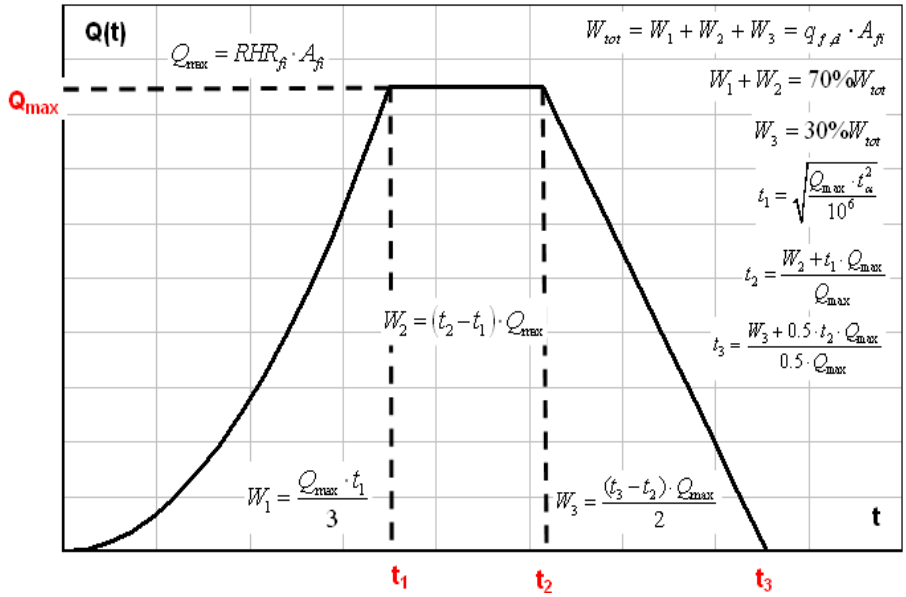

Figure 35 Heat Release Rate Curve.

From distributions of the computed characteristic times of RHR (Figure 36) we can note that the duration of fires are less than 100 minutes and that the experimental design includes cases for which there is a low specific fire load and a big compartment's floor. In this case the RHR is characterized by the absence of the steady fire. This can be observed also in Figure 37, sampled curves

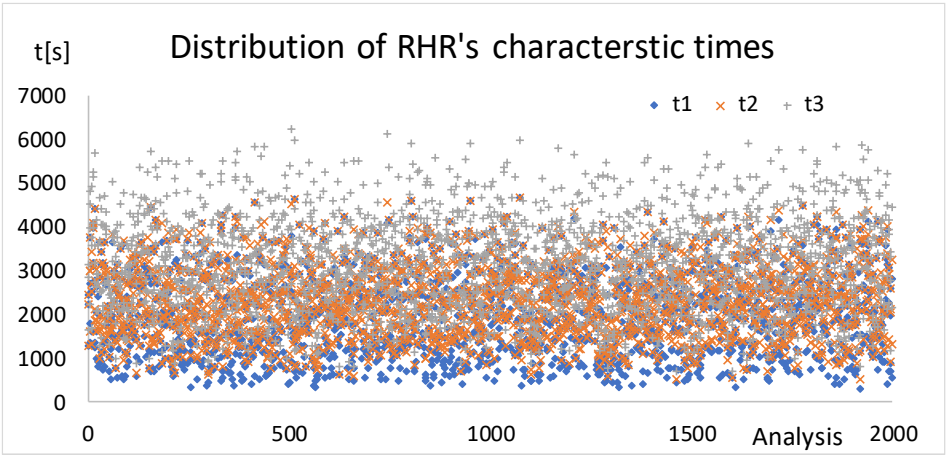

Figure 36 Computed characteristic time.

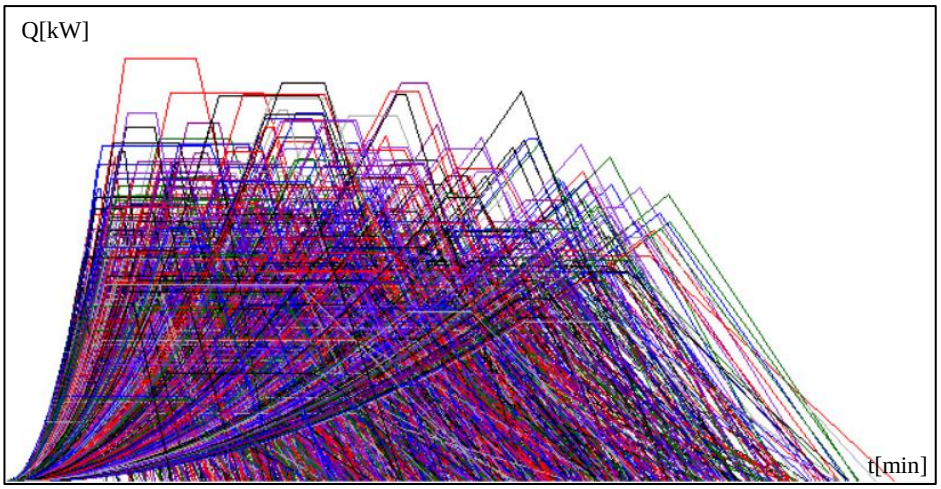

Figure 37 Sampled RHR Curves.

Once the RHR curve is defined, input and output parameters are stored into a database, then the procedure build the Fluid dynamic model and run the FDA analysis.

Thermal analysis is carried out as reported in section 2.1. The RHR curve, opening and other parameters are used as input of the Fluid Dynamic Analysis in order to assess temperature of the gas in compartment during fire. All temperature curves derive directly from the RHR curve, for this all temperature curve are characterized by a heating phase and a cooling phase.

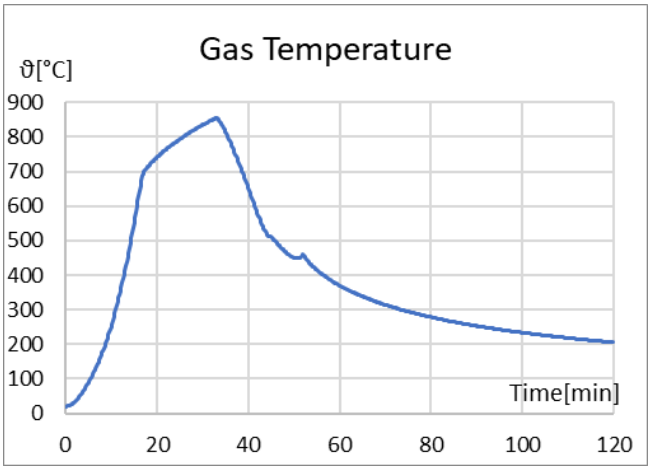

Figure 38 Temperature Curve.

In particular, the heating phase could be characterized by two branches, the first with a higher slope and the second with a lower slope. The slope of the gas temperature curve is due to the heat released in compartment and while the first branch that derives from the parabolic branch of the RHR is always present the second branch could collapse if the heat released in the growing phase and the cooling phase are so big that the energy released in these two phases is equal to the fire load in the compartment.

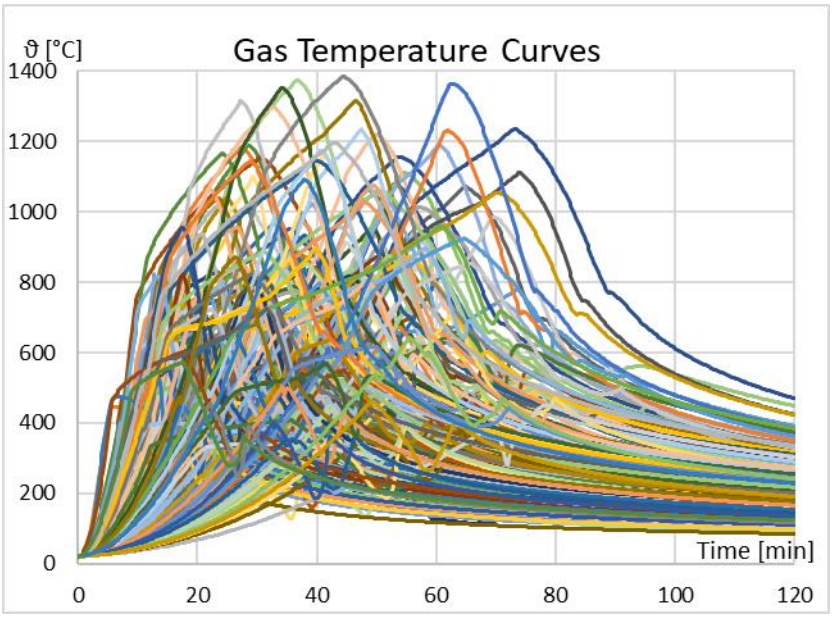

Figure 39 Gas Temperature Curves.

4.3.3 FIRE SCENARIOS AND SUBSTRUCTURES DEFINITION

When the solver finishes analysis, processor stores results and creates thermomechanical model which consisting of two parts. The first part of the model is used to characterize the moment-curvature relationship of the section in function of temperature and time, and the second one is the substructure used for the structural analysis.

In the sample array structures are characterized by beam's Inertia I_b, the I_c/I_b Factor and the Index of building IB. The procedure uses two lists to define

substructures sections: one relative to beam, which contains all IPE profiles and HEA profiles, and another relative to columns which contain all IPE and HE profiles. Both section's lists are ordered by Inertia. The identification of sections could be illustrated by a graphic way, as reported in Figure 40. Starting from the sample's value (A), the section inertia I_b (B) is multiplicated by the I_c/I_b Factor (C), then the procedure finds in section list the section of column (D) characterized by:

$$I_c = \frac{I_c}{I_b} I_b \tag{4.9}$$

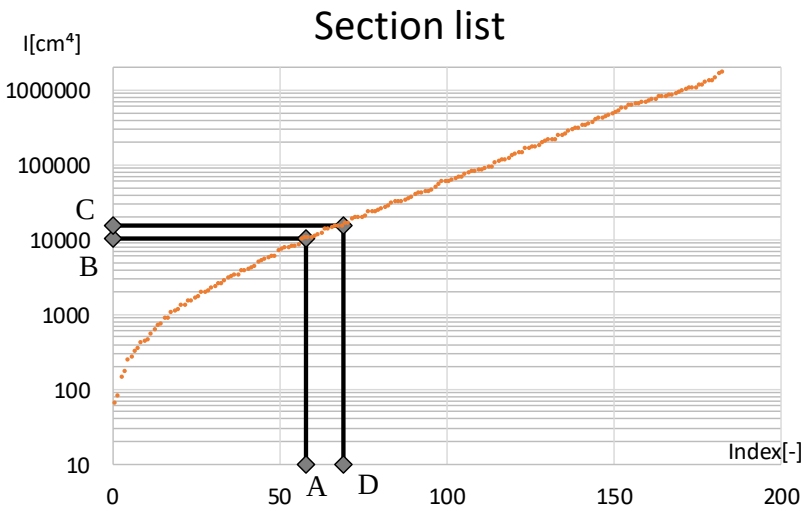

Figure 40 Section's identification.

Starting from the value relatives to I_b and I_c/I_b of sample, the procedure find in beam's section list the section associated to the extracted index, then it uses the I_c/I_b parameter to find in the list of columns a section such that the ratio between the inertia sought and the inertia of beam section is equal to I_c/I_b. Once beams and columns were defined, the algorithm pass to build the substructure.

The desired substructure is defined trough the value assumed by the variable IB. All possible substructures showed in Figure 41 can be involved in fire which affects up to three bays close together.

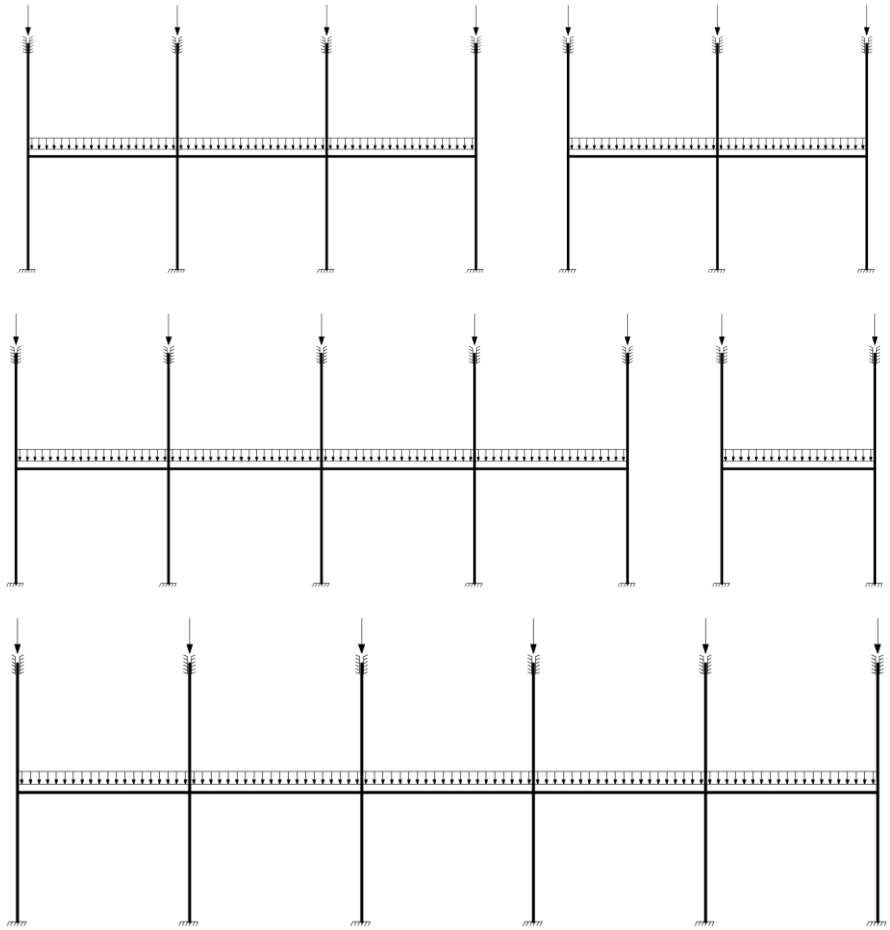

Figure 41 Standard Substructures.

As concern boundaries of substructures, there are a fix constraint on foot of columns in the first level of structure. Regarding to displacement constraints it's assumed that deck's stiffness and strength is greater than stresses in columns, so greater that bending moment, horizontal forces and vertical forces can't deform the deck. The top of the substructures is constrained to horizontal displacement and rotations. In this case the degree of freedom relatives to vertical displacements

is released and a load is placed on the head of column in order to simulate the weight of upper decks.

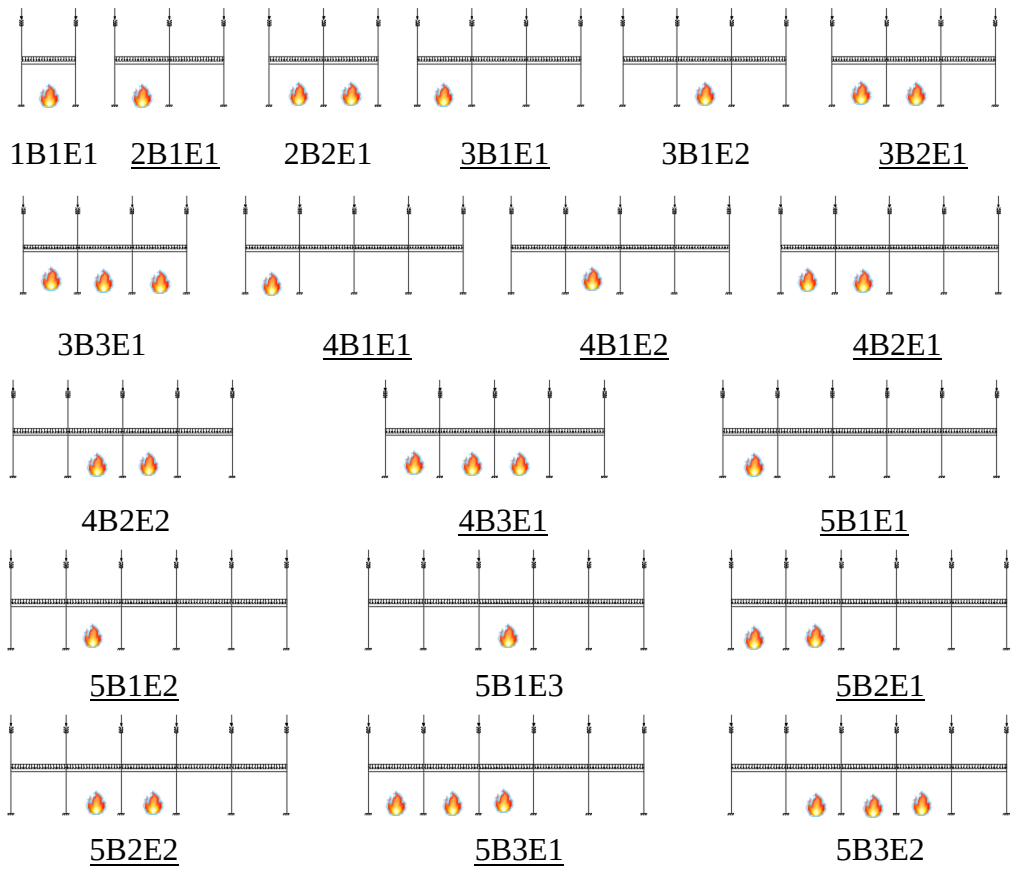

Figure 42 Fire Scenarios.

Figure 42 show some fire scenarios considered in the probabilistic study. The total of scenarios are composed of those represented in the figures plus those that can be obtained by exploiting symmetries. Fire scenarios are named with alphanumeric string of characters that depends from the number of substructure's bay, the number of bays exposed to fire and the number of the first bay exposed to fire starting from the left side. For instance, the scenario named 5B2E2 represent a substructure with 5 bays where there are two bays exposed to fire and the first bay exposed is the second bay of the structure. As already said fire scenarios represented in Figure 42 are only a part of the considered scenarios. Since substructures are characterized by the same beam length and the same geometry for all beam and for all columns respectively, in LHS sampling some

scenarios are considered two times in order to take into account symmetries. Scenarios counted twice in the sampling phase are underlined in Figure 42.

4.3.4 LOADS

Regarding loads, there are two type of loads in order to represent the load on girders and loads on columns. For this reason, two parameters of the samples identify the load condition μ_L and μ_N. Starting from μ_L which variates in the interval $0.2 \div 0.7$ the design procedure evaluates load on beam as a percentage of the load that causes beam's failure. Note that the moment M along spans could be calculated as:

$$M = \frac{q \cdot L^2}{\alpha} \qquad \rightarrow \qquad q = \frac{\alpha\, M}{L^2} \tag{4.10}$$

Where α [-] is real number, L[m] is the length of beam, and q[kN/m] is the distributed load. The crisis of the beams is attained when moment reach along the span the capacity value $M = M_{pl}$. Replacing M_{pl} with its expression in function of geometric properties of section and tensile material's strength:

$$q_{cr} = \frac{\alpha \cdot W_{pl} \cdot f_y}{L^2} \tag{4.11}$$

finally, we get the distributed load value:

$$q_L = \frac{\alpha \cdot W_{pl} \cdot f_y \cdot \mu_L}{L^2} \tag{4.12}$$

The parameter α depends from the position considered along the beam's span and from constraints, so it is hard to evaluate in this context. Since the structural typology is fixed, we know without perform analysis that the plastic hinges come up near the beam joints first and finally near the midspan of the beam. Values of α are reported in are reported in Table 5.

Structural scheme	α
Pinned-pinned beam	$[-]$
Fixed-Fixed beam	12
Fixed-Pinned beam	8

Table 5 Values of α by structural scheme

The value of α adopted in calculations is 10, thinking that bending moment distribution along the beams could change from a fixed-fixed to fixed-pinned configuration of beams. Note that $ql^2/10$ is a reference value assumed as a starting point to calibrate regression parameter related to the load level in the beam. $\alpha = 10$ was chosen because 10 is a mean value between 8 and 12 so the value of the bending moment $ql^2/10$ is similar to the real bending moment at the beam support.

As concern stresses on columns the procedure calculates the axial load N multiplying μ_N per the profiles area A_f, per the tensile strength f_y:

$$N = A_s \cdot f_y \cdot \mu_N \qquad 4.13$$

Generally, the load level μ_0 is defined as the ratio between the demand and capacity when the fire begins, and it has sense only if the collapse depends from the yield of one section of structure. In this case all structures have overabundant constraints so the stress can be redistributed to other parts of structure. Moreover both μ_L and μ_N in this context don't respect the definition of μ_0 because μ_L doesn't contains the real stress on cross section (because α isn't precisely evaluated) and μ_N doesn't take into account stability problem.

4.4 Analysis Results

As already said the thermomechanical analysis conducted in this work are named uncoupled because it was conducted in two steps: The first that consider only the thermal problem in order to compute temperatures and the second one that use calculated temperatures to characterize constitutive law of materials and use it to compute stress and displacement of structure. In next two paragraph it will be shown results of the both step of thermomechanical analysis.

4.4.1 THERMAL ANALYSIS

Thermal analysis of cross sections allows to know temperature's distribution in structural elements. Since cross sections are exposed to fire in function of its own positions in the structure, even if a structure is characterized by the same section for beam and columns, we get different temperature distribution because they are characterized by different exposure conditions. Temperature distribution in section is reported in Figure 43 as regard beam's sections (three side exposed) and Figure 44 as regard column's section (four side exposed).

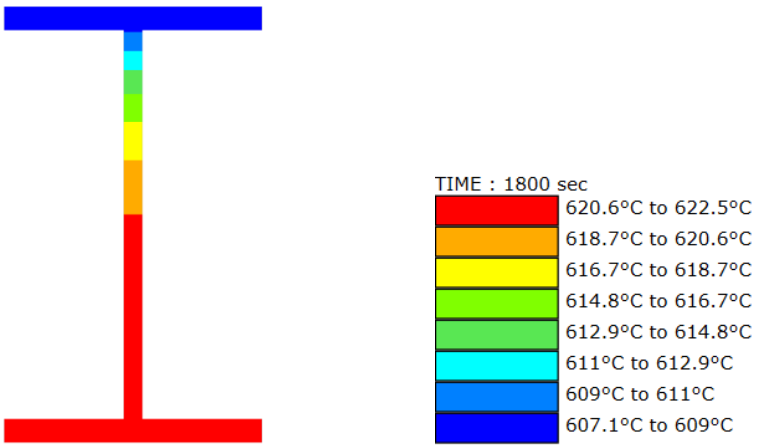

Figure 43 Section temperature distribution for three side exposure.

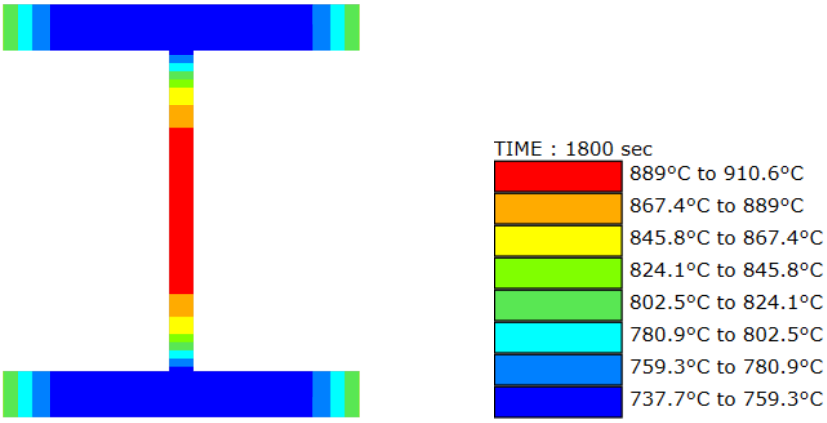

Figure 44 Section temperature distribution for four side exposure.

Thermal analysis is conducted in in time domain of 7200 seconds (2 hour) for each thermal problem and results are stored in a database that could be queried as the user want. Figure 45 show the evolution of temperature in steel element compared with the gas temperature evolution computed with the FDA. Note that temperature evolution of the steel shows two little change of slope around 30 min and 50 min, this effect is due to peak of specific heat of steel.

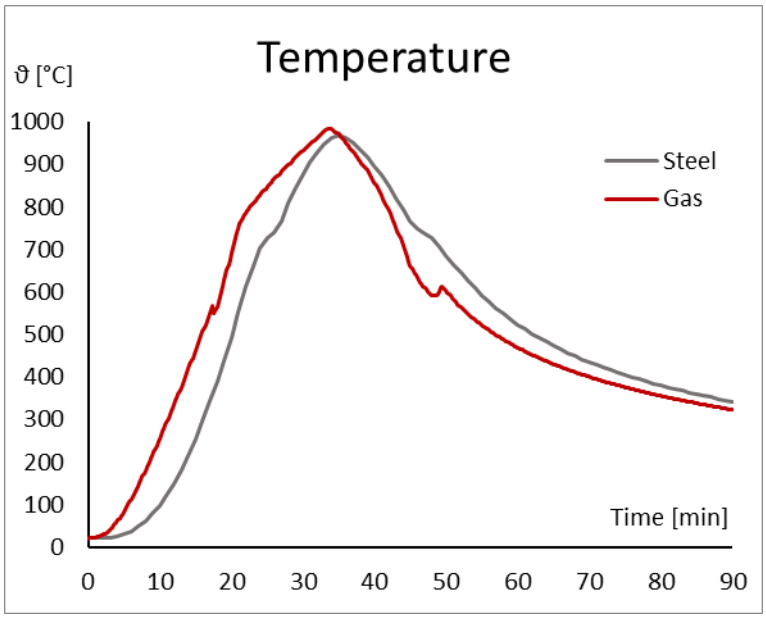

Figure 45 Temperature evolution in steel element.

Thermal effects due to steel's thermal expansion coefficient in this modelling hypotheses could be synthetized in only two quantities:N_ϑ and M_ϑ. The first is the axial load induced by thermal effects and it depends from barycentric deformations whereas the second, defined as the Moment induced by thermal effects depend from section 's curvature. These two quantities can be calculated in the fibres section's model thanks to the hypotheses of plane section deformation.

Note that using a FEM model based on discretization of the section in fibres there isn't a single reference temperature to characterize section so to synthetize data in further calculations we refer to the mean of temperature in the cross section, defined as the mean of temperatures of each fibre's mean temperature. Since the FEM analysis returns nodal temperature for all m nodes of the section, we have to mean temperature in each fibre and redo the mean weighted on the fibres' section areas:

$$\vartheta = \frac{1}{A_S}\sum_{i=1}^{n}\left(\frac{1}{m}\sum_{j=1}^{m}\vartheta_{i,j}\right)A_i \qquad 4.14$$

In 4.14, A_s is the cross section's area, A_i is the area of the i-th fibre, n is the total number of fibres of cross section, m is the number of nodes for each fibre in which the temperature $\vartheta_{i,j}$, is calculated. In further calculation it will be adopted $m = 4$ because a plane finite element with four nodes is adopted in FEM Model for thermal analysis.

4.4.2 THERMOMECHANICAL ANALYSIS

Thermo-mechanical analysis was conducted as reported in chapter 2. A in house software is developed to build geometry of substructures and assign properties starting from numbers generated from the LHS Sampling optimized through the simulated annealing method. Once the substructure is characterized with its own features (i.e. geometry loads and constraints) and thermal analysis is completed the output of this last one is used to perform the mechanical analysis in fire condition. Thermal analysis output is used as input for mechanical analysis because it is needed to define behaviour of the beam elements. As already said

the mechanical analysis returns stress, strain and displacement of structure during fire. Results of the structural analysis allows to know in a predefined time domain displacements and stresses in of structure.

Regarding stresses, the FEM core of Safir compute the stresses in each point of integration of structure for each timestep taking in account thermal effect and the decay of material properties due to temperature increasing.

Results taken into account in this study are the displacements and the stresses, in particular the Axial Force N and the bending moment in the strong axis of the sections. As we can see from next figures, the output of the analysis can be displayed in the space to appreciate the distribution of stresses at exact instant or it can be displayed in function of time.

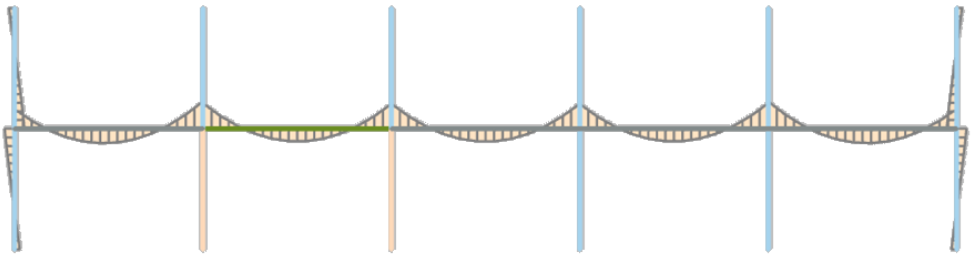

Figure 46 Bending moment distribution in space at the begin of fire.

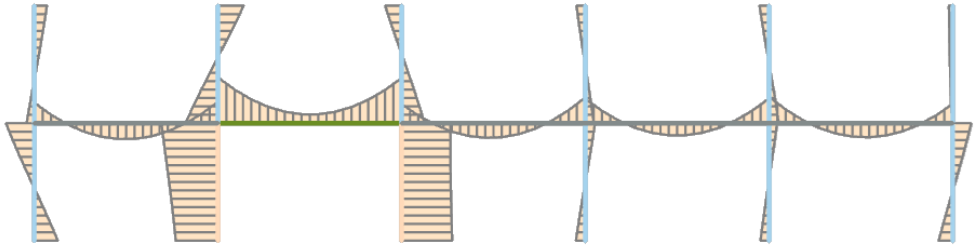

Figure 47 Bending moment distribution in space during fire.

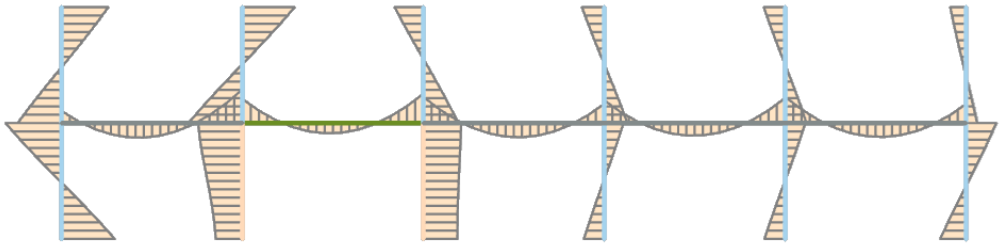

Figure 48 Bending moment distribution in space at the end of fire.

In Figure 46, Figure 47 and Figure 48 we can see the bending moment distribution within the structure at the beginning, during and at the end of fire. Note that respect the beginning of fire there is a burden of stresses due to thermal effects also at the end of fire. Figure 49 explicitly shows the same concept through the representation of the axial force in function of time.

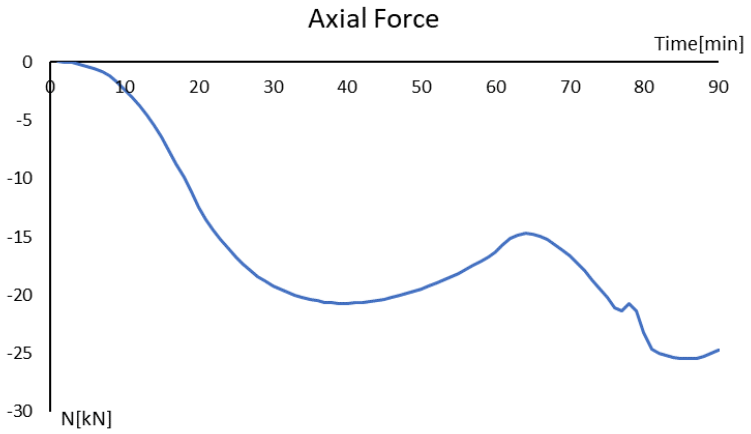

Figure 49 Axial Force in function of time.

Regarding displacement, results can be showed in the same way. Figure 50 show the deformed shape of the substructure at the beginning and at the failure, in this case we can see that the constraints adopted for the head of upper columns allows the expansion of the column and attenuates thermal effects (blue circle). Indeed, if the vertical displacement is constrained the axial force that arise due to thermal effect could cause a failure because instability. Moreover, this representation allows us to see zones of structure involved in plasticization (red circles).

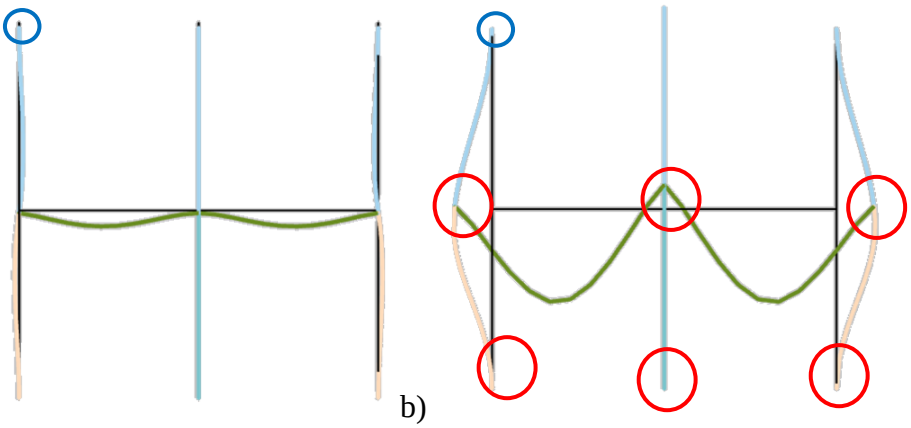

Figure 50 Displacement at the beginning of fire(a) and at failure (b).

4.5 Structural behaviour's analysis

Analysed structures are characterized by only five types of elements: beams which can be exposed or unexposed to fire and columns that can be exposed to fire by four or one side, or unexposed. Analysis results show that the structure could reach the collapse only in exposed elements, for this reason the database is characterized by the collapse mode. The purpose of this section is to interpret the results of the single analysis in order to understand the physics phenomena and illustrate the collapse modes (i.e. Beam Columns one side exposed and Columns four side exposed). Moreover, in this section there are also some more observations about structural behaviour of samples. In particular starting from the observations on of the data presented in the previous section an analysis of the structural behaviour was performed in order to interpret cluster's results.

The evolution of stresses in structure in fire are generally non-monotonic, indeed both Axial force and bending moment have an increasing phase and decreasing phase. The increasing phase is due to thermal effect of steel which want to expand but is hampered by other parts of structure.

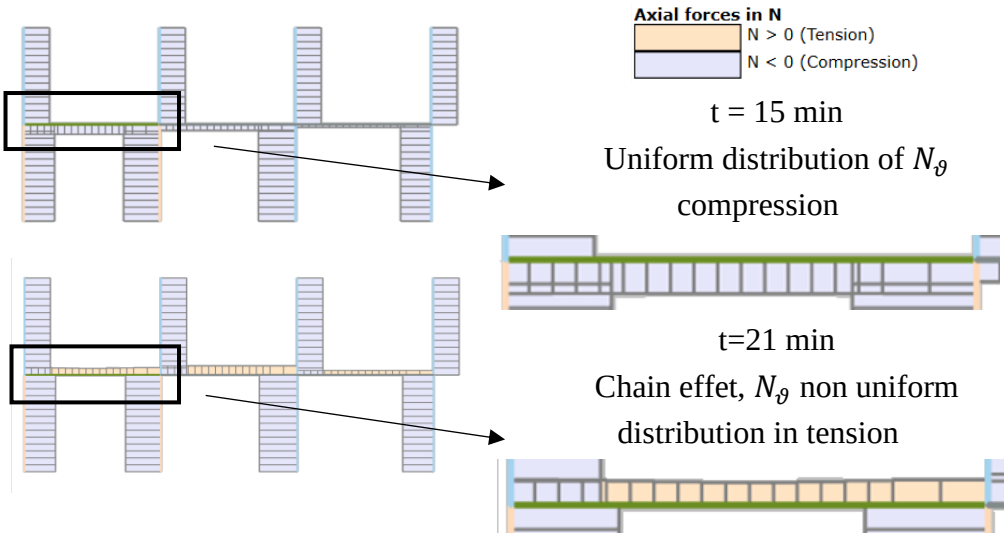

Figure 51 Chain effect.

The decreasing phase depends from the yielding of the structure and second order effects, in particular regarding to axial force, it can grow up to yielding point and amplify second order effects. It causes larger displacements so internal

stresses in the new configuration can be converted in strain thus axial forces decrease.

In other cases, it could happen that at the end of the fire the axial load distribution assumes a parabolic distribution due to the chain effect. This effect occurs when bending resistance of the beam is nearly null and the bending stiffness is very low but the structure can exploit some more the resistance of members. In this case displacements of beam tends to be very big, the bending moment tends to reduce itself and the axial load assume a parabolic shape as the theory about the equilibrium of cable says. The chain effect, to arise need also that the constraint offered by the structure is adequately big.

4.5.1 COLLAPSES

As already said, there are three types of collapse mechanism, one for each type of element exposed to fire. In this work we talk about collapse mechanism (or failure mode or collapse mode) referring to a section type of the structure, which is the first section that reach the end of its own moment-curvature diagram. This means that each collapse mechanism is defined by the first section which fails. The thermomechanical analysis output report doesn't highlight the finite element associated to the last point of the moment-curvature diagram, but it returns a warning when there is a fibre in softening in any section. In truth there is a large variability on structural collapse for these non-linear problems due to a lot of parameters. In truth the softening branch couldn't be defined as well in this type of thermomechanical analysis for various reasons: the softening branch defined in the computer program start at $\varepsilon_\sigma = 15\%$ that is a very large value of deformation too much that in these condition the fibres should be considered in their deformed configuration due to the Poisson ration ($\nu = 0.3$). Moreover, in softening branch the Elastic modulus should be negative that means that the strain rate of the material increases and this could cause the fracture of material (things didn't taken into account in this work). Finally, the hypothesis of plane section in large deformation of materials becomes less truthful.

The high number of analysis performed leads to some problems in results management. It is very hard to check all results by hand, for this reason a stratagem was needed to handle the checking phase. To do that, a process of collapse element's identification was developed. The process consists in following steps:

1. Interrupted analysis count (~780)
2. Count of the warning associated to the steel in descending branch in the output file (all timestep);
3. Creation of the elements list;
4. Association of warning messages to elements;
5. List sort in descending order;
6. Manual check of collapsed analysis to correct false positive matches (as shown in further paragraph);

Note that rarely the collapse of the structure depends from only one section, indeed there is a lot of structure where there is the yielding in several section for the same mechanism, or yielding occurs in both beams and column sections.

Following paragraphs show collapse mechanisms and report qualitative considerations on the vulnerability of structures to collapse mechanisms. This will be done through the illustration of an analysis involved in the selected mechanism type.

4.5.2 BEAM'S COLLAPSE MECHANISM

The collapse mechanism that interest the beam is the most probable mechanism in the database. As already said, the beam's collapse mechanism means that the collapsed section is placed in the beam exposed to fire. When a beam is exposed to fire it expands itself thanks to thermal effects but if the beam is bounded in axial direction by a deformable constraint the deformation isn't equal to thermal expansion of material but depends from the stiffness of constraints. The countered expansion manifests itself as load that acts on the structure and could cause instability or plasticization. When we consider geometric and material's non-linearities in thermomechanical problems, the heated beam could plasticize and lose stability due to thermal effects. In these condition the solution of the equilibrium could be not only one, indeed in some cases the excessive deformation and the loss of flexural capacity of the beam cause big displacements that can stabilize on a new point of equilibrium where the beam has a very low bending moment and the axial load change its own sign, passing from compression to tension state. When this situation occurs, it is said that the chain effect is manifested. The chain effect could appear when the frame is sufficiently stiff and resistant to horizontal forces. In this section will be presented results about two analysis in order to understand better the collapse mechanism. Analysis data are reported in Table 6.

As you can see from the table, even if structure 355 is characterized by a lower load level the structure 113 has a higher collapse temperature (755°C vs 677 °C). Moreover, we can see that the logarithm of the frame's stiffness is higher in the case of the 355 while there is a lower number of bays and a lower value of I_c/I_b ratio. By an energetic point of view the energy released by the fire evaluated in the fluid dynamic context is transferred to the structure trough exposed surfaces, for this reason structure 355 is involved in a fire much burdensome than the structure 113 so this last should collapse later if it is exposed to the same fire . In this context means that the structure 113 should collapse for higher temperature because can store more energy that come from fire.

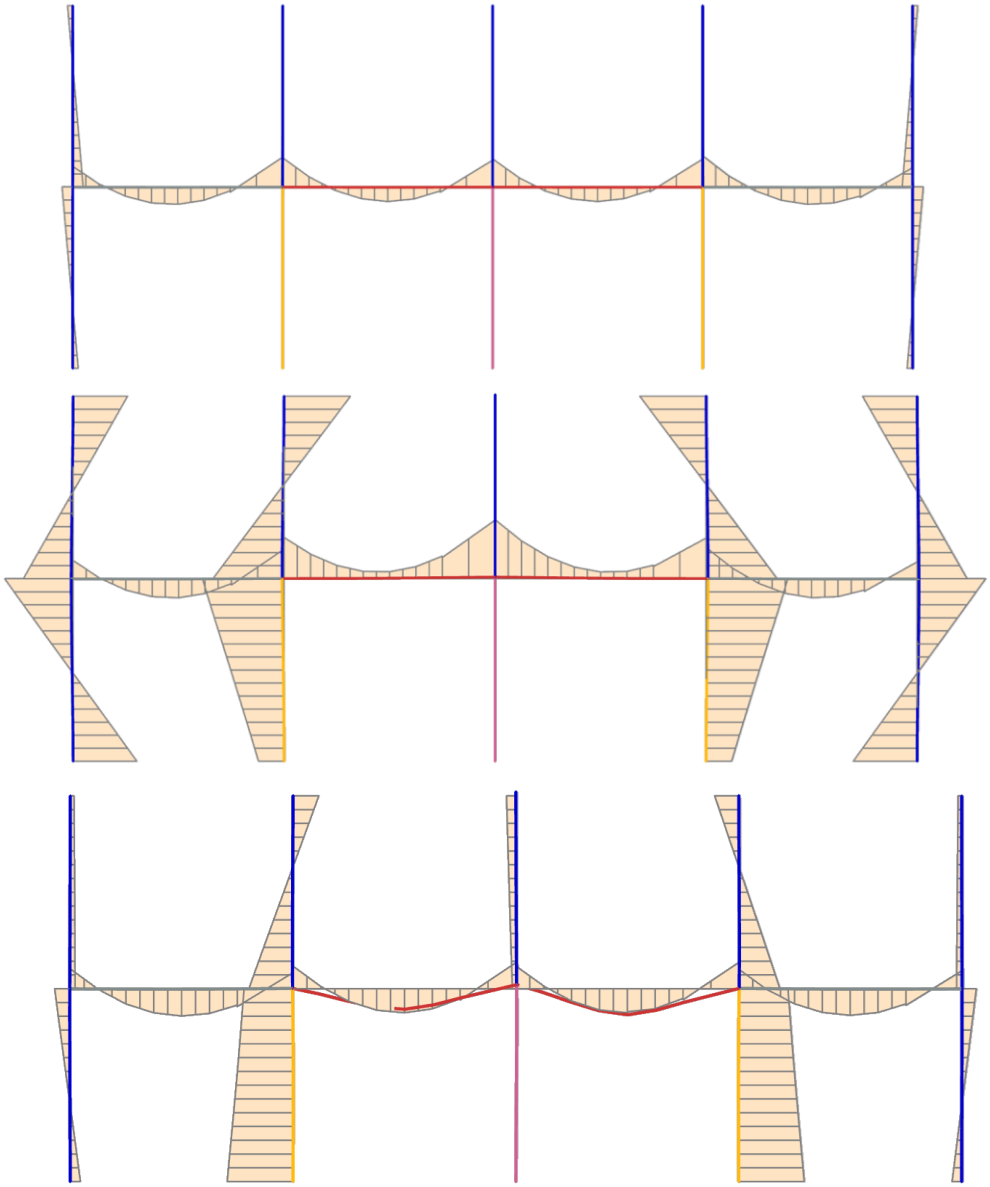

Figure 52 Structure 355. Bending moment distribution t=0 min, t=15 min, t =24 min.

n°	L	H	Bays		μ_L	μ_N	I_c/I_b	Beam	Column	Log(K_χ)	ϑ [°C]
			Tot	Exp							
355	4.2	3.7	4	2	0.42	0.08	0.93	IPEA330	HE260A	4.58	677
113	5.4	3.4	5	1	0.6	0.23	0.97	IPEO240	HE160M	4.49	755

Table 6 Characteristics values of analysis considered for beam's mechanism.

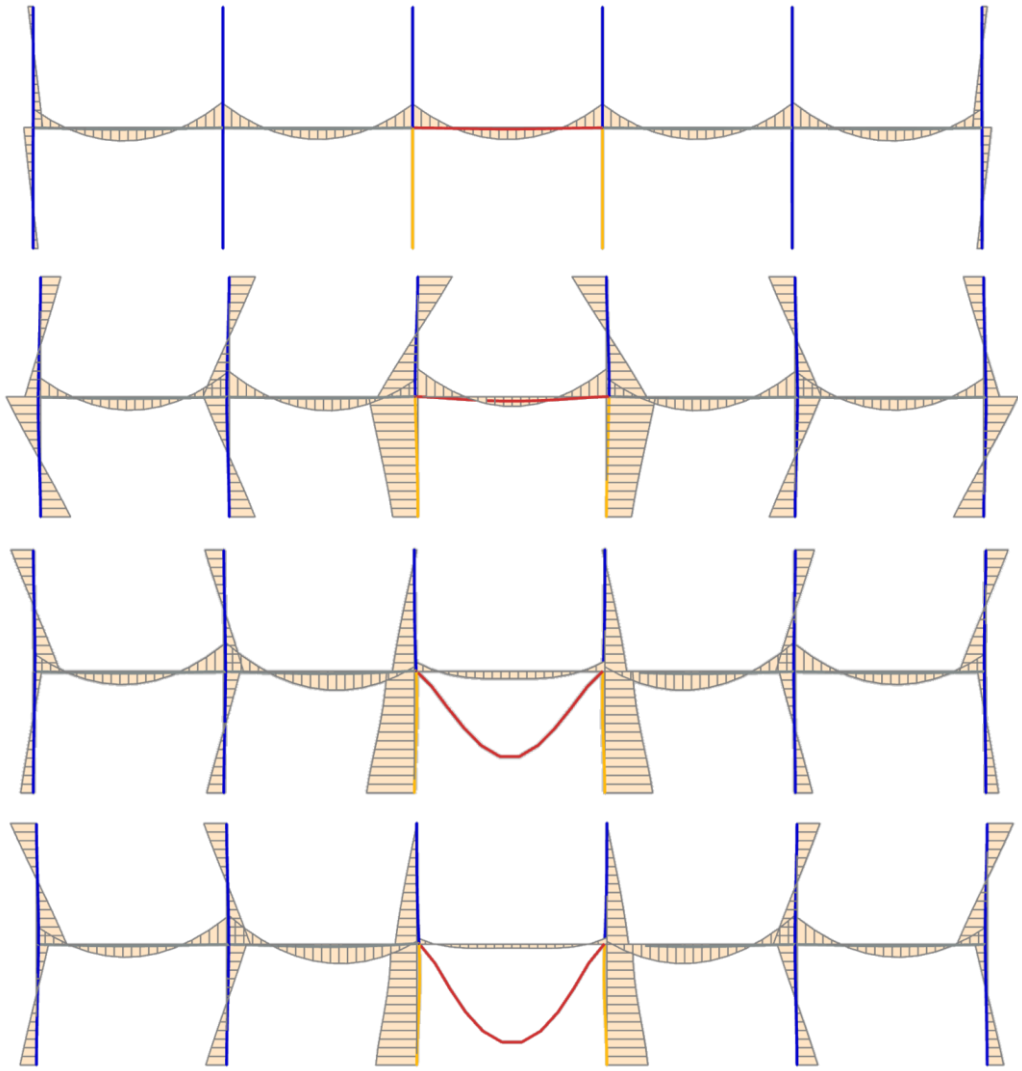

Figure 53 Structure 113. Bending moment distribution t=0 min, t=27 min, t= 37 min and t =42 min.

Figure 52 and Figure 53 show the bending moment distribution for analysis 355 and 113 respectively. As we can see from the illustration of Figure 52, the central bays are exposed to fire (red), so the substructure results symmetric respect the central column. On the contrary the structure 113 (Figure 53), have a total of five bays and only one is exposed to fire. In this case the axis of symmetry cut the midspan of the exposed beam.

Regarding structure 355, when the fire begins the bending moment distribution change from the typical configuration relative the service state to a configuration where there is the maximum effect of thermal loads (t =15min). After that the stresses tends to decrease but not for the attenuation of the fire but the effect of geometrical and material's non-linearities. Indeed, at as you can see from the figure at t = 24 min the beams reach a high deflection while the bending moment is quite equal to the bending moment at the fire beginning.

In beams exposed to fire in the first phase the bending moment tends to grow because thermal curvature. In case of Analysis 355 the thermal effects in terms of curvature exceed the effect of girder's load (bending moment doesn't change sign along the span at t=15 min). At the end of fire, we can see that because the deformation of the beam due to plasticity the bending moment tend to return equal to the bending moment at t =0 min because the plastic deformations dispel thermal effects. After t = 24 min the structure lose completely the capacity to redistribute stresses to stiffer and more resistant elements, for this the plastic deformation increase in the beam compatibly with the constitutive law. When the moment-curvature diagram of the section reaches the softening branch, displacement diverge and the structure collapse.

Regarding to columns, the one exposed to four side tends to expand due to temperature increasing, and in this case doesn't change the bending moment distribution because the structure is symmetric. Columns exposed to one side (orange), when the fire begin thermal effects on the structure can be seen on the bending moment diagram, indeed the maximum moment variation can be seen on these structural elements because in these the temperature induced curvature is the highest. If we observe the bending moment diagram on the unexposed columns, we can see that it is nearly zero at the beginning of the analysis, then it increases up to 15 min and the peak, that coincides with the deck's level facing always the outside of the structure. This effect is caused by the axial force that arise in the beam due to thermal expansion.

As Concern the Analysis 113, the behaviour of the structure during the fire is quite different. Regarding the evolution of stresses also in this case distribution

of bending moment starts from the service state (t = 0 min) increase due to thermal effects (t = 27 min) and finally decays up to the failure (t = 42 min). In the case of analysis 113 when the fire begins the bending moment on the beam tend to increase but due to the higher value of μ_L and the length of the beam, the thermal effect doesn't exceed the load induced stresses. For this reason, the bending moment along the span assumes both positive and negative values.

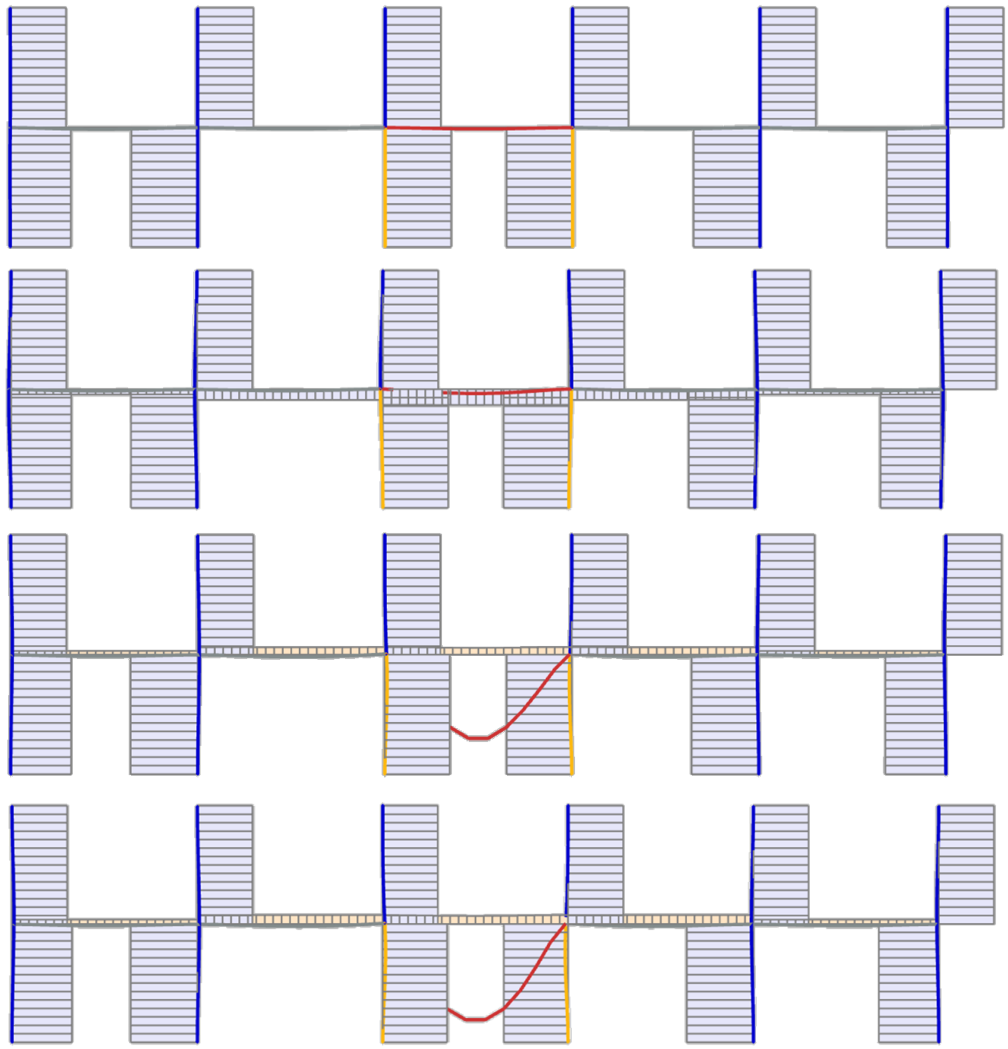

Figure 54 Structure 113. Axial force at t=0 min, t=27 min, t= 37 min and t =42 min. (compression violet, tension peach)

Another interesting thing about structure 113 is relative to the distribution of bending moment at t = 37 min and t = 42 min. The bending moment in the joint section and in the midspan decrease monotonically from the 27 mins up 37 min but since this instant the bending moment along the exposed beam remains nearly constant. The reason of this condition is the excessive displacements induced by flexural resistance decays that now tends to be zero. In this situation the structure 355 is collapsed but in this case the incipient collapse is blocked by a new equilibrium position that is given by the configuration of chain-shape of the beam (chain effect).

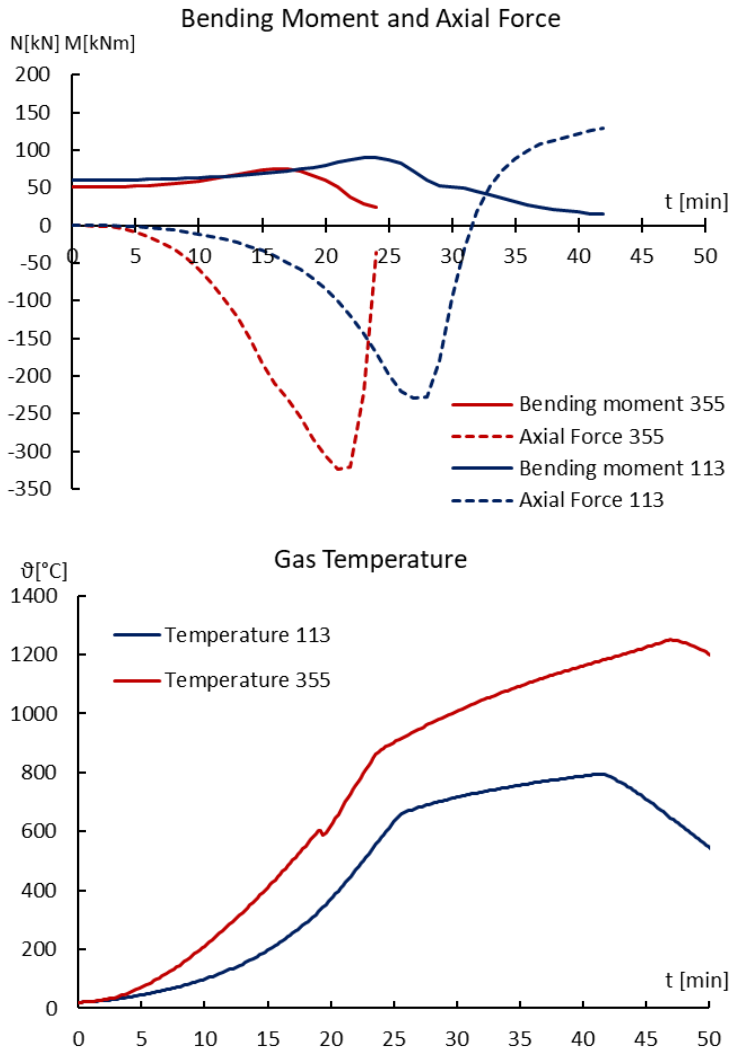

Figure 55 Evolution of M and N.

The chain effect gives to the structure an additional resistance thanks to the axial bearing capacity of the beam. If we at the same time look at the distribution of the axial stresses within the structure, we can see that the axial force which is a compression force has changed becoming a tension force (Figure 54). Note that when chain effect manifests itself bending moment on columns of the frame in this condition change sign (Figure 53). The same observation can be done if we look at the diagram that represent the bending moment and the axial force in function of time (Figure 55).

Finally, it must be said that also if the chain effect gives an over resistance to the structure in terms of stresses, regarding temperature the reward isn't very high. Generally, this effect can be appreciated during the stationary phase of the RHR, where gas temperature tends to increase slowly. If the variation of temperature in time is too high the new stable configuration became incompatible with the plastic resistance of the beam and structure collapse immediately.

To summarize we can say that the collapse of beams could be retarded due to chain effect. This means the collapse temperature increase and the structural context play a central role in structure's resistance. Moreover, regarding to post-crisis mechanism that increase the capacity of structure, they depend from several condition and can't be predicted as well. For this reason, there is a higher variability of the collapse temperature that in the further chapter will result as a higher variance on the collapse temperature.

4.5.3 FOUR SIDE EXPOSED COLUMN'S MECHANISM

The most probable mechanism of collapse after the beam's mechanism is the failure mode that involves the columns exposed by four side. The C4s mechanism occurs when the first element that can't achieve the equilibrium is a column exposed by four side. This type of mechanism is related to the stability of the column and the stability of the frame which in steel structure plays a central role. The stability problem gives place to brittle collapse and the structure can't rely on post crisis resistance. For these reasons the collapse temperature distribution is characterized by a lower variability.

In order to show this type of collapse it was analysed the structure 718 (Figure 56) characterized by parameters reported in Table 7.

n°	L	H	Bays		μ_L	μ_N	I_c/I_b	Beam	Column	Log(K_χ)	ϑ [°C]
			Tot	Exp							
718	5.2	4.8	4	2	0.37	0.19	1.35	IPE120	HE100B	2.84	614

Table 7 Characteristics values of analysis considered for C4s mechanism.

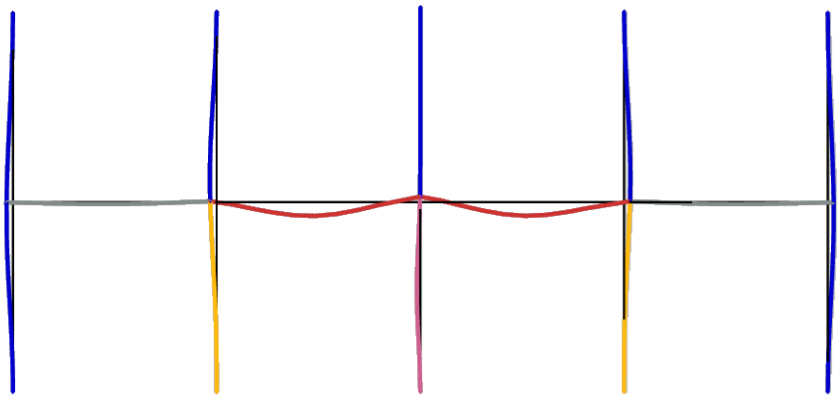

Figure 56 C4s Mechanism, structure 718 displacements at failure (t = 20 min).

Figure 56 shows the structure 718 at the collapse time. As you can see from the figure the structure is symmetric as concerns the geometry and the fire the maximum displacement of the structure is about 38 mm that is very small if we compare this displacement with the displacement achieved by the C1s mechanism (will be defined in further paragraph). If we compare the value reported in Table 6 and Table 7 we can note the different value associated to the load level of the beams and the load level associated to the columns. These two parameters play a central role in the definition of the collapse mechanism indeed we start from a higher value of μ_N most likely the structure will fail due to columns exposed by four side. Moreover the comparison of the two tables shows also a different value of I_c/I_b and a different value of $Log(K_\chi)$ that means that the structure should be characterized by high over resistance of the cross section of the column and a discrete deformability of the frame in fire condition.

a)

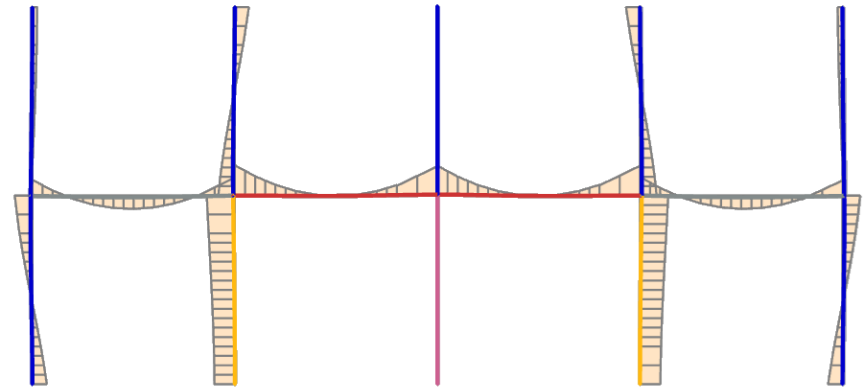

b)

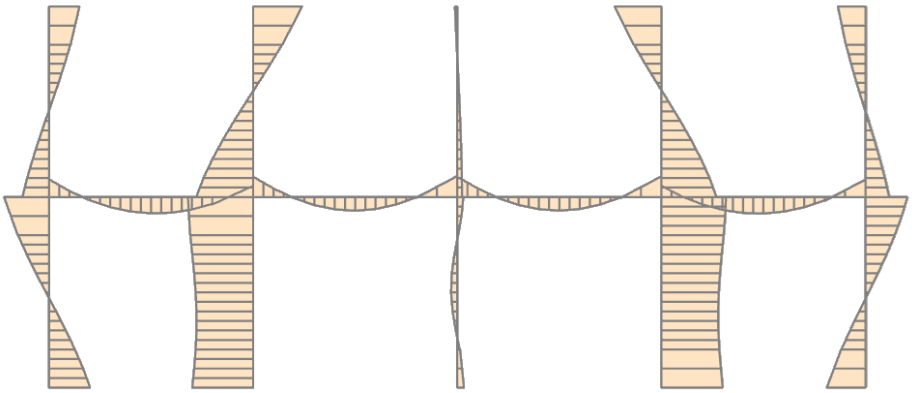

Figure 57 C4s Mechanism, structure 718, bending moment distribution a) t = 12 min b) t = 20 min.

Observing the distribution of the bending moment in the structure at collapse (Figure 57) we can see that around the central column that is the one exposed to four side by fire the bending moment is characterized by a sinusoidal shape. This particular distribution of the bending moment in the column exposed by four side is due to the stability loss of the column and it preannounces the collapse of the structure.

A non-linear analysis was performed in order to build the M-N interaction diagram (Compagnone et al. 2018) taking in account mechanical and geometrical non linearities. Figure 58 shows that the collapse occurs due to attainment of N_{cr}.

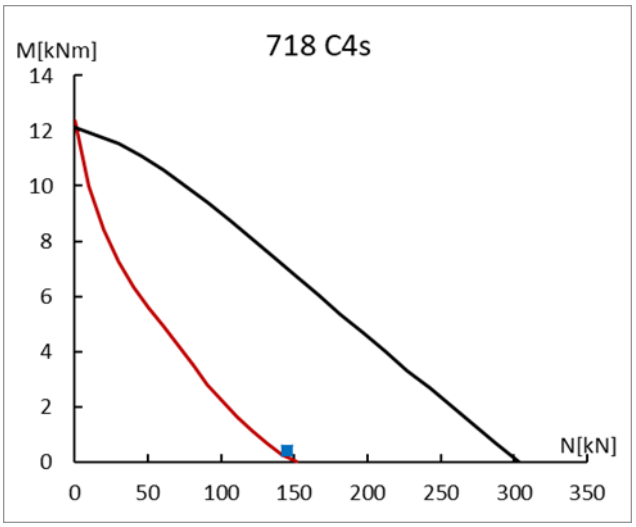

Figure 58 C4s Mechanism, safety check at collapse.

Regarding to the axial force (Figure 59), in structure 718 due to the low value of the $Log(K_\chi)$, there normal stress in beams aren't big as in the case of beam's mechanism. Moreover, the axial force in the beam, in case of structure 718 wasn't characterized by the classic evolution (increase decrease) because the deformability of the structure allows displacements and the heated beams doesn't risk the stability loss.

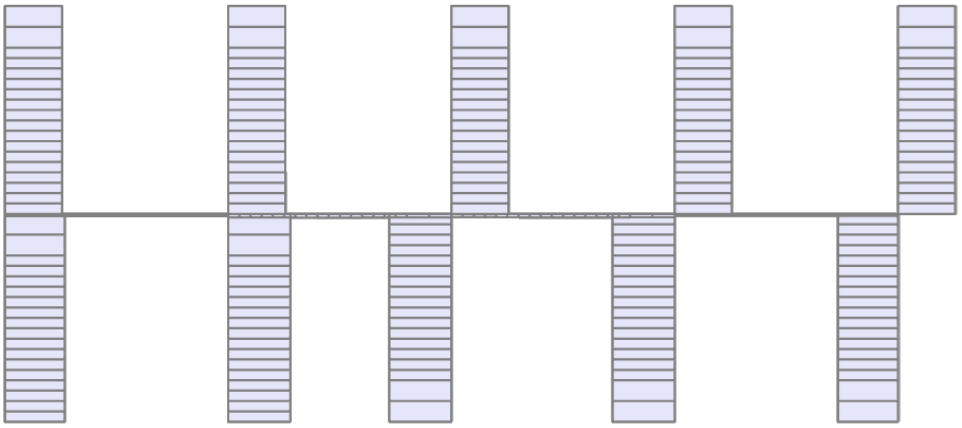

Figure 59 C4s Mechanism, structure 718, axial force distribution (t = 20 min).

4.5.4 ONE SIDE EXPOSED COLUMN'S MECHANISM

The C1s mechanism is the mechanism of collapse that involve columns exposed to fire by one side. In this mechanism of collapse temperature of structural elements, could be very low because the failure of the structure depends from the lateral stiffness of the frame and by the number of bays exposed to fire. In this type of collapse mechanism we have also the case of the single bay exposed to fire because this type of fire scenario (xB1Ex) there are only column exposed to fire by one side, so if the beam section is characterized by a low load level the collapse will be reached through the column failure. In Table 8 are reported principal parameters that identify the structures 1051 and 1187 defined as reported in 4.3 from the sample of the LHS simulation.

n°	L	H	Bays		μ_L	μ_N	I_c/I_b	Beam	Column	Log(K_χ)	ϑ [°C]
			Tot	Exp							
1051	5.7	5.6	4	3	0.54	0.28	1.05	IPE120	HE100A	2.47	174

Table 8 Analysis 1051Characteristics values. C1s mechanism.

In Figure 60 is reported the deformed shape of the structure 1051 in collapse condition. This structure collapse after 17 min, but the configuration of structure changes suddenly.

As you can see from the figure, two minutes before the collapse (Figure 60a) the structure's displacements are shaped as the B mechanism or C4s mechanism but when the structure fail the displacement of the left part of the structure are very different from displacements of the right part (Figure 61). In this case the columns exposed to fire are distributed asymmetrically in the substructure, for this reason when the temperature increase thermal effect are contrasted in different way form the two part of the structure. In particular, the unexposed column in the right part of the structure act as a spring.

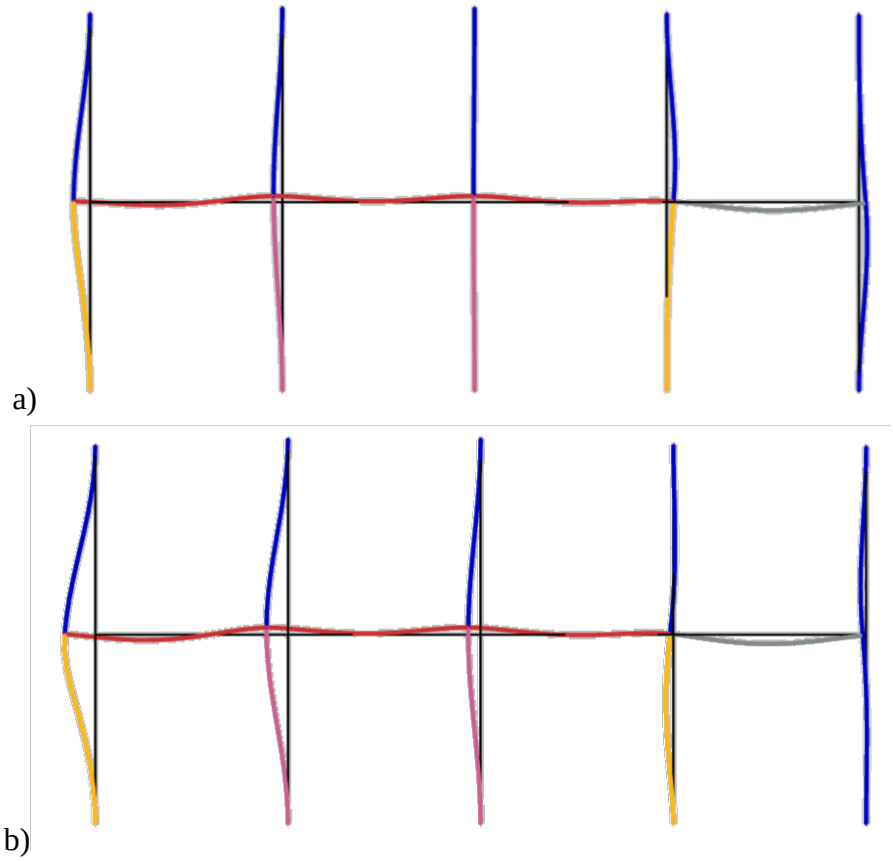

Figure 60 C1s Mechanism, structure 1051 at a) t = 15 min, b) t = 17min.

When thermal effects and the structural damage due to fire reach the limit of stability the one side exposed column in the left part of the structure tends to displace. While in the first part of the fire one side exposed column take part in the resistant mechanism and it is useful to transfer the load on the unexposed column pushing it to right, now due to stiffness and resistance loss displacement tends to diverge and the unexposed column is pushed by the unexposed column to left because this last structural element tends to discharge itself. In last seconds the displacement of the one side exposed column are too big that the unexposed column see the rest of the structure as a lateral load, indeed to stabilize the structure the unexposed column tends to contrast the displacement but it is not enough resistant and the whole substructure collapse (Figure 60b).

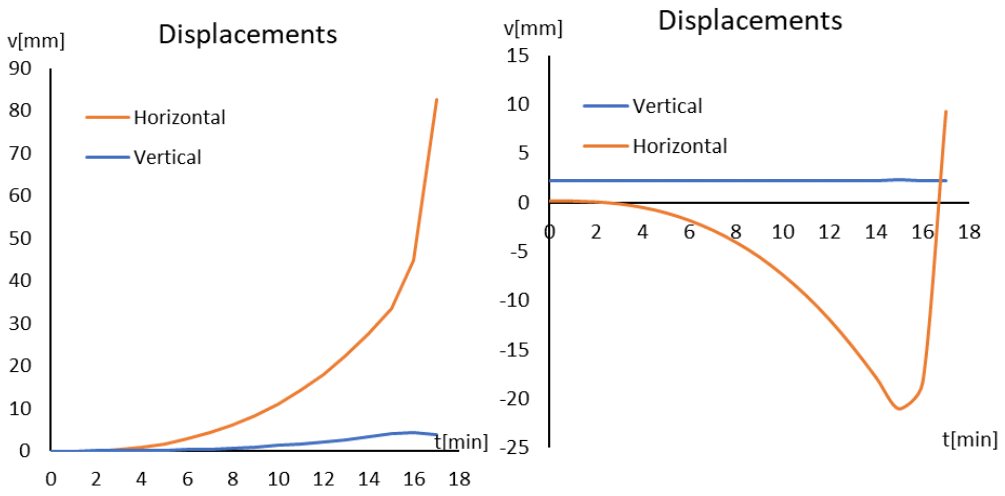

a) b)

Figure 61 Structure 1051 displacements, structure 1051 of a) left node, b) right node.

The C1s collapse happen when the frame's columns are characterized by a very low inertia, big temperature gradients and structural' asymmetry. If the inertia of the column is sufficiently high the first element that collapse with a high probability is the beam. If the structure is gradually heated the failure should depends from the column exposed by four side because there is a higher flow that enter in the cross section. The structural asymmetry influences this mechanism of collapse because the C1s failure as already shown is triggered by the lateral displacement of the structure.

n°	L	H	Bays		μ_L	μ_N	I_c/I_b	Beam	Column	Log(K_χ)	ϑ [°C]
			Tot	Exp							
1187	4.7	5.4	2	1	0.43	0.02	1.35	IPE270A	HE180M	3.68	92

Table 9 Analysis 1187. Characteristics values. C1s mechanism.

As regard structure 1187, it is displayed in Figure 62. This structure is characterized by a very low collapse averaged temperature (92°C) and collapse cross section's maximum temperature (202°C). As you can see from figure, the structure after 15 min (collapse) is characterized by a burden of stresses in columns due to bending moment induced by thermal effects, whereas the bending moment in beams doesn't change much. Moreover, the asymmetry of the fire causes a bigger displacement in the left side of the structure.

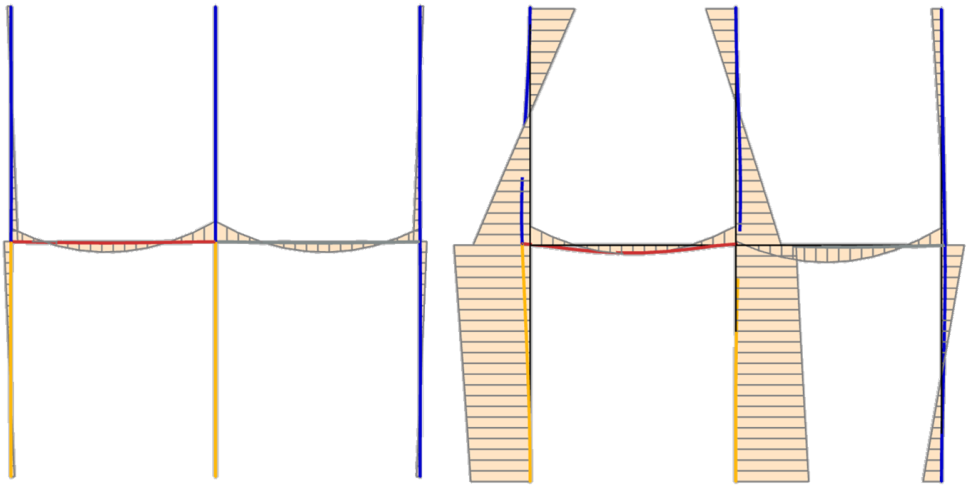

Figure 62 Structure 1187 at t =0 min (left) and t=15 min (right).

Note that while temperature in the collapsed element is 92°C temperature in the exposed beam is 603 °C. In this condition the beams have almost yield because considering the reduction factor $k_{y,\vartheta}(600) = 0.47$, but the collapse happen because the resistance is equal to the demand in the left column. If we consider Table 2, also if we assume the maximum temperature uniform in the cross section we obtain only a reduction of 10% of the Eulerian Buckling load. For this reason, we can say that collapse was induced by thermal effects of the beam that should be added to thermal effect on the columns. In order to investigate this phenomenon, it was performed a second analysis where the column exposed to one side was replaced by column exposed by four side (1187mod).

The structure with the four-side exposed column, displayed in Figure 63 characterized by the same collapse time (15 min) but in this case the structure fails due to stiffness decay of columns. In the new structure 1187 temperature in column is higher more than 4 time the original structure, indeed the mean temperature is 411 °C and the maximum temperature is 451 °C.

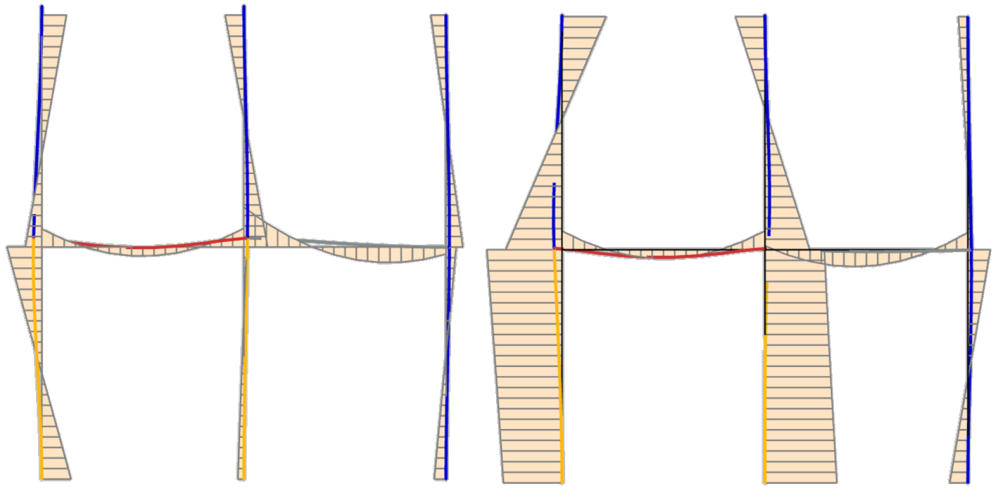

Figure 63 Structure 1187mod with four side exposed columns vs structure 1187 with column exposed by one side.

Observing Figure 63 we can see that the bending moment in unexposed column for structure 1187 is higher than the bending moment in the case of 1187mod. The stress burden in the unexposed column is due to thermal effect in column: since the column is heated from the side of the exposed beam the column should displace itself to outside causing the bending moment increase in the unexposed column.

Finally note that the slope of the bending moment on the perimetral exposed column for structure 1187mod is higher than structure 1187. This means that the shear on column in higher in 1187mod and this phenomenon can be justified if we think at the thermal effect on central column. In 1187 thermal effects in the central column push to the right the structure and stresses the unexposed column. The displacement of the central column allows the elongation of the exposed beam and for this reason the shear on the left column is lower than 1187 mod. In Figure 64 are displayed safety checks in section involved in collapse. Demand's points referring to stresses in column at collapse instant. Points on the right side are relative to the stress at foot of central column whereas points on the left referring to head of perimetral column.

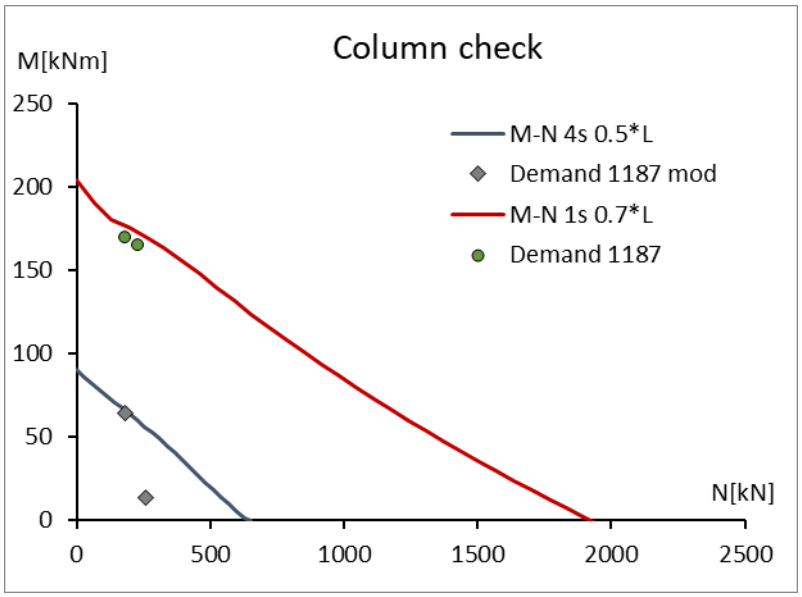

Figure 64 Safety checks for Structure 1187mod and Structure 1187.

4.6 Formulation of the probabilistic model

We refer to the critical temperature of the generic structural element ξ (i.e., $\xi = T_{c,b}$ for the beams, $\xi = T_{c,4s}$ for the columns exposed on 4 sides and $\xi = T_{c,3s}$ for the columns exposed on 3 sides.

On the basis of the idea of Gardoni et al. (2002a), the probabilistic model can assume a formulation expressed by the following equation:

$$C_\xi(\mathbf{x}, \boldsymbol{\Theta}_\xi) = \hat{c}_\xi(\mathbf{x}) + \gamma_\xi(\mathbf{x}, \boldsymbol{\theta}_\xi) + \sigma_\xi \varepsilon \qquad 4.15$$

This expression is a function of a global set of unknown parameters $\boldsymbol{\Theta}_\xi = (\boldsymbol{\theta}_\xi, \sigma_\xi)$, in which $\boldsymbol{\theta}_\xi$ represents the subset of the unknown parameters and σ_ξ is the standard deviation of the model error; $\hat{c}_\xi(\mathbf{x}) = ln[\,\hat{\xi}(\mathbf{x})]$ is the deterministic model and $\gamma_\xi(\mathbf{x}, \boldsymbol{\theta}_\xi)$ are the correction terms.

4.6.1 DETERMINISTIC MODELS FOR THE CRITICAL TEMPERATURE

As already said, the probabilistic study aims to correct a deterministic model by adding some quantities that depends from model parameters. For the deterministic model of the critical temperature we refer to the empirical formula implemented in the EN 1993-1-2:

$$\hat{\vartheta}(\mathbf{x}) = 39.13\, ln\left(\frac{1}{0.9674 k_1 k_2 \mu_0^{3.833}} - 1\right) + 482 \qquad 4.16$$

where $\mu_0 = E_{fi,d}/R_{fi,d,0}$, in which $E_{fi,d}$ represent stresses at and $R_{fi,d,0}$ represent the resistance at the beginning of fire. Coefficients k_1 and k_2 variates between 0.7 and 1 in dependence of exposition of elements to fire.

The simplified model of EC3 was chosen because widely accepted till now. The simplified analysis through deterministic model of EC3 is based on some hypotheses:

1. Single member Analysis: this simplification is assumed safe enough to perform structural analysis without taking into account the variation of internal stresses due to thermal actions that could arise in structural members;
2. No Combined Actions: The method of the critical temperature is based on the disequation:

$$\frac{S}{k_y(\vartheta)R_{t_0}} \leq 1$$

where S is the force and R is the resistance. If the resistance at each analysis timestep can be written as the resistance at the time t_0 multiplied for the reduction factor $k_y(\theta)$, if we define the load level as

$$\mu_0 = \frac{S}{R_{t_0}} \quad \rightarrow \quad \frac{\mu_0}{k_y(\vartheta)} \leq 1 \quad \rightarrow \quad \mu_0 \leq k_y(\vartheta)$$

If there is no combined actions this operation can be easy done, but if we take into account instability or an advanced safety criteria the resistance has non linear dependence by $k_y(\vartheta)$ so this method can't be used. Note that if a simplified linearized model of resistance's criteria is adopted the critical temperature method remains valid also in case of combined actions;

$$\frac{N}{k_y(\vartheta)N_{pl,t_0}} + \frac{M}{k_y(\vartheta)\, M_{pl,t_0}} \leq 1$$

3. No second order effects and no instability: this simplifications neglects second order effects that can arise due to stiffness' decay;
4. Steel strength decay defined as $k_y\,(\vartheta)$, which is a deterministic variable.

Using the regression model that was calibrated on the results of structural non linear analysis with two zone fire model, we can remove all hypotheses excepting hypothesis 4.

This deterministic model is generally not recommended when we deal with natural fire curves, but even if it has a lot of limitation it is characterized by a very simple formulation and returns not too wrong results, as it will be observed in section 5.4.

4.6.2 MODELS' CORRECTIONS

Referring again to Gardoni et al. (2002a), the correction terms $\gamma_\xi(\mathbf{x}, \boldsymbol{\theta}_\xi)$ can be written, for example, as a complete first order polynomial

$$\gamma_\xi(\mathbf{x}, \boldsymbol{\theta}_\xi) = \boldsymbol{\theta}_\xi^T \mathbf{h}(\mathbf{x}) = \sum_{i=0}^{n} \theta_{\xi,i} h_i(\mathbf{x}) \qquad 4.17$$

in which $\mathbf{h}$ is a vector of explanatory functions $h_i(\mathbf{x})$ obtained by applying the Yang transformation expressed in Eqs. (2) and (3) to a set of basis functions $\eta_{k,i}(\mathbf{x}_k)$, that is $h_i(\mathbf{x}) = ln[\,\eta_i(\mathbf{x})]$.

To develop the proposed models, we consider as an initial candidate explanatory function $h_0(\mathbf{x}) = 1$, in order to capture the potential bias of the deterministic models of each of the two components, that is independent of $\mathbf{x}$. Specifically, to inspect the potential bias associated to each component of $\mathbf{x}$, we also consider $\eta_2(\mathbf{x}) =$ Area $[m^2]/200$, $\eta_3(\mathbf{x}) = o$, $\eta_4(\mathbf{x}) = q_f[MJ/m^2]$, $\eta_5(\mathbf{x}) = RHR_{fi}/500kW/m^2$, etc.

4.6.3 MODEL SELECTION

A stepwise deletion process is used to simplify the models, removing the unimportant terms and obtaining the most parsimonious form of the model. In this paper, we use a stepwise deletion process developed by Gardoni et al. (2002a) that is applicable to all data types. The normality assumption of the model error has been verified by diagnostic plots at each step of the process as indicated by Rao and Toutenburg (1999). The stepwise deletion process, adopted for the generic set of data q-th set of data $(\mathbf{y}_{\xi,q}, \mathbf{x}_q)$, concerns the following steps:

1) Compute the posterior mode of the parameters $\boldsymbol{\Theta}_\xi$ and the related approximation of covariance matrix using the formulation $\boldsymbol{\Sigma}_{\boldsymbol{\Theta}_\xi \boldsymbol{\Theta}_\xi} = -\{\nabla\nabla\, ln[L(\boldsymbol{\Theta}_\xi|\mathbf{y}_{\xi,q})p(\boldsymbol{\Theta}_\xi|\mathbf{y}_{\xi,1}, \dots, \mathbf{y}_{\xi,q-1})]\}^{-1}$, referring to Richards (1961).

2) Identify the term $h_i(\mathbf{x})$ whose coefficient $\boldsymbol{\theta}_\xi$ has the largest coefficient of variation (C.o.V.). Such a term is the least informative among all the explanatory functions, so one can choose to drop it from the correction term $\gamma_\xi(\mathbf{x}, \boldsymbol{\theta}_\xi)$.

3) Assess the reduced model by checking if the value σ_ξ has not increased by an unacceptable amount. If so, accept the reduced model and repeat the step 1 and 2 for further reductions. Otherwise, the performed reduction is not desirable and the model form before such a reduction is as parsimonious as possible.

4) Compute the posterior statistics of the parameters $\boldsymbol{\Theta}_\xi$ as described in the section 3.8.3.

It is worth noting that what makes unacceptable the increase of σ_ξ is the level of accuracy and, at the same time, of parsimony desired for the specific problem.

4.6.4 BAYESIAN UPDATING, DEFINITION OF THE LIKELIHOOD FUNCTION AND PRIOR DISTRIBUTION

The Bayesian updating rule for the generic set of data q-th set of data $(\mathbf{y}_{\xi,q}, \mathbf{x}_q)$, expressed in the Equation 4.18 can be written as

$$p(\boldsymbol{\Theta}_\xi|\boldsymbol{y}_{\xi,1}, \dots, \boldsymbol{y}_{\xi,q}) = \kappa_\xi L(\boldsymbol{\Theta}_\xi|\boldsymbol{y}_{\xi,q}) p(\boldsymbol{\Theta}_\xi|\boldsymbol{y}_{\xi,1}, \dots, \boldsymbol{y}_{\xi,q-1}) \qquad 4.18$$

where $p(\boldsymbol{\Theta}_\xi|\mathbf{y}_{\xi,1}, \dots, \mathbf{y}_{\xi,q})$ is the posterior distribution of the unknown parameters $\boldsymbol{\Theta}_\xi$, $L(\boldsymbol{\Theta}_\xi|\mathbf{y}_{\xi,q})$ is the likelihood function, $p(\boldsymbol{\Theta}_\xi|\mathbf{y}_{\xi,1}, \dots, \mathbf{y}_{\xi,q-1})$ is the prior distribution and $\kappa_\xi = [\int L(\boldsymbol{\Theta}_\xi|\mathbf{y}_{\xi,q}) p(\boldsymbol{\Theta}_\xi|\mathbf{y}_{\xi,1}, \dots, \mathbf{y}_{\xi,q-1}) d\boldsymbol{\Theta}_\xi]^{-1}$ is the normalizing factor, all related to the q-th updating.

Observed values of the failure lead to the following expression of the l-th residual $r_{\xi,q,l}$ related to the transformed reading $C_{\xi,q,l}(y_{\xi,q,l})$:

$$r_{\xi,q,l}(\boldsymbol{\theta}_\xi) = C_{\xi,q,l}(y_{\xi,q,l}) - \hat{c}_\xi(\boldsymbol{x}_{q,l}) - \gamma_\xi(\boldsymbol{x}_{q,l}, \boldsymbol{\theta}_\xi) \qquad 4.19$$

that is $r_{\xi,q,l}(\boldsymbol{\theta}_\xi) = \sigma_\xi \varepsilon_l$. Cases where the failure is not observed in the considered element can be treated as censored data. It means that $r_{\xi,q,l}(\boldsymbol{\theta}_\xi) < \sigma_\xi \varepsilon_l$

and, wherever ξ have a physical upper bound ξ_{lim}, also that $r_{\xi_{lim},q,l}(\boldsymbol{\theta}_\xi) \geq \sigma_\xi \varepsilon_\xi$, in which

$$r_{\xi_{lim}}(\boldsymbol{\theta}_\xi) = C_{\xi_{lim}} - \hat{c}_\xi(\boldsymbol{x}_{q,l}) - \gamma_\xi(\boldsymbol{x}_{q,l}, \boldsymbol{\theta}_\xi) \tag{4.20}$$

Under the assumption of statistically independent observations, we obtain the general form of the likelihood function

$$L(\boldsymbol{\theta}_\xi, \sigma_\xi | \boldsymbol{y}_{\xi,q}) \propto \prod_{\text{Equality Data } l} P[\sigma_\xi \varepsilon_l = r_{\xi,q,l}(\boldsymbol{\theta}_\xi)] \times \prod_{\text{Censored Data } l} P[r_{\xi,q,l}(\boldsymbol{\theta}_\xi) \geq \sigma_\xi \varepsilon_l > r_{\xi,q,l}(\boldsymbol{\theta}_\xi)] \tag{4.21}$$

Since ε has a standard normal distribution, we can write:

$$L(\boldsymbol{\theta}_\xi, \sigma_\xi | \boldsymbol{y}_{\xi,q}) \propto \prod_{\text{Equality Data } l} \left\{ \frac{1}{\sigma_\xi} \varphi \left[\frac{r_{\xi,q,l}(\boldsymbol{\theta}_\xi)}{\sigma_\xi} \right] \right\} \times \prod_{\text{Censored Data } l} \left\{ \Phi \left[\frac{r_{\xi_{lim},q,l}(\boldsymbol{\theta}_\xi)}{\sigma_\xi} \right] - \Phi \left[\frac{r_{\xi,q,l}(\boldsymbol{\theta}_\xi)}{\sigma_\xi} \right] \right\} \tag{4.22}$$

where $\varphi(\cdot)$and $\Phi(\cdot)$ respectively represent the standard normal probability density function and the corresponding cumulative distribution function.

Considering a non-informative prior distribution for the parameters $\boldsymbol{\theta}_\xi$, and referring to Box and Tiao (1992), it is possible to proof that it is locally uniform, while, following Gardoni et al. (2002a), for σ_ξ we adopt $p(\sigma_\xi) \propto 1/\sigma_\xi$, so that the prior distribution assumes the form

$$p(\boldsymbol{\theta}_\xi) \propto \frac{1}{\sigma_\xi} \tag{4.23}$$

4.6.5 CALIBRATED PROBABILISTIC MODELS

Structural steel is commonly considered as non-resistant above a limit of 1200°C. Thus, we consider $C_{\xi_{lim}} = ln(\xi_{lim}) = ln(1200)$. In order to well understand the developed regression model, the estimation of parameters was conducted in two ways. First a regression with all possible parameters was created, based only on information about the failure of the structures (equality data). Once regression parameters were estimated a stepwise deletion process was implemented in order to simplify the model. Finally, to observe the effects of information about non-failed structures a second set of data was used to estimate one more time parameters of regression models. The second set contains information about failed structures and information about non-failed structures used as lower bounds for the critical temperature estimation (named set of censored data). Information of non-failed structures influences the computation of likelihood function (Eq. 4.22).

The regression model was developed using results of 2D thermomechanical analyses. Even if structural analysis was performed without taking into account the out-of-plane flexural buckling the regression model predict the critical temperature independently from the direction of the stresses respect the strong (or weak) axis of the section. In case we are analysing the frame where columns are disposed on the weak axis, parameters should be computed (in this case $W_{pl,col}$) referring to the weak axis of the column. Of course, the developed model can't be used in case of combined flexural bending moment actions M_x, M_y.

4.6.5.1 PROBABILISTIC MODEL FOR THE CRITICAL TEMPERATURE OF BEAMS

The results of the stepwise deletion and the estimation of the posterior statistics of the parameters $\boldsymbol{\Theta}_{T_{c,b}}$ for the two set of data are presented here. Considering first the complete model with all the candidate explanatory functions and using the first set of data ($\mathbf{y}_{T_{c,b},1}, \mathbf{x}_1$), we find that the parameter $\theta_{T_{c,b},10}$ has the largest COV (=2.37); hence, to simplify the model, we drop the term $\theta_{T_{c,b},10}\, ln(I_c/I_b)$. Next, we assess the reduced model and repeat the steps of the stepwise deletion. After 15 steps, the model selection process identifies $h_2(\mathbf{x})$, $h_3(\mathbf{x})$, $h_5(\mathbf{x})$, $h_7(\mathbf{x})$, $h_{15}(\mathbf{x})$ and $h_{17}(\mathbf{x})$. Figure 65 summarizes the stepwise

deletion, showing the values of the COV of the model parameters and the posterior mode of the model standard deviation $\sigma_{T_{c,b}}$.

The posterior statistics, reported in Table 10, define the following form of the probabilistic model $C_{T_{c,b}}(\mathbf{x}, \boldsymbol{\Theta}_{T_{c,b}}) = ln[\,T_{c,b}(\mathbf{x}, \boldsymbol{\Theta}_{T_{c,b}})]$:

$$
\begin{aligned}
&ln[\,T_{c,b}(\boldsymbol{x}, \boldsymbol{\Theta}_{T_{c,b}})] \\
&\quad = ln\left[39.13\, ln\left(\frac{1}{0.9674\mu_0^{3.833}} - 1\right) + 482\right] + \theta_{T_{c,b},2}\, ln(o) \\
&\quad + \theta_{T_{c,b},3}\, ln(q_f) + \theta_{T_{c,b},5}\, ln(h) + \theta_{T_{c,b},7}\, ln(\mu_L) \\
&\quad + \theta_{T_{c,b},15}\, ln(Area, b) + \theta_{T_{c,b},17}\, ln(\mu_0) + \sigma_{T_{c,b}}\varepsilon
\end{aligned}
\qquad 4.24
$$

Considering then the second set of censored data $(\mathbf{y}_{T_{c,b},2}, \mathbf{x}_2)$, we obtain that the regression's parameters tends to remain the same and the deviation of estimated parameters decrease. This aspect can be predicted because the set of censored data contains even lower bounds that allows to increase the confidence of the regression model but can't radically change results of the computation. These oscillations don't influence the error of the regression, indeed $\sigma_{T_{c,b}}$ in both regressions is equal to 0.08. The posterior statistics, reported in Table 11.

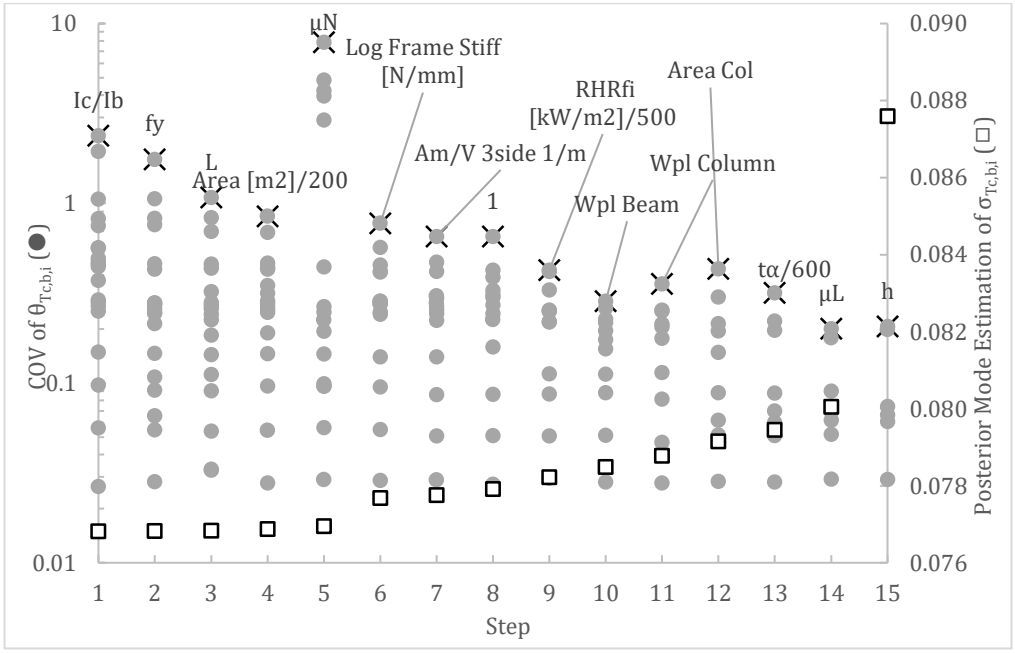

Figure 65 Stepwise deletion process of the critical temperature model for beams, using the first set of equality data.

	$\theta_{T_{c,b},2}$	$\theta_{T_{c,b},3}$	$\theta_{T_{c,b},5}$	$\theta_{T_{c,b},7}$	$\theta_{T_{c,b},15}$	$\theta_{T_{c,b},17}$	$\sigma_{T_{c,b}}$
Mean	−0.03	0.10	−0.11	−0.17	−0.05	0.23	0.08
SD	0.006	0.006	0.023	0.016	0.004	0.013	0.002
$\theta_{T_{c,b},3}$	−0.10						
$\theta_{T_{c,b},5}$	0.71	−0.45					
$\theta_{T_{c,b},7}$	−0.07	0.14	−0.09				
$\theta_{T_{c,b},15}$	0.14	−0.78	0.06	−0.05			
$\theta_{T_{c,b},17}$	0.04	−0.01	0.04	−0.79	0.09		
$\sigma_{T_{c,b}}$	0.04	−0.04	0.05	0.03	0.02	−0.05	

Table 10 Posterior statistics of parameters in the critical temperature model for beams. Equality data

	$\theta_{T_{c,b},2}$	$\theta_{T_{c,b},3}$	$\theta_{T_{c,b},5}$	$\theta_{T_{c,b},7}$	$\theta_{T_{c,b},15}$	$\theta_{T_{c,b},17}$	$\sigma_{T_{c,b}}$
Mean	−0.03	0.09	−0.07	−0.18	−0.05	0.23	0.08
SD	0.006	0.006	0.021	0.015	0.003	0.012	0.002
$\theta_{T_{c,b},3}$	−0.06						
$\theta_{T_{c,b},5}$	0.66	−0.45					
$\theta_{T_{c,b},7}$	0.00	0.14	−0.03				
$\theta_{T_{c,b},15}$	0.17	−0.76	0.06	−0.05			
$\theta_{T_{c,b},17}$	0.00	−0.02	0.03	−0.77	0.08		
$\sigma_{T_{c,b}}$	0.05	−0.04	0.09	−0.06	0.01	0.04	

Table 11 Posterior statistics of parameters in the critical temperature model for beams. Equality data and censored data

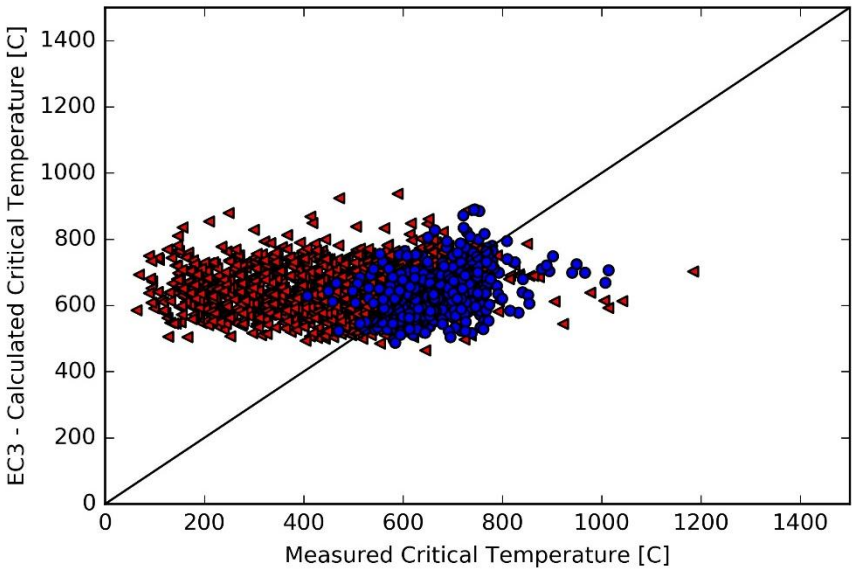

Figure 66 Comparison between measured and predicted the critical temperature for beams based on deterministic model.

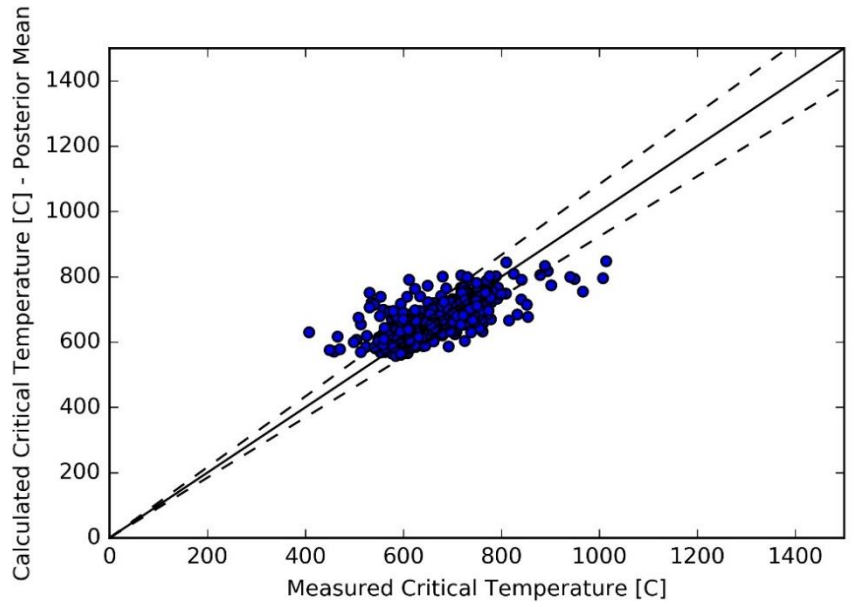

Figure 67 Comparison between measured and predicted the critical temperature for beams based on probabilistic model calibrated with the equality data.

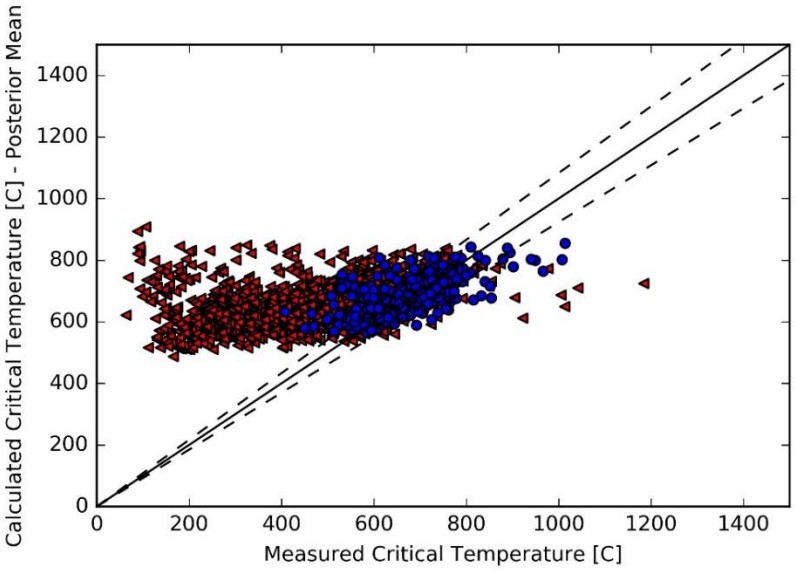

Figure 68 Comparison between measured and predicted the critical temperature for beams based on probabilistic model calibrated with the equality data and the censored ones.

4.6.5.2 PROBABILISTIC MODEL FOR THE CRITICAL TEMPERATURE OF COLUMNS EXPOSED ON 4 SIDES

As for the critical temperature of beams, the stepwise deletion is performed to reduce number of elements of $\boldsymbol{\Theta}_{T_{c,4s}}$. Figure 69 summarizes the stepwise deletion process. Considering the first set of data we note that the specific fire load lose its significance respect to the model evaluated for beams because the coefficient of variation of this parameter is the highest in this regression model (Figure 69). At the end of the deletion process the regression model assume the form reported in equation 4.25. This regression model is characterized by the dependence from a larger number of parameters respect the model of beam's mechanism.

Estimated parameters are characterized by a low standard deviation except for the constant $\theta_{T_{C4s},0}$ which is characterized by a CoV = 1.505.

The posterior statistics, reported in Table 12, define the following form of the probabilistic model $C_{T_{c,4s}}(\mathbf{x}, \mathbf{\Theta}_{T_{c,4s}}) = ln[\,T_{c,4s}(\mathbf{x}, \mathbf{\Theta}_{T_{c,4s}})]$:

$$
\begin{aligned}
& ln[\,T_{c,4s}(\mathbf{x}, \mathbf{\Theta}_{T_{c,4s}})] = \\
&= ln\left[39.13\, ln\left(\frac{1}{0.9674\mu_0^{3.833}} - 1\right) + 482\right] + \theta_{T_{c,4s},0} \\
&\quad + \theta_{T_{c,4s},7}\, ln(\mu_L) + \theta_{T_{c,4s},8}\, ln(\mu_N) + \theta_{T_{c,4s},9}\, ln(L) \\
&\quad + \theta_{T_{c,4s},11}\, ln\left(W_{pl,columns}\right) + \theta_{T_{c,4s},13}\, ln(Area, col) \\
&\quad + \theta_{T_{c,4s},18}\, ln\left(\frac{A_m}{V}\right) + \sigma_{T_{c,4s}}\varepsilon
\end{aligned}
\qquad 4.25
$$

Adding the second set of censored data, the standard deviation associated to parameters' estimation tends to decrease. In particular as regard the constant of the regression model, the standard deviation associated to $\theta_{T_{c4s},0}$ became 0.016. Finally, we have to highlight that considering the lower bounds information collected in the set of censored data the standard deviation of the whole model increase $\sigma_{T_{C4s}}^{Equality} = 0.07 < \sigma_{T_{C4s}}^{Censored} = 0.08$. This can be observed also comparing blue markers in Figure 71 and Figure 72, where for the regression model calibrated on the set of censored data we can see that blue markers tends to be more dispersed than the same markers in Figure 71.

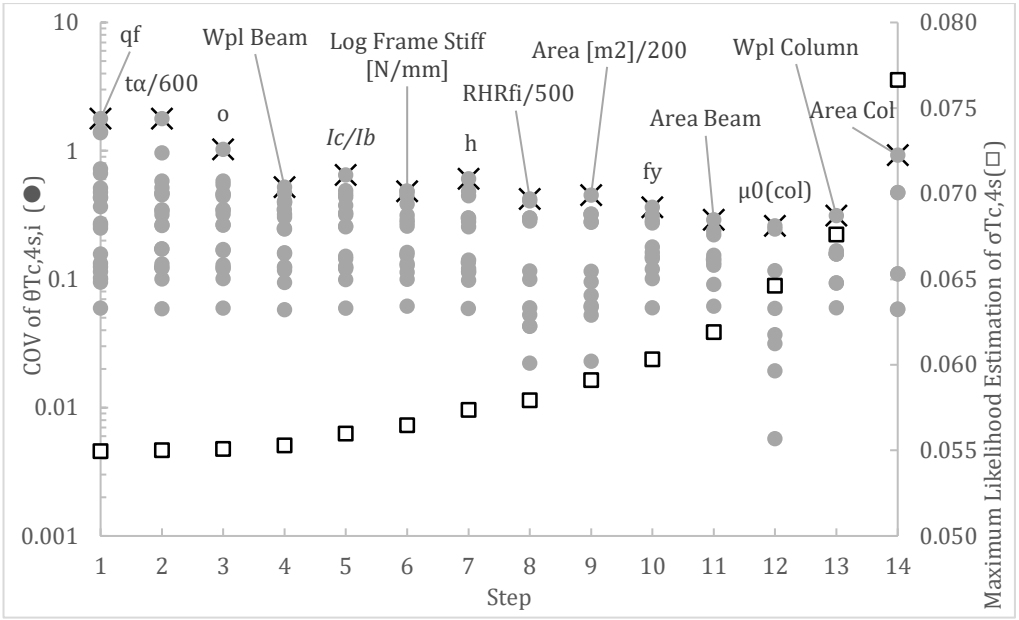

Figure 69 Stepwise deletion process of the critical temperature model for columns exposed on 4 sides, using the first set of equality data.

	$\theta_{T_{c,4s},0}$	$\theta_{T_{c,4s},7}$	$\theta_{T_{c,4s},8}$	$\theta_{T_{c,4s},9}$	$\theta_{T_{c,4s},11}$	$\theta_{T_{c,4s},13}$	$\theta_{T_{c,4s},18}$	$\sigma_{T_{c,4s}}$
Mean	−9.32	0.178	−0.11	0.10	−0.47	1.05	0.56	0.07
SD	1.505	0.017	0.010	0.031	0.077	0.171	0.095	0.004
$\theta_{T_{c,4s},7}$	−0.10							
$\theta_{T_{c,4s},8}$	0.19	0.09						
$\theta_{T_{c,4s},9}$	−0.18	0.13	−0.04					
$\theta_{T_{c,4s},11}$	0.97	−0.17	0.19	−0.15				
$\theta_{T_{c,4s},13}$	−0.99	0.14	−0.19	0.16	−0.99			
$\theta_{T_{c,4s},18}$	−0.98	0.07	−0.16	0.13	−0.92	0.95		
$\sigma_{T_{c,4s}}$	0.00	0.01	−0.01	0.00	0.00	0.00	−0.01	

Table 12: Posterior statistics of parameters in the critical temperature model for columns exposed on 4 sides.

	$\theta_{T_{c,4s},0}$	$\theta_{T_{c,4s},7}$	$\theta_{T_{c,4s},8}$	$\theta_{T_{c,4s},9}$	$\theta_{T_{c,4s},11}$	$\theta_{T_{c,4s},13}$	$\theta_{T_{c,4s},18}$	$\sigma_{Tc,4s}$
Mean	−9.70	0.20	−0.11	0.11	−0.53	1.15	0.54	0.08
SD	0.016	0.020	0.007	0.028	0.022	0.026	0.017	0.006
$\theta_{T_{c,4s},7}$	−0.72							
$\theta_{T_{c,4s},8}$	−0.15	0.17						
$\theta_{T_{c,4s},9}$	−0.67	0.19	0.04					
$\theta_{T_{c,4s},11}$	−0.31	−0.16	−0.21	0.05				
$\theta_{T_{c,4s},13}$	0.29	0.22	0.23	−0.11	−0.98			
$\theta_{T_{c,4s},18}$	−0.27	−0.06	−0.03	−0.10	0.89	−0.91		
σTc,4s	0.00	−0.11	0.03	−0.01	−0.02	0.07	−0.12	

Table 13 Posterior statistics of parameters in the critical temperature model for columns exposed on 4 sides.

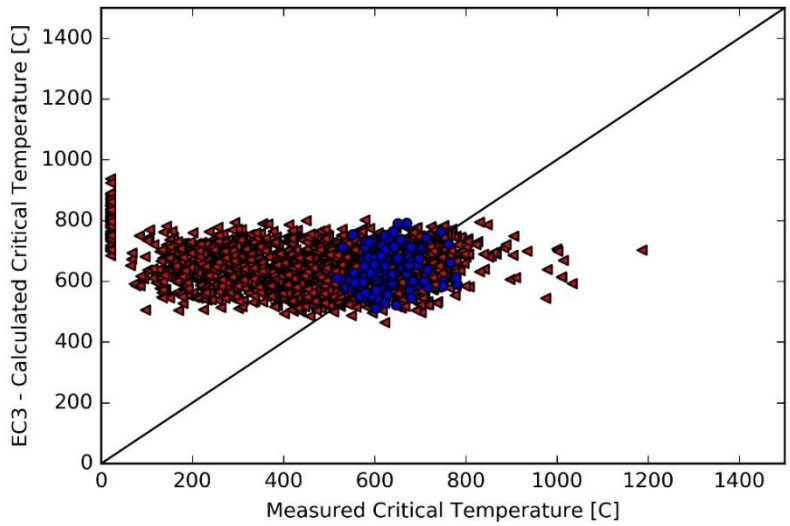

Figure 70 Comparison between measured and predicted the critical temperature for columns exposed on 4 sides, based on deterministic model.

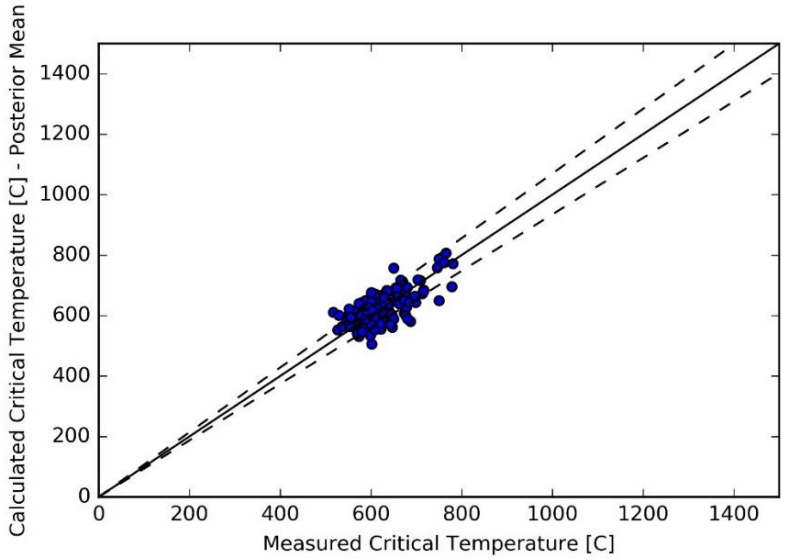

Figure 71 Comparison between measured and predicted the critical temperature for columns exposed on 4 sides, based on probabilistic model calibrated with the equality data.

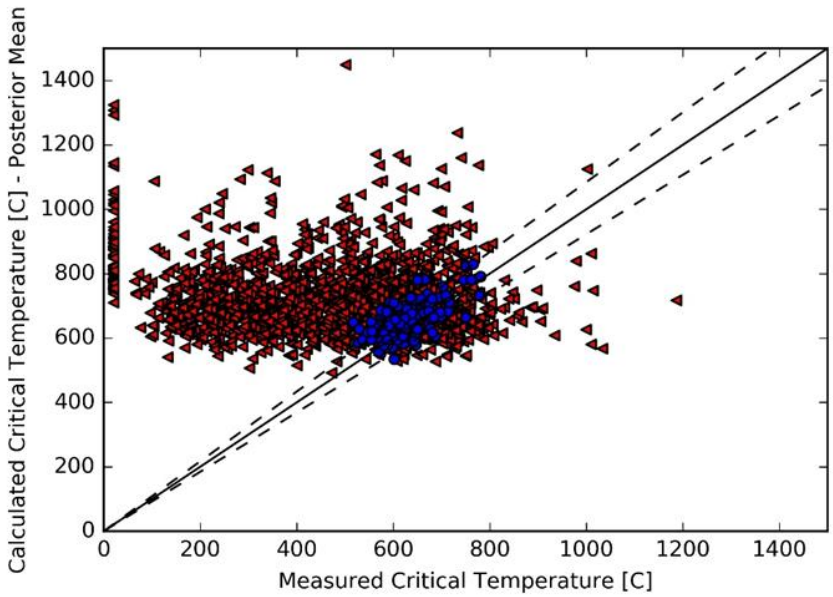

Figure 72 Comparison between measured and predicted the critical temperature for columns exposed on 4 sides, based on probabilistic model calibrated with the equality data and the censored ones.

4.6.6 APPLICATION

To test the developed probabilistic model the regression was applied neglecting last term of both formulation in order to use it as deterministic. Regression model was applied to the database in order to bench performances respect to the Eurocode 3 model. There is a comparison for each mechanism first, then the regression was applied to entire structures to test the accuracy of the model without take into account the collapse results, as in a real situation.

Regression model is calibrated on framed structure analysis results, critical temperature take into account thermal gradients and second order effects. Note that since critical temperature depends from the structure there are two types of thermal effects:

- Thermal effects that arise in analysed member and influence internal stresses;
- Thermal effects that arise in other part of the structure and influence external load applied on the analysed member.

Regression model takes into account both.

As regards second order effects are related to ones can arise in the substructure due to thermal expansion and due to large displacements.

Hypothesis on the damage law $k_y\ (\vartheta)$ for the steel constitutive law remain also in the regression model.

4.6.6.1 BEAM MECHANISM

In Figure 73 are reported on the x axis the ratios between the critical temperature measured with the deterministic model of Eurocode 3 and the measured critical temperature, whereas on the y axis the rations between the proposed model estimation and the measured critical temperature. As you can see from the figure, the proposed model has a best estimate more accurate than the EC3 model, indeed the distance between the dashed lines and the continuous lines for the proposed model is little than the Eurocode model. Since the proposed model is calibrated on the existing model (Eurocode 3), the regression adjusts results of the Eurocode where it is possible, otherwise the critical temperature tends to be equal to the temperature evaluated through EC3 model. For this reason, results have a positive correlation. Moreover, it was applied the model of the Eurocode 3 without taking

into account the correction factor of the load level for the beams (k = 1 instead of k =0.7). In this case, the error of the Eurocode model increase (Figure 74).

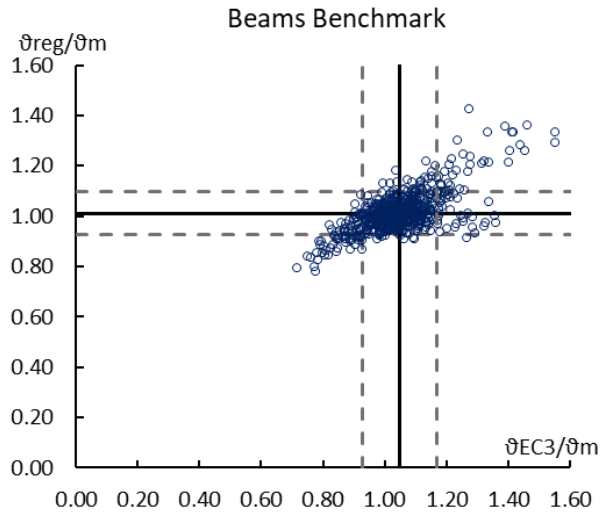

Figure 73 Comparison between the regression model, Eurocode model and measured Temperature.

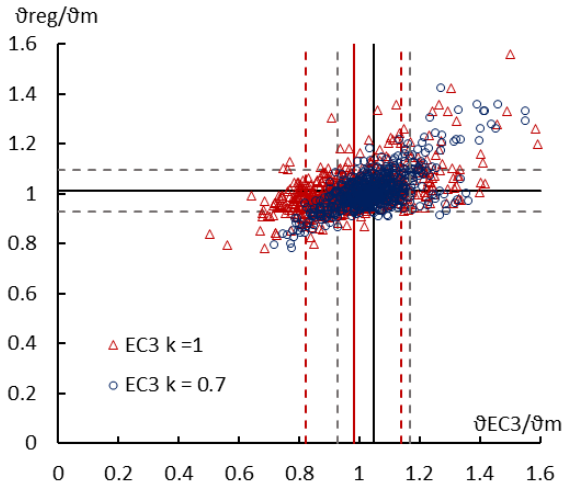

Figure 74 Comparison between the regression model, Eurocode model with k = 0.7, k = 1 and measured Temperature.

Regarding statistics, in Table 14 are reported the performance of the three models. As already said, the proposed model provides more accurate results, in terms of mean (101% vs 96%) and in terms of deviation (11.5% vs 8.4%). Despite

good results, note that the proposed model has an unsafe mean, but this can be adjusted with a safety factor.

	$\vartheta_{EC3,k=1}/\vartheta_m$	$\vartheta_{EC3,k=0.7}/\vartheta_m$	$\vartheta_{reg}/\vartheta_m$
Mean	98.2%	104.7%	101.1%
Dev. St.	15.8%	12.0%	8.4%

Table 14 Comparison of methods for beams.

4.6.6.2 COLUMNS MECHANISM

Regression applied to equality data relative to the C4s mechanism shows that the estimation of the critical temperature is slightly unsafe for both methods. This can be seen also from Table 15. The mean of the regression model is slightly lower than the Eurocode 3 model but it has a higher deviation.

	$\vartheta_{EC3}/\vartheta_m$	$\vartheta_{reg}/\vartheta_m$
Mean	106.1%	99.2%
Dev. St.	10.0%	8.5%

Table 15 Comparison of methods for columns.

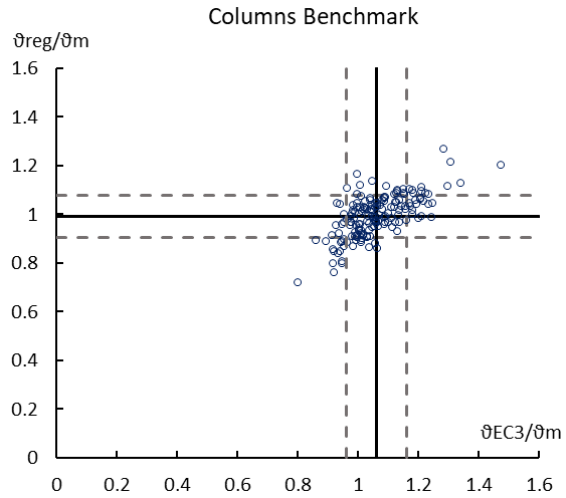

Figure 75 Comparison between the regression model, Eurocode model and measured Temperature.

4.6.6.3 EXAMPLE

This section shows four examples of application of the developed model. Selected substructures are reported in Table 17. As you can see from Table 17, substructures are heterogeneous and characterized by a number of bays exposed higher than one. For this reason, thermal effects related to elements exposed to fire could be very high, and in these structures, it can arise the chain effect due to the high number of spans.

N°	Sections		h	L	μ_L	μ_N	q_f	Bays	
	Beam	Column						Exposed	Total
[-]	[-]	[-]	[m]	[m]	[-]	[-]	[MJ/m²]	[-]	[-]
1411	IPEO400	HE340B	3.45	3.41	0.39	0.10	589	3	4
1611	IPE400	HE300B	4.00	4.25	0.33	0.29	255	2	5
180	IPEA160	HE120B	3.47	4.99	0.45	0.22	178	3	5
1391	IPEO200	HE160B	5.69	4.48	0.33	0.17	416	3	5

Table 16 Selected Substructures.

In Table 17 are reported other significant quantities needed by the regression model.

Parameters that user musts calculate to estimate the critical temperature is

$$\mu_L = {\frac{qL^2}{10}}\Big/{W_{pl}f_y}$$
$$\mu_N = {N_d}\Big/{A_c f_y} \qquad 4.26$$
$$\frac{A_m}{V}_c = \frac{p_c}{A_c}$$

Where N_d is the load applied on the top of the upper column of the substructure, q is the distributed load on the beams, f_y is the steel yield strength, A_c and W_{pl} are the column's cross section area and beam's cross section plastic modulus respectively and p_c is the perimeter of the column's cross section.

Moreover, to estimate the critical temperature it is needed the value of μ_0 and the ventilation factor of compartment exposed to fire. Regarding to μ_0 it is defined as the maximum load level of the substructure:

$$\mu_0 = max\left(\frac{N_d}{A\, f_y} + \frac{M_d}{W_{pl} f_y}\right) \qquad 4.27$$

The maximum load level μ_0 is calculated using a linear yield criterion. Note that the parameter μ_0 is lower than μ_L in some cases because this last is calculated assuming as bending moment in the joint the quantity $\frac{qL^2}{10}$. This assumption is due to the hypothesis that beams behaviour is in the middle between a fixed-pinned beam and a fixed-fixed beam. In truth, rotational deformation at the end of the beams depends from the structural context, so the real load level could be lower than μ_L and at the same time it should be even higher than μ_N because this dummy load level doesn't take into account the load transferred by the beams to the columns.

Regarding to ventilation factor o, it is defined as:

$$o = \frac{A_{v,tot}\sqrt{\frac{\sum_i h_i A_{v,i}}{A_{v,tot}}}}{A_{tot}} \qquad 4.28$$

Where $A_{v,i}$ and h_i are the vent's area and vent's height respectively, $A_{v,tot}$ is the sum of the vent's areas and A_{tot} is the total surface area of the compartment.

N°	h	L	μ_0	μ_L	μ_N	q_f	o	A_b	A_c	$W_{pl,c}$	$\frac{A_m}{V}_c$
[-]	[m]	[m]	[-]	[-]	[-]	MJ/m²	$[m^{1/2}]$	[mm²]	[mm²]	[cm³]	[1/m]
1411	3.45	3.41	0.36	0.39	0.10	589	0.042	9260	16464	2408	112
1611	4.00	4.25	0.38	0.33	0.29	255	0.017	8067	14282	1868	124
180	3.47	4.99	0.34	0.45	0.22	178	0.014	1548	3277	165	215
1391	5.69	4.48	0.25	0.33	0.17	416	0.004	3072	5232	353	180

Table 17 Other parameters needed by capacity models.

The application of the regression model starts with a thermal analysis of the section, which can be performed in several ways. In this case it was performed a non-linear transient analysis using as input the thermal data obtained from a two-zone model analysis. Once temperatures evolution in steel cross sections are known, it is possible to apply regression model for beams and columns in order to assess critical temperatures related to the single mechanism. To compute critical temperature we have to evaluate equations 4.24 and 4.25 using as input parameters values reported in Table 17.

In order to compare performance of the method with the numerical experimentation and the Eurocode model, critical temperatures computed with these methods were reported in Table 18. Observing temperatures in Table 18 we can see that the regression model let us to assess a more accurate critical temperature, improving the accuracy of the estimation of averaged percentage of 9 points. Moreover, as you can see from Table 18, the application of the regression model through the two expressions allows to improve the reliability of the method.

N°	***Eurocode 3***		***Regression***		***Numeric***		*Columns*		*Beams*	
	$\vartheta_{EC3,b}$	$\vartheta_{EC3,c}$	$\vartheta_{reg,b}$	$\vartheta_{reg,c}$	$\vartheta_{m,b}$	$\vartheta_{m,c}$	$\frac{\vartheta_{EC3,c}}{\vartheta_{m,c}}$	$\frac{\vartheta_{reg,c}}{\vartheta_{m,c}}$	$\frac{\vartheta_{EC3,b}}{\vartheta_{m,b}}$	$\frac{\vartheta_{reg,b}}{\vartheta_{m,b}}$
[-]	[°C]	[°C]	[°C]	[°C]	[°C]	[°C]	[-]	[-]		[-]
1411	689	664	677	679	691	682	0.97	1.00	1.00	0.98
1611	749	630	655	606	595	564	1.12	1.07	1.26	1.10
180	699	683	663	628	636	578	1.18	1.09	1.10	1.04
1391	742	710	718	669	631	607	1.17	1.10	1.18	1.14

Table 18 Results obtained through capacity models.

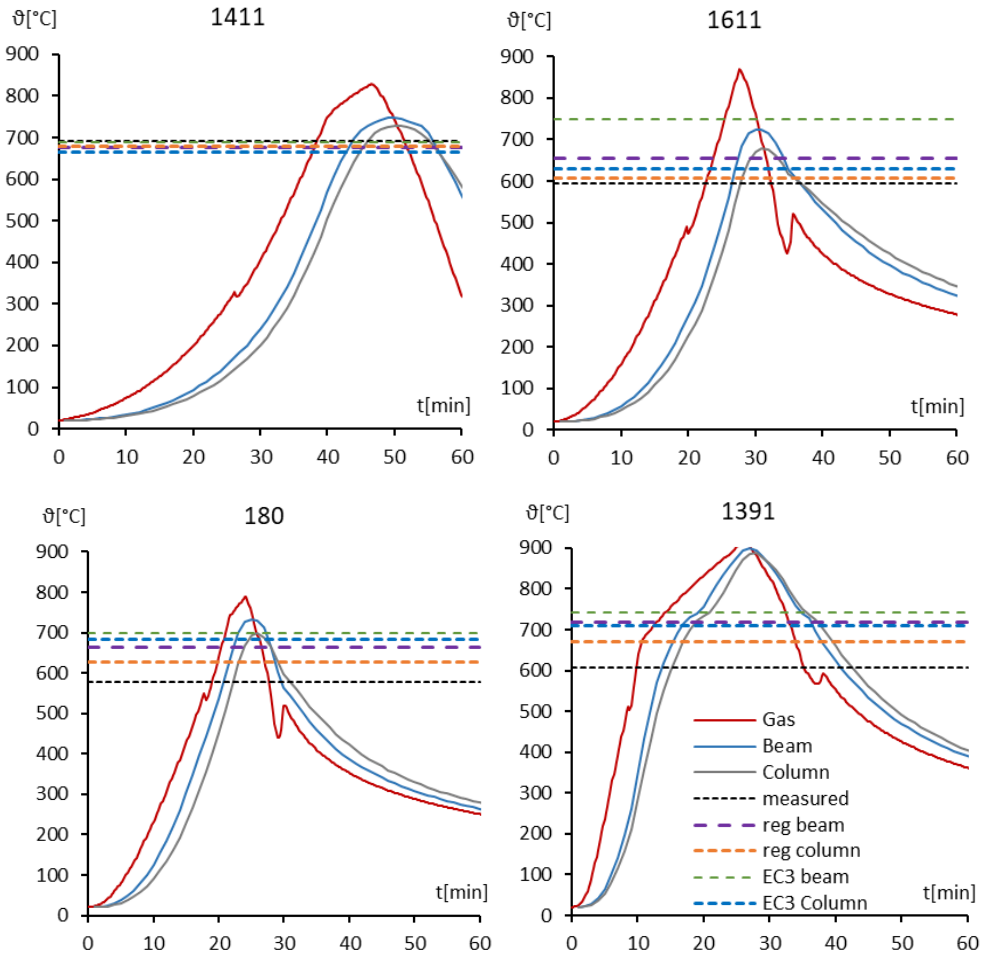

Figure 76 Thermal Analysis compared with critical temperatures.

When there is a bad prediction provided by a mechanism regression model the other mechanism cut off temperature adjusting results. Indeed, if the one regression model returns bad results, we can rely on the other regression that estimate another collapse temperature.

Figure 76 shows the results of thermal analysis conducted on considered substructures. Temperatures in cross sections (grey and blue lines), calculated using the fire analysis results (red line) show a delay in the heating phase and in the cooling phase due to the specific heat of the steel. The material's peak of specific heat traduces itself in a variation of the heating speed around 700 °C.

Values computed in Table 18 was displayed in these graph (dashed lines) in order to render the difference in terms of estimation of time and temperatures.

By the point of view of collapse time, we can see that even if critical temperature's estimation scatter is equal to 1.10 the structure's time of resistance assessment is very accurate. Moreover, due to the difference in the estimation of critical temperatures of column and beams we can obtain a wrong assessment of the collapse mechanism. This effect has a low influence on the results because temperatures difference in structural elements is generally lower than 100° C and critical temperatures are quite similar, for this reason even if the model return a wrong result, the real collapse mechanisms occur in a couple of minutes.

Analysed substructures are displayed in Figure 77. This figure shows also the deformed shape structures exposed to fire at failure. Note that structures Figure 77a and Figure 77b fail due to the collapse of the beams whereas Figure 77c and Figure 77d collapse due to the failure of the columns. Observing the deformed shapes of substructures we can see that while in Figure 77a the most disadvantaged element is the beam in the middle of spans involved in fire, the structure 1611 (Figure 77b) could cause uncertainty because even if the collapse registered is due to the beam failure the column is pushed to the right by the beam involved in fire.

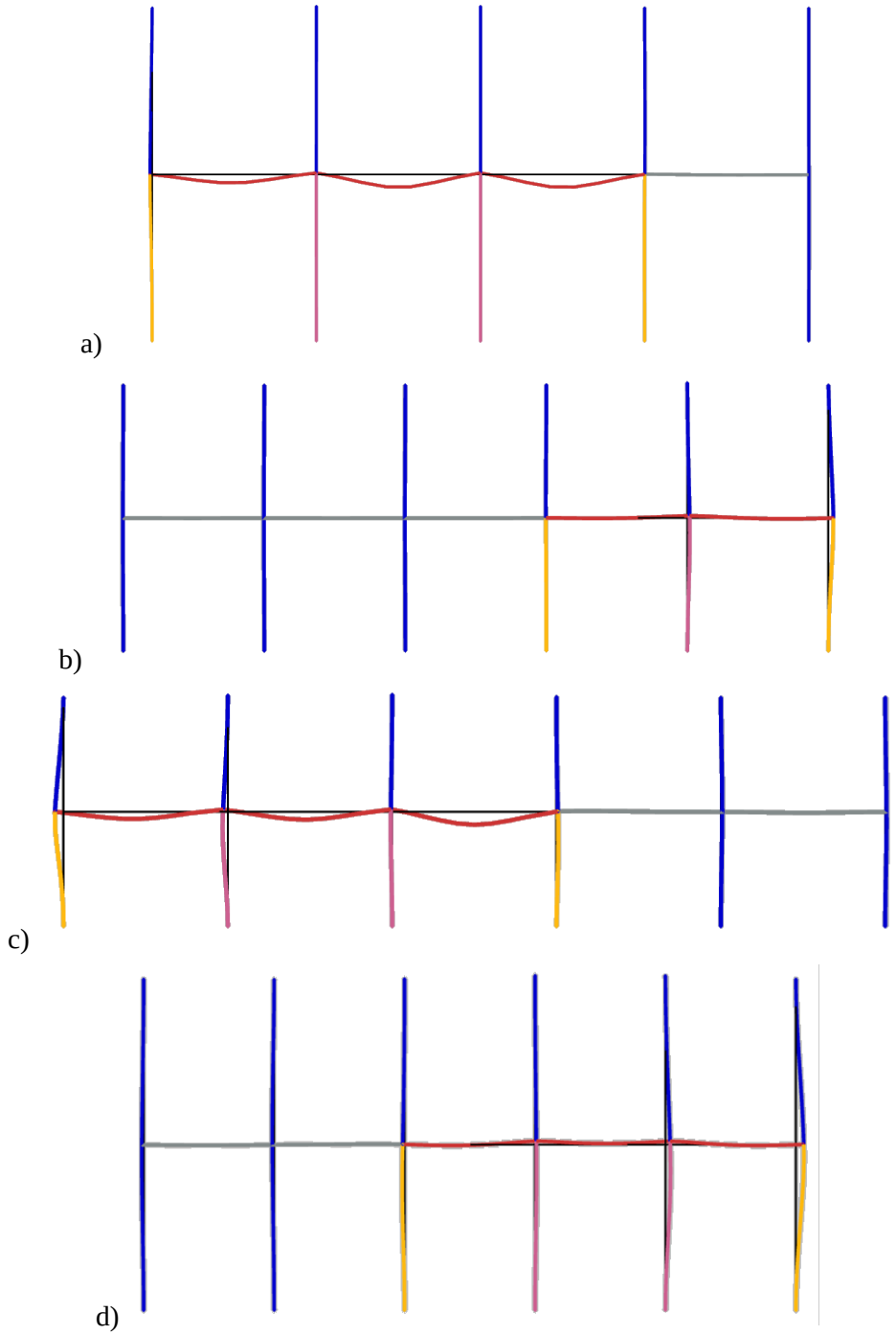

Figure 77 Analysed substructures a) 1411 b) 1611 c) 180 d) 1391.

Chapter 5

5 Observations on cluster

Database exploited to build regression model contains a lot of data that regard statistics of fire analysis and thermal analysis. In this section it will be analysed all analysis results in order to do some interesting observations on structural behaviours and other results.

Before that, a quick summary is needed in order to frame the context. The fist observation that we can do on the database regards the number of collapses and about the mechanism of collapse in order to do preliminary considerations. As you can see from Table 19, there are a high number of not collapsed structure. Regarding to collapsed substructures, we can see that the 762 (38.1%) samples can be classified in function of the failure mechanism. Table clearly shows that the more recurrent collapse mechanism is that relative to the beam's failure that characterize almost 75% of collapsed structures. On the contrary the failure of one side exposed column is a mechanism of collapse with lowest frequency of occurrence, indeed it interest only the 6% of collapsed structures, that decrease up to 2% considering the total amount of analysed structures.

	Collapsed			**Not collapsed**
	Beams	**Col4s**	**Col1s**	
Samples	601	166	29	1204
	796			
% total	0.300	0.083	0.014	0.602
% collapse	0.755	0.208	0.036	0

Table 19 Collapse's frequencies.

Next paragraph is focused on the Sampling results, where there will be proved the quality of sampling procedure through a comparison with a sample base four times little than the sample base used in regression model. Then will be showed the results obtained in terms of gas temperature in compartments. In this case some regression will be done to do some observation that can be used to rapid assessment of temperature in compartments. Once the aspects related to fire modelling are discussed, it will be analysed the stresses distribution in structures before fires, in particular regarding to the transformation of random variables given in input to the internal stress distribution evaluated in output of analysis. Finally, it will be showed the results of the sample base in order to draw conclusion about the rapid structural assessment relative to the collapse temperature.

5.1 Sampling results

The LHS and optimization procedure through the simulated annealing method allow to build correlation-controlled sample database. Using this procedure, we can be sure that the sample is representative of the entire population but bring with it some defects like the loss of flexibility. In simple Monte Carlo Simulation (MCS), if a cut off of the sample base is needed for any reason it can be done if the new sample base is big enough, thanks to the large numbers' law. Sampling in simple MCS, as already said is based on the random extraction of samples from CDF, and the desired correlation is achieved because there is a high quantity of numbers sampled on a set of CDFs related to each other. In this case the Latin Hypercube Sampling allow to build a small sample base, but without the simulated annealing the desired correlation cannot be achieved. The LHS optimized through the SA build a special sample that can't be modified after its creations but it allows to build very small samples, representative of entire population. Prove of that is reported in Figure 78, where are reported raw results in terms of collapse temperature of substructures. The figure shows the comparison between the results obtainable from two different sample base. The first is a small sample that was built to test tools used to manage FDA and MA, whereas the second one shows the raw results obtained from analysis of two thousand samples used in regression model. Observing Figure 78 we can see that the distribution of collapse temperature is very similar for both samples, changes regard only the density of the data.

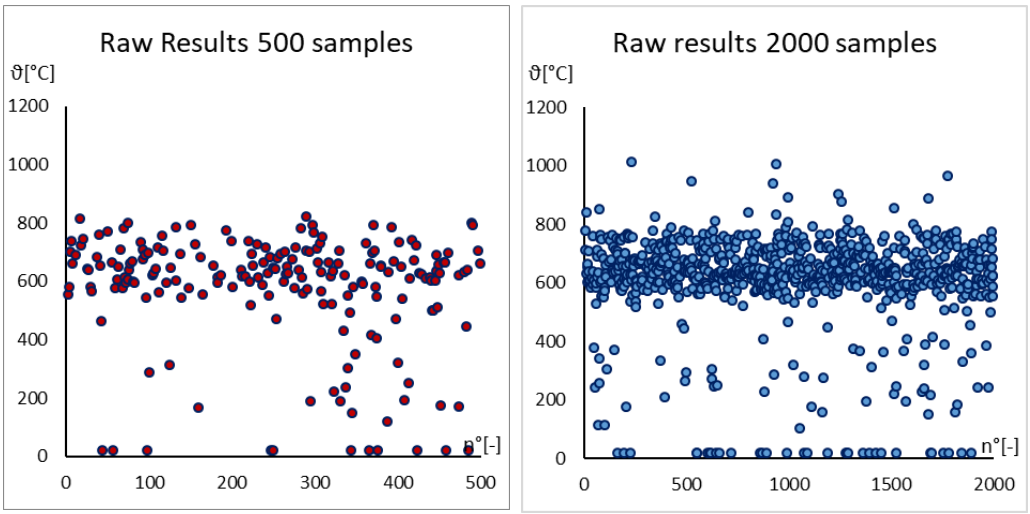

(a) (b)

Figure 78 Raw results of sample base: 500 Samples(a) and 2000 Samples(b).

5.2 Gas Temperature

Regarding to gas temperatures, the maximum temperature reached in compartment was stored in database. These data were processed in order to study their probability of occurrence.

The marginal probability was studied first, so it was defined 26 classes of temperatures where each one corresponds to a temperature interval of 50 °C then a relative frequency histogram was constructed. The division into classes was carried out using the criterion of equation 5.1:

$$x_j \in c_i \qquad if \qquad \delta_i \leq x_j \leq \delta_{i+1} \tag{5.1}$$

Where x_j is the single data of the sample, $c_i$is the i-th class, δ_i and δ_{i+1} are the separation's element that identify the class c_i.

The height of the i-th column relatives to the i-th class is evaluated as the ratio between the number of cases n_i that belong to the class c_i over the total number of cases.

$$h_i = \frac{n_i}{n_{tot}} \qquad 5.2$$

The frequency histogram was compared with several model of random variable, in particular they were considered the Normal Model, the Log-Normal Model and the Weibull Random Variable (Figure 79).

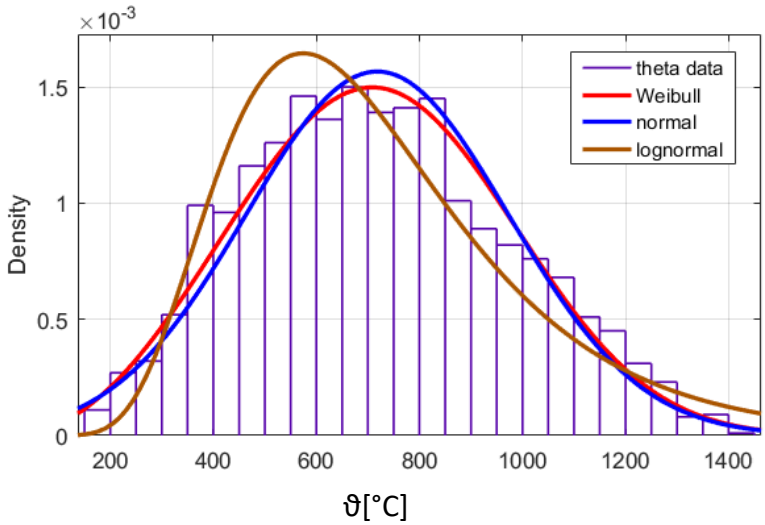

Figure 79 Frequency histogram, comparison between random variables.

This can be seen also from the probability plot (Figure 80) and CDFs (Figure 81). In particular from the probability plot we can see that the Lognormal distribution is the ones that has a good fit also for the data relatives to lower temperatures.

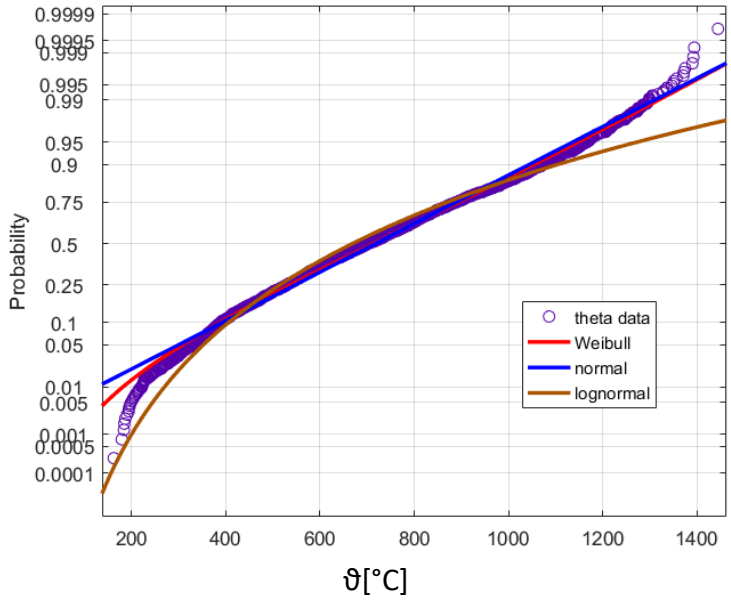

Figure 80 Probability plot.

In Table 20 estimated parameters for each random variable was reported. If we focus on the Normal distribution's parameters, we can see that the standard deviation is very high. Thanks to the property of the Gaussian distribution we know that the sum of mean and standard deviation coincides with the 84° percentile and the sum $\mu + 2\sigma$ is near the value of the 95° percentile.

Distribution	$\boldsymbol{\mu}$ ***or*** $\boldsymbol{\lambda}$		$\boldsymbol{\sigma}$ ***or*** $\boldsymbol{k}$	
	Estimate	*Std. err.*	*Estimate*	*Std. err.*
Weibull	804.20	6.14	3.08	0.053
Normal	718.08	5.69	254.73	4.02
Log Normal	6.50	0.008	0.39	0.006

Table 20 Temperature's distribution parameters.

If we calculate these two quantities, we obtain temperatures that correspond to the 84° percentile is equal to 972 °C, whereas temperature that corresponds to 95° percentile is equal to 1226 °C.

Figure 81 show the CDF associated to the three random variables compared to data.

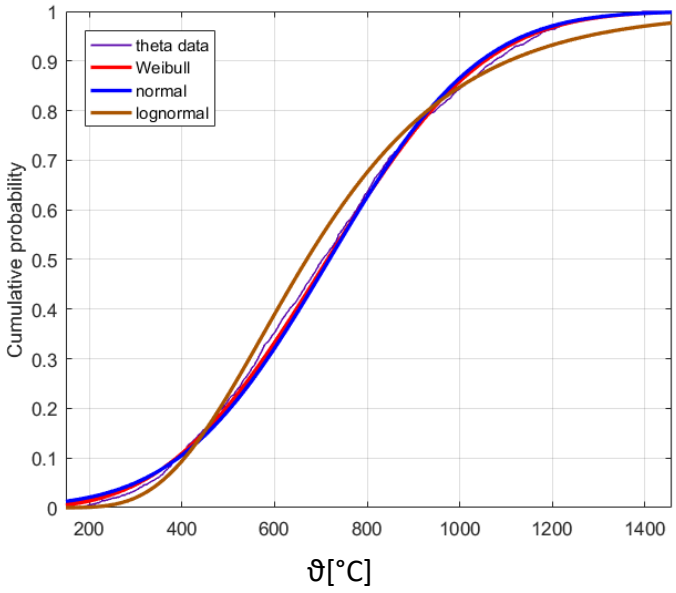

Figure 81 CDFs.

The result obtained in Figure 81 says only that temperature have a certain probability of occurrence, but the high value of variance doesn't allow us to draw conclusions.

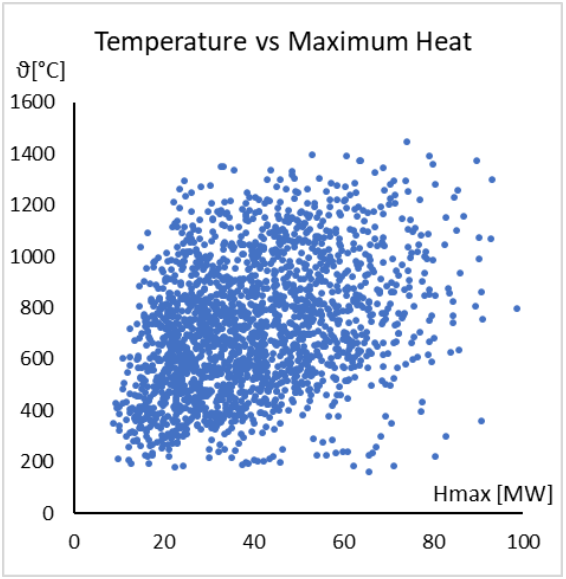

Figure 82 Maximum temperature vs Maximum heat released.

If we disaggregate results and study the probability of occurrence of temperatures in function of the maximum heat released in compartments, calculated as $H_{max} = RHR_{fi} \cdot A_f$ and expressed in $[MW]$, we can see the correlation between these two parameters (Figure 82).

The correlation means that there is a relation between parameters, that could be used to provide indications useful to rapid assessment. The Bivariate model of Normal distribution for dependent random variables can be expressed as a function of the random variable X, random variable Y and a parameter that depends from the covariance of the two random variables named correlation coefficient ρ:

$$\rho = \frac{Cov[X,Y]}{\sigma_X \sigma_Y} \tag{5.3}$$

The expression of the bivariate normal distribution is

$$N(x,y) = \frac{1}{2\pi\sigma_X\sigma_Y\sqrt{1-\rho^2}} e^{-\frac{1}{2(1-\rho^2)}\left(\frac{(x-\mu_x)^2}{\sigma_x^2} - 2\rho\frac{(x-\mu_x)(y-\mu_y)}{\sigma_x\sigma_y} + \frac{(y-\mu_y)^2}{\sigma_y^2}\right)} \tag{5.4}$$

This model was applied to the logarithm of the random variables in order to obtain a bivariate lognormal model. Starting from data showed in Figure 82 and assuming as random variable the maximum temperature and the maximum heat released in compartment, mean and standard deviation of each RV and covariance was calculated. All mentioned parameters were reported in Table 21. As you can see, the value of $\mu_{\ln(x)}$ and $\sigma_{\ln(x)}$ are equal to these reported in Table 20. Moreover, note that there is a relatively high value of the coefficient of correlation.

$\boldsymbol{\mu_{ln(x)}}$	$\boldsymbol{\mu_{ln(y)}}$	$\boldsymbol{\sigma_{ln(x)}}$	$\boldsymbol{\sigma_{ln(y)}}$	$\boldsymbol{Cov[ln(X), ln(Y)]}$	$\boldsymbol{\rho_{ln(x),ln(y)}}$
6.50	10.48	0.153	0.200	0.0619	2.02

Table 21 Bivariate distribution parameters.

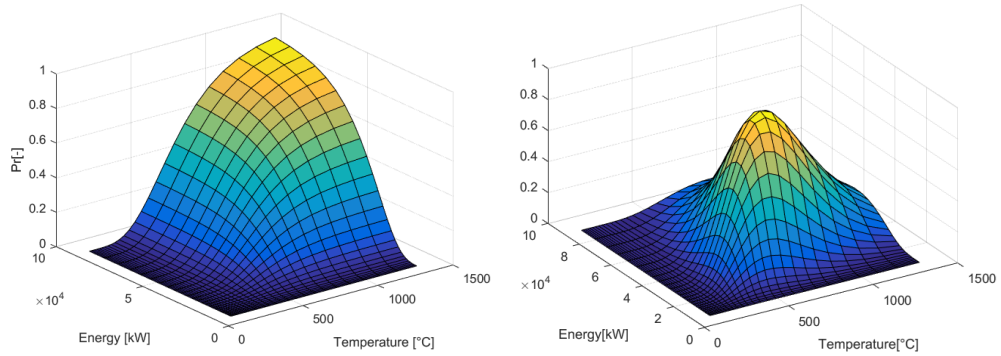

Figure 83 3D representation of Multivariate CDF and pdf.

Figure 83 show the cumulative (left) and the density (right) distribution function of the bivariate random variable in a 3D space. The same surface can be showed better using iso-contour, as reported in Figure 84. This representation highlights the dependence of temperature from the maximum heat released in compartment during fire. In other words, curves in Figure 84 represent the probability of occurrence of a maximum temperature respect to maximum energy released in compartment, which is $P(\vartheta \leq \bar{\vartheta}, H_{max} \leq \bar{H}_{max})$. This figure allows us to predict the probability taking in account two random variable.

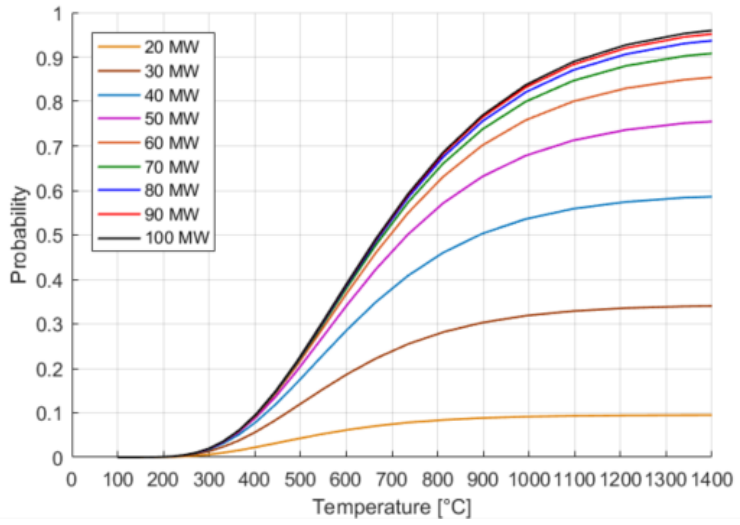

Figure 84 Multivariate CDF, Iso-contours. $P(\vartheta \leq \bar{\vartheta}, H_{max} \leq \bar{H}_{max})$.

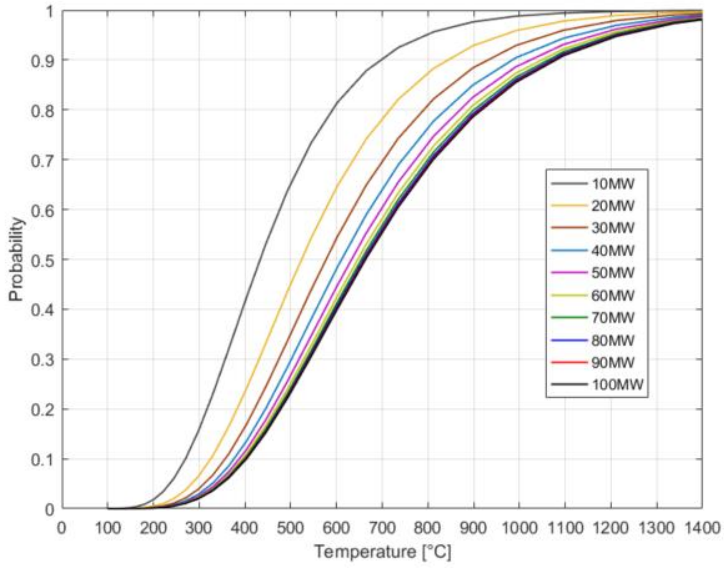

Figure 85 Multivariate CDF. Iso-contours, $P(\vartheta \leq \bar{\vartheta} \mid H_{max} \leq \bar{H}_{max})$.

In order to highlight the dependence we can see the probability of occurrence of a maximum temperature given the value of maximum heat released in compartment during fire, in other words $F(\vartheta \leq \bar{\vartheta} \mid H_{max} \leq \bar{H}_{max})$ (Figure 85).

As you can see from this graph, with a Maximum energy released of 30 MW that correspond to a peak $RHR_{fi} = 250kW/m^2$ in a compartment of 120 m² there is a probability of 84% of reach a peak temperature lower than 850 °C. We obtain the same probability in a compartment of 80 m², characterized by the same value of $RHR_{fi} = 250kW/m^2$ with a temperature of 750°C.

Finally, in Figure 86 and Figure 87 show the comparison between the computed model and the experimental data regarding to the pdf and the CDF.

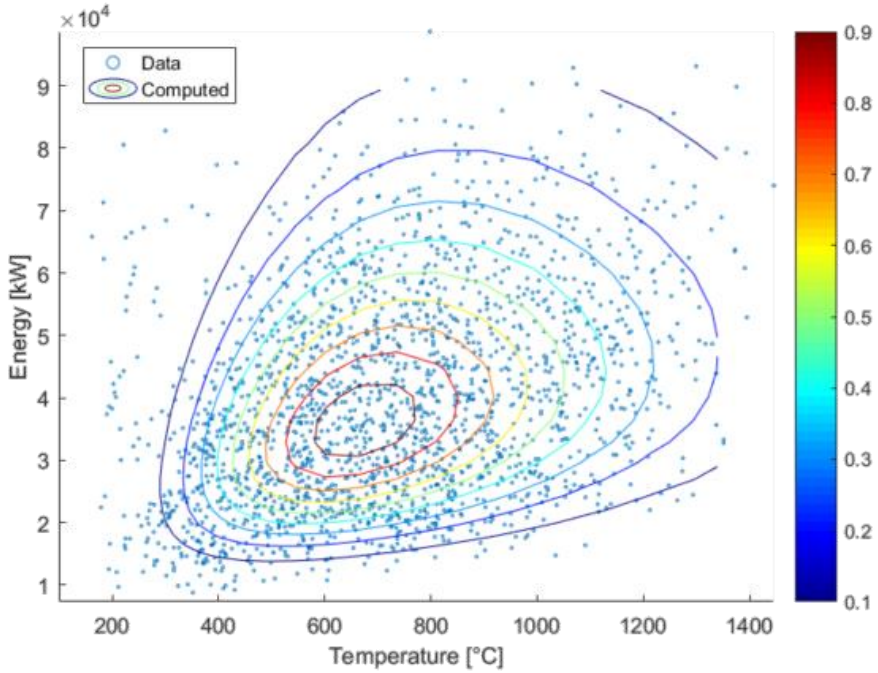

Figure 86 Calculated multivariate pdf vs experimental data.

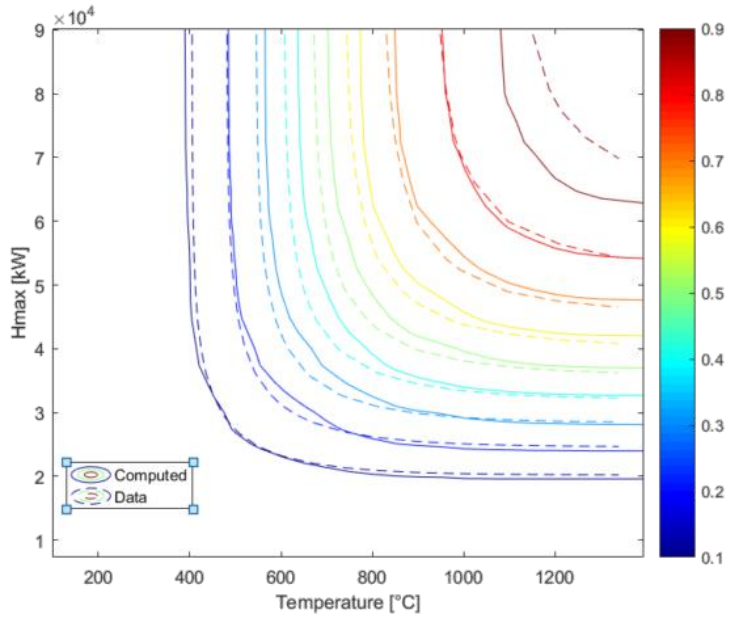

Figure 87 Multivariate Cdf Experimental (dashed) vs Computed (continuous).

5.3 Probability distribution of stresses

Figure 88 shows the value of axial load applied on column's head for each analysis of sample. At glance we immediately realize that the distribution of the axial load applied on columns isn't uniform (because if we consider any area of the graph the density of point change with the considered N interval), even if sampled parameters are all defined as uniform distribution in sampling phase.

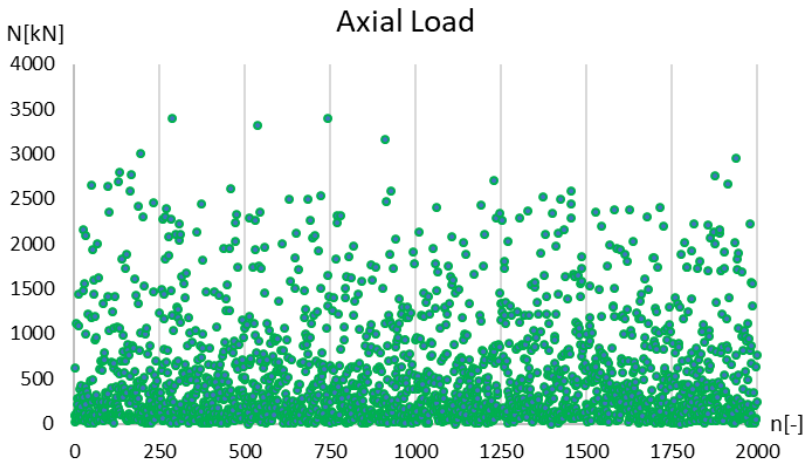

Figure 88 Axial load of columns.

In this study it was defined two parameters μ_N and μ_L that was used to identify load on columns and beams respectively. In particular these parameters were defined as the ratio between demand and capacity of beam and columns, calculated assuming a certain structural scheme:

$$q_L = q_{pl} \cdot \mu_L \qquad N = N_{pl} \cdot \mu_N \qquad 5.5$$

where q_{pl} is the value of distributed load that yield beams and N_{pl} is the value of the axial load that plasticize the column. Expanding previous equations, we obtain:

$$q_L = \frac{\alpha \cdot W_{pl} \cdot f_y \cdot \mu_L}{L^2} \qquad N = A_s \cdot f_y \cdot \mu_N \qquad 5.6$$

Equation 5.6 clearly show the dependence of loads from random variables, moreover regarding to q_L the value of α depends from structural geometry so it is a random variable also. For these reasons loads are distributed with a random variable that results of the composition of several random variables and is different from the distribution given during the sampling phase. As the central limit theorem says, the composition of several random variables, whatever distributed, tends to a Gaussian random variable. Thanks to CLT we can fit distribution of results using a Normal or a Lognormal Distribution. For instance in Figure 89 is displayed the cumulative distribution function of the Axial Load computed with the 5.6 we can see that it can be fitted with a lognormal distribution with an error on fit smaller than 10 %.

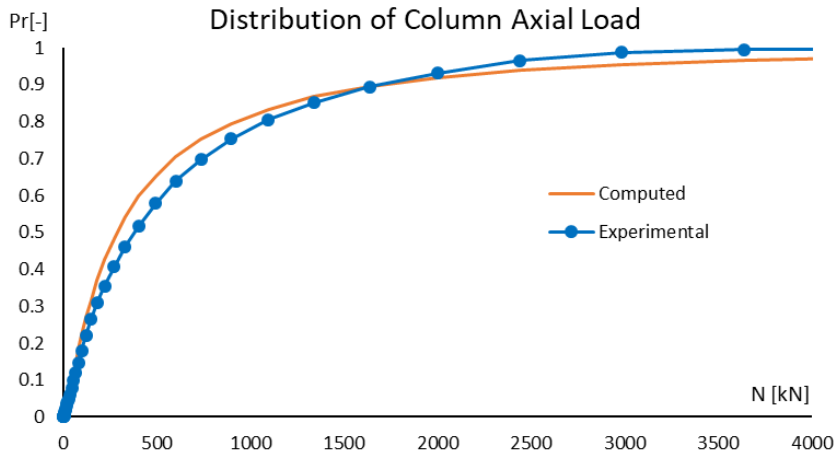

Figure 89 Probability distribution of real Load Level.

The same observations can be done if we read structural output of analysis, in particular observing the distribution of the real load level in the structure. Since the load levels of beam and columns are defined thanks to the assumption of the structural scheme (that fix the value of α) parameters μ_L and μ_N aren't the real loads level in beam and columns but allows us to understand the magnitude of the load level of the structure. Moreover μ_L and μ_N are parameters relative to a

specific section and was defined in the Eurocode for single elements analysis, so they lose their sense in a structural context. To keep this parameter meaning, a redefinition of the load level is needed. In particular we can define the load level of the structure μ_0 as the maximum section's load level in structure. It can be defined in symbols as:

$$\mu_0 = \max\left(\frac{N}{N_{pl}} + \frac{M}{M_{pl}}\right) \qquad 5.7$$

Where all terms are calculated at the beginning of fire, for this reason the value of μ_0 can be evaluated through a mechanical analysis in ambient condition of the substructure.

The structural load level takes into account combined action of axial force and bending moment in each point of structure, for this it's value could be much bigger than μ_N and μ_L. Note that the structural load level μ_0 is always bigger than the load level of the columns μ_N because to the value of the axial load that acts on the top of the columns it will be summed the shear of beams. ϕ

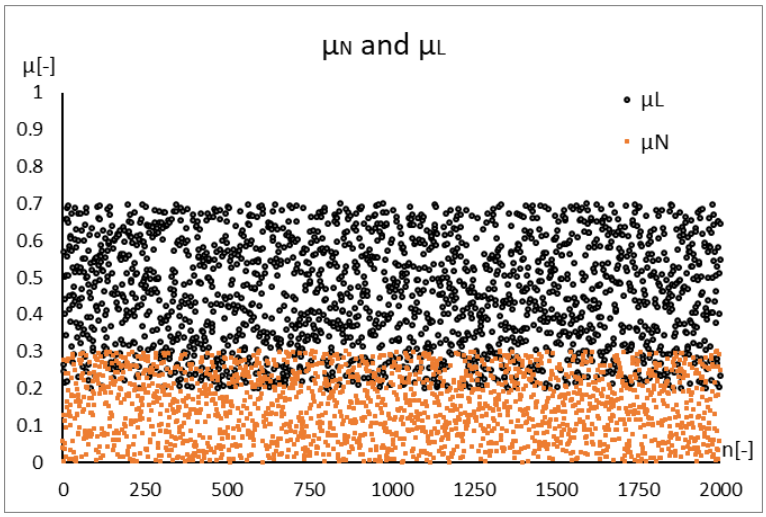

Figure 90 Values of real load level μ_N and μ_L.

Comparing Figure 90 and Figure 91, we can see that the distribution of the load level of the structure is very different from the distribution of the load levels relatives to beams and columns. In particular the load level is always bigger than 0.1 and can reach also high value due to the random assignment of the geometries. In some cases we reach also value of μ_0 very near to 1 (0.97), because it can be that the sampling define a structure with high value of μ_N and μ_L and a small value of inertia's ratio I_c/I_b.

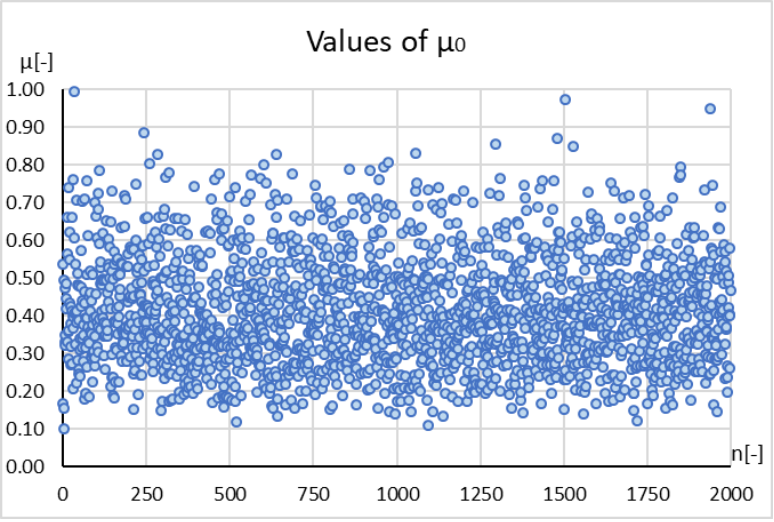

Figure 91 Values of real load level μ_0.

Even in this case we can analyse the distribution of the structural load level obtaining a pdf that tells us something about order of magnitude of this quantity in structural context.

Figure 92 shows the results of load level's analysis. Graph show that also in this case the parameter is distributed as a lognormal random variable characterized by parameter reported in Table 22.

Mean	Dev. St.	Median	Cov
0.413	0.155	0.40	0.375

Table 22 Load level distribution parameters.

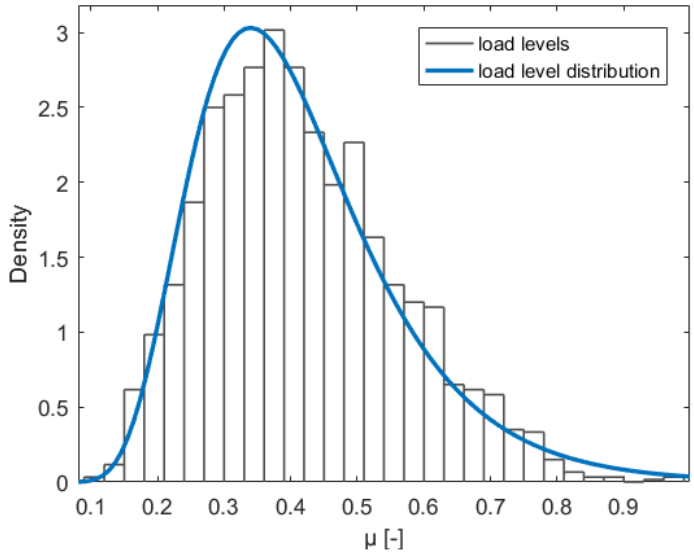

Figure 92 Real Load Level pdf.

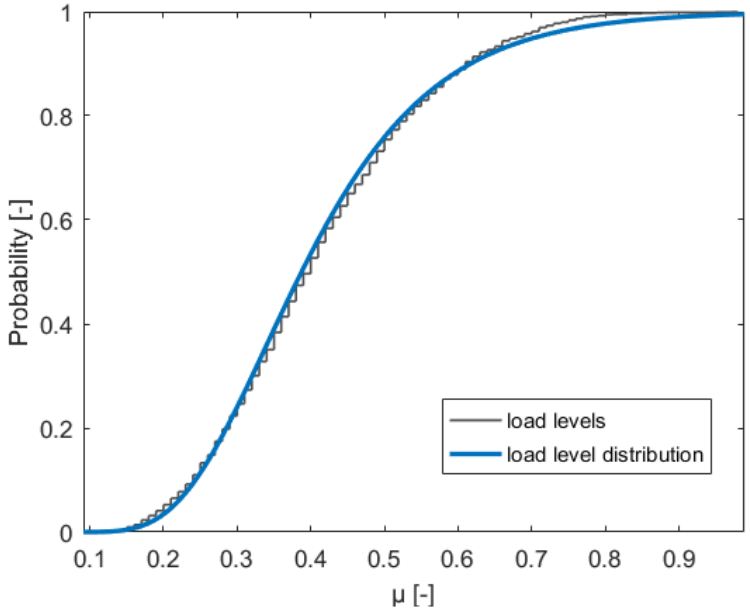

Figure 93 CDF of real Load Level.

5.4 Failure

The probabilistic study discussed in paragraph 5.2 doesn't take into account the structural behaviour but focus on the probability of occurrence of a given maximum temperature in compartments. In this section the structural response in terms of resistance will be treated starting from the observation on cluster.

Raw results in function of the analysis number are reported in Figure 94, and they were represented in function of the collapse mode. It was observed that analysed substructures could collapse in three ways: by failure of the beam, failure of the column exposed by four side and column exposed by one side.

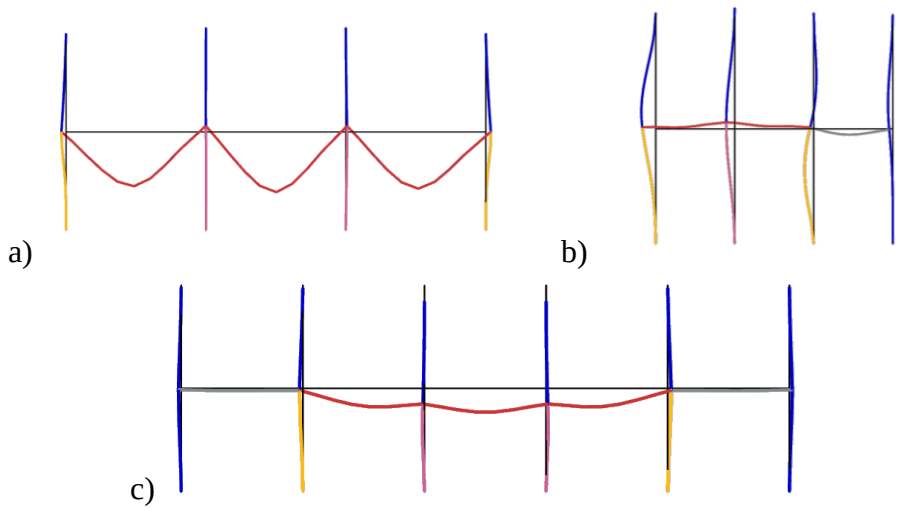

Figure 94 Collapse modes. a) Beam, b) One sides exposed column, c) Four side exposed column.

The collapse due to beam's failure (beam mode) is the most probable collapse mode, and it occurs when the section of the beam isn't able to carries the load and in the most of cases the crisis happens in the joint due to the shape of the bending moment diagram.

The failure of columns exposed by four side (4sCol mode) is the second most probable collapse mode and it happens due to decay of the resistance of the column. Since the beam is the meanly most loaded element in substructures this collapse should happen with a very low frequency if we consider only the plastic resistance of elements, but if we consider the stability of columns the frequencies of this type of collapse increase.

Finally, the failure of one side exposed columns (1sCol mode) is the collapse mode with the lower associated probability of occurrence, this kind of collapse happens when thermal effects cause big displacements in horizontal direction. Moreover, this type of collapse tends to occur when the constraint offered by the unexposed part of the substructure is asymmetrical.

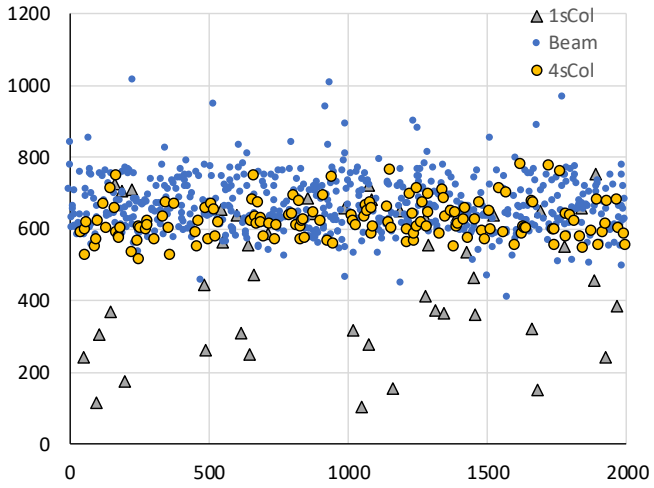

Figure 95 Raw Results.

As Figure 94 shows, most of collapses happen between the 500 °C and 800 °C, that corresponds to a coefficient of reduction $0.11 \leq k_{y,\vartheta} \leq 0.78$. Observing for single collapse mode we can see that the beam's mode seems to have a mean of collapse temperature lightly higher than all other collapse modes. Regarding to the distribution of the 4sCol mode, we can see that the temperature distribution is slightly shifted to downward. This distribution is due to the stability check that is very severe for steel structures in fire condition. As concern the 1sCol mode, it is characterized by a much lower temperature respect to other collapse mode but this doesn't mean that the maximum temperature is equal to the collapse temperature. In this graph is reported the temperature of the collapsed elements, and since these types of columns are exposed to only one side the total heat fluxes is lower than the heat flux of other elements. For instance, in the case of the Analysis n° 202 that collapse with 1sCol mode, temperature in one side exposed column is 175°C whereas we reach 510 °C and 480 °C in the beam and in the four-side exposed column respectively.

Note that the temperature displayed in these graphs are weighted average. In the simplified method proposed in standard temperature distribution in steel

structure are considered nearly constant through the cross section due to thermal properties of steel. In truth the thermal gradient could give place to temperature difference of several percentage points. In order to quantify difference for failure data it was calculated the scatter between weighted average temperature and the maximum temperature in the section at the collapse time using the formula

$$s = 1 - \frac{\vartheta_{mean}}{\vartheta_{max}} \qquad 5.8$$

Figure 96 show the scatter s vs the record index in the failure dataset. As you can see the scatter between mean and max temperature change its magnitude in function of the section type. The lower scatter was registered for the four side exposed columns (c4s) where the scatter value doesn't exceed the 10%. If we consider the beams, the maximum scatter value increase up to 20% due to the different exposure condition of the beam section (three side exposure) and the maximum value of the scatter (60%) is registered for the C1s. Note that while Beams and C4s vary in the interval 0÷10% and 0÷20% respectively, the scatter of C1s vary in the interval 24÷60%. We can say that the mean temperature is very different from the maximum temperature in all cases.

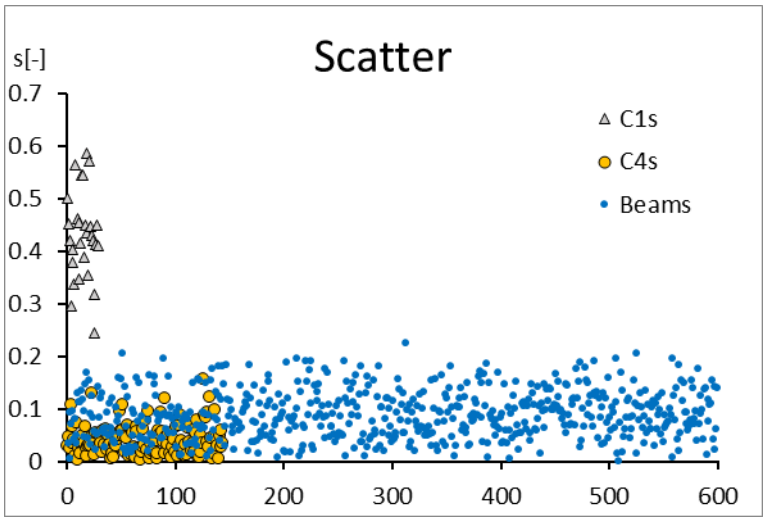

Figure 96 Value difference between maximum temperature e mean temperature.

The study of results started from the comparison with the critical temperature calculated as reported in the Eurocode. The equation of the Eurocode 3 gives temperature of collapse of an element exposed to the fire curve ISO-834 in function of the load level parameter μ_0 and a coefficient k that depends from exposure condition of structural elements:

$$\vartheta_{crit} = 39.19 \ln\left(\frac{1}{0.9674\, k_1 k_2\, \mu_0^{3.833}} - 1\right) + 482 \qquad 5.9$$

The coefficient $k = k_1 \cdot k_2$ where $k_1 = 1$ if the cross section is four side exposed (columns) or $k_1 = 0.7$ if the section is exposed by three side (beams). Regarding k_2 it is equal to 1 if the structural element is uniformly heated along its length and equal to 0.85 if not.

Note that this equation derives directly from the equation that describe strength's decay and by neglecting thermal effects because it was thought for applications of the prescriptive approach to fire.

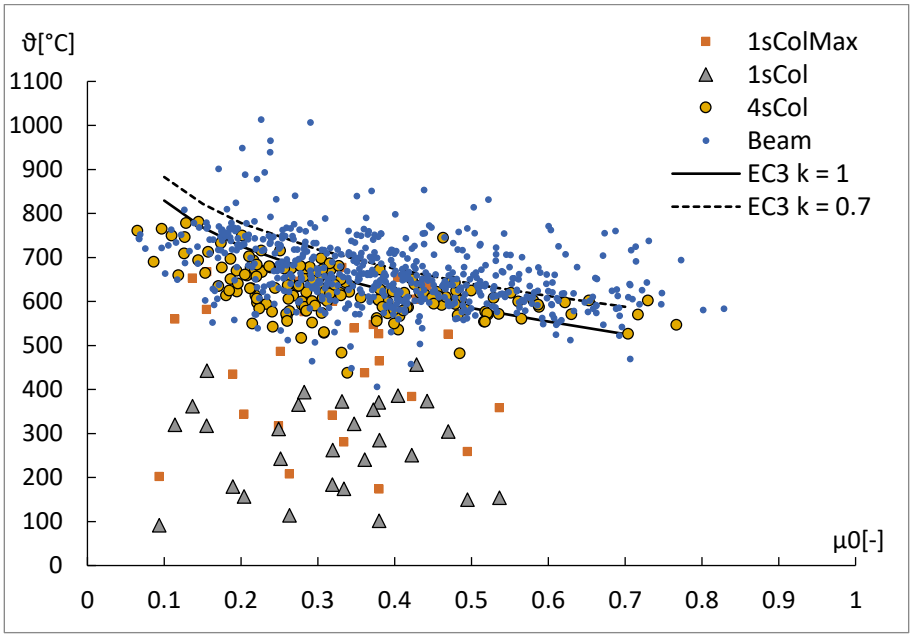

Figure 97 Critical Temperature of substructures.

Figure 97 show collapse temperatures in function of load level of collapsed elements. In this figure is displayed also the equation 5.9. Observing this figure, we can say that even if the Eurocode equation for critical temperature has a good fit with results that come from substructures exposed to natural fires, there is a large scatter on results if we consider thermal effects that arise in not statically determinate structures. In particular the real critical temperature has a lower dependence from the load level.

The scatter can be seen better in Figure 98, that shows the ratio between the critical temperature observed from the analysis results and the critical temperature predicted by the Eurocode. Also, in this graph results are showed in function of load level. As we can see from the Figure 98, the error tends to remain constant in function of the load level.

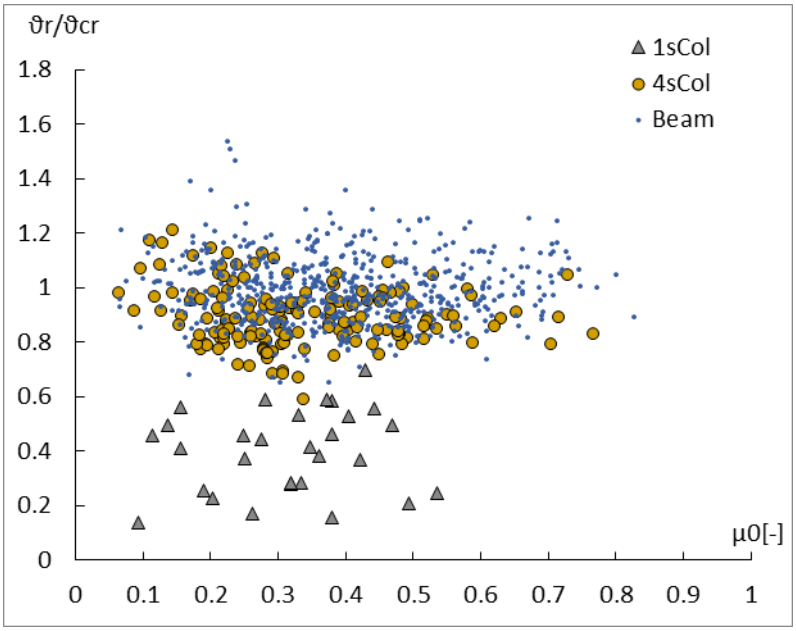

Figure 98 Scatter diagram of Critical Temperature.

Also, in this diagram results are classified by collapse mode and it's easy to note that while we have a good prediction of critical temperature for beams and four side exposed column, there is a very bad results if we try to assess the critical temperature of the one side exposed column. The bad prediction is due to the fact that the critical temperature for one side exposed column have a strong

dependence from other parameters of the structure like the stiffness of the frame and the heating speed of structural elements.

Just presented results seem to say that the prescriptive method could return unsafe assessment of the collapsed temperatures in some cases, but this is not true. While the Eurocode formulas could return unsafe results due to the presence of thermal effects, by the point of view of the time. It is well known that prescriptive method is much conservative, especially on estimation of resistance in terms of time. Figure 99b shows the comparison between time needed to reach the collapse temperature using the ISO standard fire (Figure 99a) and the actual time obtained from calculations. From the figure it can be noted that using the prescriptive method the time needed is much lower than once calculated through the RHR. Considering that temperatures evaluated with ISO-834 fire curve are a function of the time and that collapse temperatures are mainly concentrated in the band 500°C - 800 °C, time estimation of temperature is distributed in a certain interval for all samples independently from the grow speed of the fire.

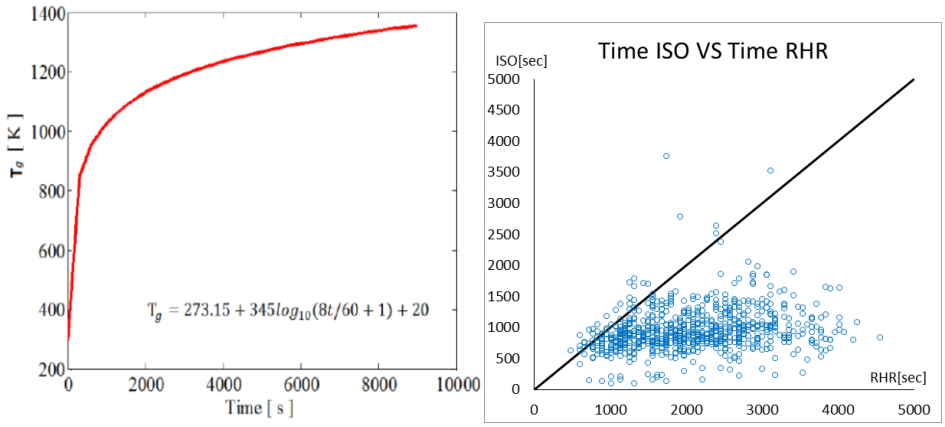

a) b)

Figure 99 a) ISO 834fire curve, b) Time needed to reach the collapse temperature with the ISO-834 and the RHR.

Some other observation can be done on collapse temperature if they are displayed in function of other parameters. In Figure 100 critical temperatures are displayed in function of the frame's stiffness. This quantity is defined as the translational stiffness of the frame not exposed to fire and calculated in the hypothesis that there is no rotation of deck's nodes. Exploiting this hypothesis,

the stiffness of a single column is calculated as the stiffness of a fixed-fixed column:

$$k_{lat} = \frac{12EI}{l^3} \qquad 5.10$$

Where I is the inertia of the column section, E is the young modulus of the steel and l is the column's height. The frame stiffness k_χ of the entire structure could be calculated as:

$$k_\chi = \left(2 \cdot b_{tot} - b_{exp} + 1\right) \cdot k_{lat} \qquad 5.11$$

Where b_{tot} and b_{exp} are the total number of bays and the number of fire exposed bays respectively. This equation takes into account bottom and top column of the substructure and is a function of aleatory variables given in input of the experimental design.

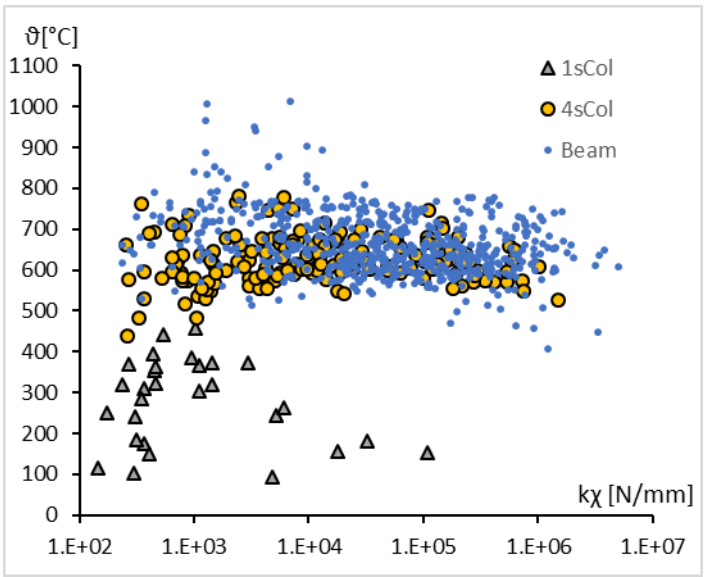

Figure 100 Critical Temperature of substructures.

From this figure, we can note that substructures tend to collapse with 1sCol mode if there is a very low frame stiffness. A reason of that is the fact that if structures are characterized by a low lateral stiffness thermal effects of the beam cause larger displacements of the columns. On the contrary, other collapse modes seems to be independent from the frame stiffness.

By a probabilistic point of view, collapse temperatures could be processed as already done with stresses and gas temperatures. In Table 23 are reported the probability of occurrence of single type of collapse referred to the entire sample and conditioned to the collapse. The table show that there a lot of samples survived to the fire: 62% of analysed structures. It is very interesting to see that the most of collapses are due to beam's failure, indeed three on four structures collapsed due to beam's failure.

Starting from these data, it is possible to process analyses in order to obtain the probability distribution of collapse temperatures. In order to process analysis and obtain the distribution of temperatures we have to distinguish the three collapse modes and get the distribution for each of them.

	Beams	Col4s	Col1s	Any
Total	0.300	0.083	0.014	0.398
Conditional	0.755	0.209	0.036	1

Table 23 Probabilities of occurrence.

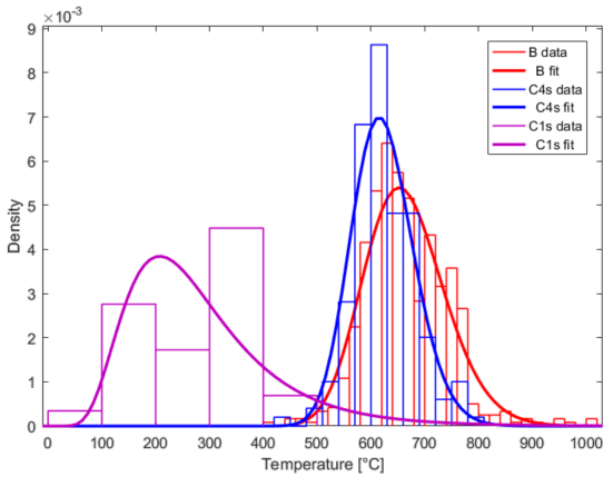

Figure 101 Collapse temperature distribution (pdf).

All distribution, as you can see from Figure 101, was assumed as lognormal and the parameters was evaluated in order to compare the computed distribution with the distribution obtained from aggregated results.

Distribution's parameters are reported in Table 24. Observing values reported in this table we can see that the Col4s Mechanism have a little lower mean collapse temperature than the beam's mechanism and that both Beams and Col4s modes are characterized by a low coefficient of variation. On the contrary, the Col1s mechanism have a very high coefficient of variation if we compare it to CoV of other distributions. A reason of that could be that the temperature used in Col4s and beam's mechanism coincides with the maximum temperature in the structure whereas in Col1s data the temperature could be much lower than the maximum registered in steel. The quality of the fit could be seen in Figure 102 also. In this figure we can see that the computed distribution overlaps the experimental results in case of both Beams and Col4s mode, the distribution computed for Col1s mode doesn't have a best fit.

	Beams	Col4s	Col1s	B + C4s	Any
μ	664	623	281	655	645
σ	75	57	134	73	146
CoV	0.113	0.091	0.477	0.111	0.226

Table 24 Parameters of distributions.

Regarding to distribution of aggregated results, it seems to fit bad the results because data of Col1s tend to lower the quality of the aggregated sample (Figure 102). The best way to obtain a good fit on the aggregated results consists to combine distributions. In other words, to obtain the aggregated results we have to sum the probability of having a collapse of beams, collapse of columns exposed to four side and collapse of one side exposed columns (Figure 102).

In alternative It is possible to consider the sample constituted only from B and C4s data. Results (Figure 103) show that in this case there is a significative deviation of results only in the first part of the aggregated probability distribution.

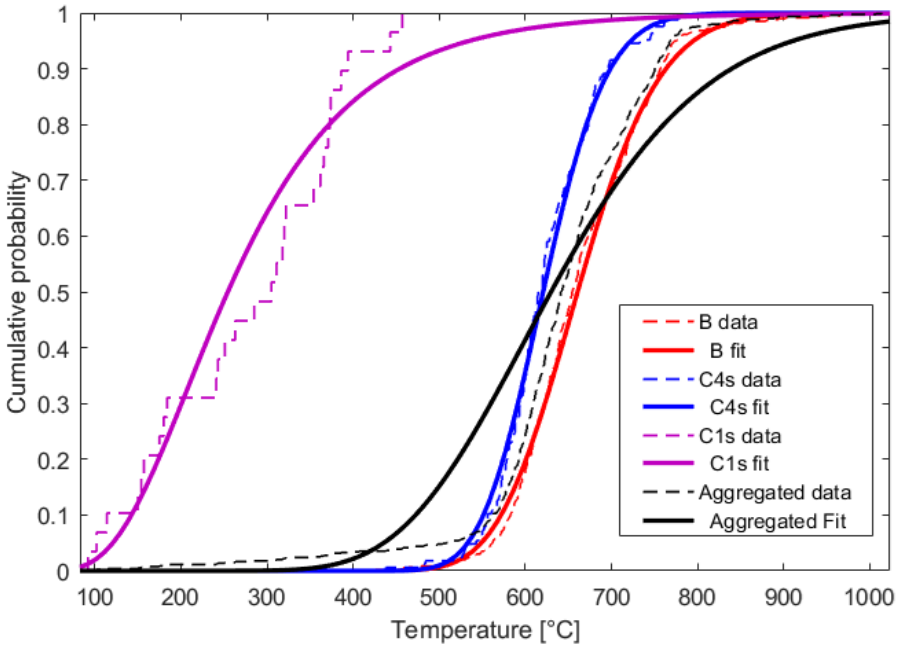

Figure 102 Collapse temperature distribution (CDF).

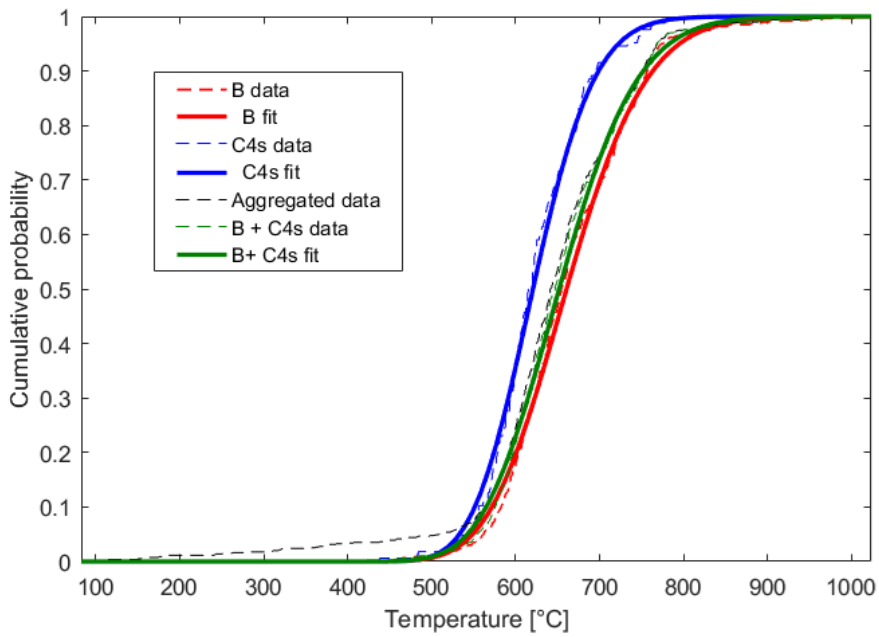

Figure 103 Collapse temperature distribution B+C4s (CDF).

Just calculated distributions express the probability of collapse $P(\vartheta \leq \bar{\vartheta}|M_i)$ in function of temperature ϑ lower or equal to $\bar{\vartheta}$ for a defined collapse mechanism (M_i). In order to combine these probabilities, we have to apply the total probability theorem and hypothesize that

- the failure modes are statistically independent between them;
- the structure fail (event F) only due to Beams mechanism (event B) or Col1s mechanism (event C_{1s}) or Col4s mechanism (event C_{4s});

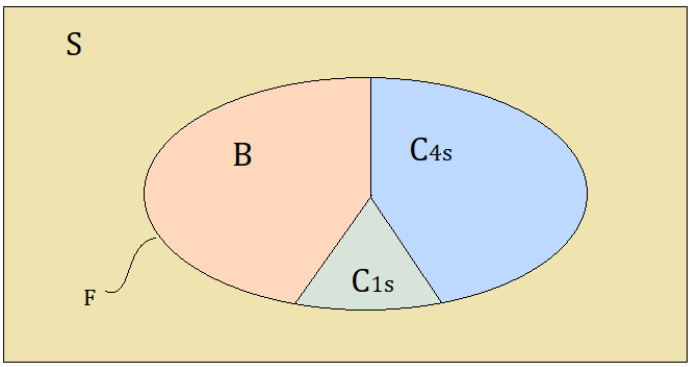

Figure 104 Eulero-Venn Diagram. Sample space(S) Collapsed Structures(F), B, C_{1s} and C_{4s} mechanism

Using this hypothesis, we can say that the probability failure for any mechanism is equal to:

$$P(F) = P(B \cup C_{4s} \cup C_{1s}) = P(B) + P(C_{4s}) + P(C_{1s}) \qquad 5.12$$

Where the value of $P(B)$, $P(C_{4s})$ and $P(C_{1s})$ can be read from the second row of the Table 23 Probabilities of occurrence Applying the total probability theorem we obtain the probability curve that express the probability of failure for any mechanism due to temperature ϑ lower or equal to $\bar{\vartheta}$:

$$P(\vartheta \leq \bar{\vartheta}|F) = \sum_{i=1}^{3} P(\vartheta \leq \bar{\vartheta}|M_i) \cdot P(M_i) \qquad 5.13$$

$$= P(\vartheta \leq \bar{\vartheta}|B) \cdot P(B) + P(\vartheta \leq \bar{\vartheta}\,|C_{4s}) \cdot P(C_{4s}) + P(\vartheta \leq \bar{\vartheta}\,|C_{1s}) \cdot P(C_{1s})$$

Where values $P(\vartheta \leq \bar{\vartheta}|B)$, $P(\vartheta \leq \bar{\vartheta}\,|C_{4s})$ and $P(\vartheta \leq \bar{\vartheta}\,|C_{1s})$ are known because we know the CDF of the random variables.

In Figure 105 we can see the comparison with the distribution computed on the aggregated data and the probability estimation using the equation 5.13. Note that the distribution computed on the aggregated data return a bad estimation of the collapse temperature. In particular there is an overestimation (safe prediction) of the probability of failure in the range 400 °C – 600 °C, and an underestimation (unsafe prediction) in the band 700 °C-1000 °C.

If it is needed a rapid estimation of the probability of collapse and it isn't required a high level of precision it can be used the prediction of the distribution computed on the aggregated data sample, taking in account that the failure assessment can be differ from the real value even 10%.

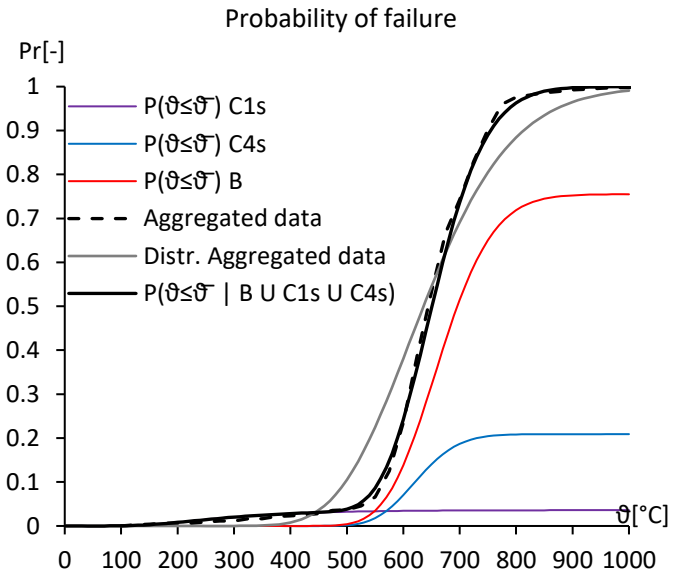

Figure 105 Collapse temperature distribution.

Chapter 6

6 Conclusions and Further developments

This section summarizes the work developed in previous chapter starting from the objective of the thesis.

The structural analysis in fire condition can be performed in two ways. The first approach consist in the application of simplified models neglecting some thermo-mechanical effects based on a standard design fire, whereas the second approach is interdisciplinary and consist in application of advanced models useful to determine thermal field in compartments, structural elements and the effect of the indirect actions on the structural behaviour.

The first approach, simplified, is very simple to be implemented and allows the designer to neglect some aspects of the fire (e.g. the structural redundancy), if the designer uses a standard design fire, named ISO-834 standard fire. The main characteristics of this fire curve is the high growth rate of the temperature in compartment that causes a high resistance loss because induces high temperatures in structural members. Furthermore, the simplified method can be applied in single member analysis, that means the thermos-mechanical effects induced by thermal expansion and gradient restrained by the rest of structure could be neglected.

The second approach is performance-based and allows obtaining results more accurate than first approach, through the modelling of a more realistic fire in the compartment and then a more realistic thermal field in structural members. Moreover, with the second approach the modelling of the whole structure or significant substructures is performed in order to take account of the indirect actions of fire (e.g. thermal restraint). Finally, the performance-based approach allows modelling the non-linear behaviour of the structure. Hence, the structure

can count on resistance reserves that could not be exploited using the simplified approach.

Unfortunately both approaches have pros and cons. The ISO-834 standard fire simulates the furnace test performed on single structural members, where the gas temperature reach 750°C in less than 20 minutes. Hence, if we perform a structural simplified analysis, we get that only structures characterized by a load level around 0.15 can resist more than twenty minute. As concern the performance based approach, as already said, it allows us to exploit the nonlinearities of structure and model the real fire that could arise in s compartment, but the application of Fire Safety Engineering methodologies requires a deep background knowledge in fire analysis and thermo-mechanics. Moreover, the advanced modelling of the fire situation in some cases could require very long analysis time due to complexity of the FEM model. Finally, the nonlinear modelling of the problem makes it difficult to implement in a parametric study.

This thesis has as objectives the reduction of the gap between these two approaches. This aim was pursued through the purposing of a new simplified formulation to estimate the critical temperature of a steel member in the context of FSE. In other words the simplified proposed model allows to use a general fire curve instead of the ISO standard fire, take into account the nonlinearities of the structures and at the same time bypass the structural analysis of the nonlinear FEM model, thanks to the calibration on 2D Analysis results set.

6.1 Sampling

In order to reduce the gap between the simplified approach and performance-based approach, the hypothesis of ISO standard fire need to be removed and to do this a better understanding of the structural behaviour in fire condition is needed.

Since it was decided to develop a regression model, a set of data that come from numerical experimentations was analysed. Using standard sampling methods, it is very difficult to develop regression model because the regression model should be sensitive to several fluid-dynamic and thermo-mechanical parameters. To describe the behaviour of the structure in fire, 13 parameters, were identified and divided into 4 groups, as follows. Note that some parameters actually play a dual role: for instance, the length of the beams influences the geometry of the substructures and also the mechanical response of the structure.

- Fire modelling Parameters (five):

    - A_f Floor's Area of the compartment;
    - A_v/A_f Ratio between Vent's area and floor's area;
    - RHR_f the maximum heat release rate per unit area;
    - q_f the specific fire load;
    - t_α the growth rate parameter of the fire;
- Geometrical Parameters (four):
    - h the height of columns;
    - L the length of beams;
    - n_b a parameter that indicate the size of beam's section;
    - I_c/I_b the ratio between the Column's Inertia and the beam's inertia.
- Mechanical Parameters (three):
    - f_y the tensile strength of the steel (S235, S275, S355);
    - μ_L a parameter that indicates the load level of the beam;
    - μ_N a parameter that indicates the load level of the column.
- Fire Scenario (one):
    - IB index of building, univocally determinate the number of bays of the substructure, number of bays exposed and place of fire

Due to the high number of parameters, a complete parametrical analysis would require a lot of fluid-dynamic and thermo-mechanical analyses to investigate the problem. In order to resolve this issue, a particular process of sampling was used, named Latin Hypercube Simulation. The *Latin Hypercube Sampling* (LHS) procedure could be used in *Monte Carlo* (MC) simulation in order to obtain small number of realizations but preserving quality of the samples. This sample technique is based on the simultaneous stratification for all variables. In other words, thanks to this procedure the samples are characterized by the same probability of occurrence and for this have high meaningfulness.

Since several random variables involved in the problem and sampling technique allows to use small samples, particular attention must be paid to the correlation between random variables. In order to do this, an optimization technique was used in order to build samples that assembled in the sample base return a predefined correlation. The Simulated Annealing optimization method

was implemented to achieve the correlation control, and in this case the correlation matrix is assumed as diagonal (no samples correlation). This optimization technique is characterized by a duality in the behaviour that makes it a very powerful method when it is applied to problems characterized by high nonlinearity. The main characteristic of the simulated annealing method is that at the beginning the algorithm behave as a random search technique and after some iteration it tends to exclude domain's regions characterized by a low probability of find in these the optimal solution of the problem.

6.2 Modelling

Fire model and structural model are based on several modelling hypotheses which could influence results. Regarding to fire analysis, it was conducted with Cfast computer program that implement a two-zone model and for this reason fire parameters taken into account are only five. CFD analysis, that is the more accurate tool to study the evolution of temperature, is based on the numerical integration of differential equations that express the balance of energy, the balance of mass and the balance of momentum of motion. The two-zone model analysis the third equation (momentum) is neglected. This assumption allows using smaller calculus's resources but neglect the effect of the fluid's motion through the compartment. Using this type of analysis we hypothesize the energy is released in the compartment uniformly and the fluid's velocity field doesn't influence temperature in analysis domain (constant temperature through the hot zone). This implies that the study is focused on full developed generalized fire. For this reason, the study was limited to compartments characterized by a floor area smaller than 200 m^2.

Computed temperature of the hot zone was applied uniformly on beams and columns. In order to better simulate the fire scenarios structural elements were exposed differently in function of their position in the structure. All beams involved in fire was exposed by three side, whereas the columns were exposed by four side o by one side if they are placed in the middle of the zone involved in fire and in the borderline of the zone involved to fire, respectively. This hypothesis is conservative because if we refer to fire analysis results, the temperature in the column's foot is generally lower than the temperature at the top.

Thermomechanical analysis of the structural members is based on the hypothesis that plane section remain plane during fire. Moreover, each section is

considered adiabatic, hence there is not heat transfer in the longitudinal direction of structural elements.

6.3 Analyses results

Fire, thermal analysis and thermomechanical analysis was performed with Cfast and Safir Software through AGL. In order to validate the analysis a sample of results was analysed in details.

Regarding to fire analysis they were observed the output temperature curves of the analysis. It was observed that maximum temperature in some cases exceed the temperature estimated through the ISO standard fire, so the simplified method in some cases could be not conservative.

As concerns thermal analysis, it was observed the weight of the hypothesis of constant temperature through the cross section of element. Temperature's gradient in some cases can be very high, in particular when we approximate to the mean temperature the thermal field of columns exposed by one side where mean temperature and maximum temperature in the section can differ of 50%-60%. Thermal gradients are much lower in beams (up to 20%) and in columns exposed by four sides (10%).

About thermo-mechanical analysis, a particular attention was paid to the study of the structural behaviour. In particular it was observed the types of collapse mechanism. Analysis results show that the collapse can happen in three ways: by the failure of the beams exposed to fire (B) or by the collapse of column exposed by one side (C1s) or by the failure of columns exposed by four side (C4s). These types of collapse influence the value of collapse temperature and oscillation associated to the collapse mean temperature.

As regards the B mechanism, associated to the failure of a beam exposed to fire, the collapse occurs due to the excessive plasticization of the end sections of the beam or middle section of a beam. When the frame is characterized by an adequate lateral stiffness and resistance, the beam changes its own configuration and behave as a cable (chain effect). We can appreciate it only if consider in the analysis the geometrical non-linearity. This effect provides to the structure an over resistance that traduces itself in a higher critical temperature and cause a deviation of the critical temperature around 12% with respect the model of the Eurocode 3.

The C4s mechanism is due to the stability loss of columns exposed to fire by four sides. Indeed, if we observe the structural behaviour, we can see that the bending moment in proximity of the collapse tends to assume a sinusoidal shape,

this means that the column collapses due to stability loss. Moreover, bending moment assumes the value zero in the middle of the columns.

The C4s collapse's type is characterized by a mean temperature of 624 °C, little lower than the B mechanism and if we compare the temperature evaluated through the numerical experimentation with the critical temperature calculated according to Eurocode (mean 659°C), we can see through the scatter that the Eurocode formula returns values like an upper bound. Indeed the best estimate of the scatter (mean plus standard deviation) is equal to one.

As Concern C1s, the mechanism that involve the column exposed by one side, it occurs much less frequently than others. The C1s mechanism depends from a lot of factors like the inertia of the section, the position of the fire and the number of bays exposed to fire. When compartment's temperature increase, structural element increases their temperature in different ways because they are exposed to fire by different number of side and have different massiveness. For this reason, mean temperature of columns exposed by one side is much lower than mean temperature of other structural elements. Moreover, due to high value of thermal gradient these structural elements are characterized by stress burden induced by thermal effects. When this collapse occurs, columns exposed by one side collapse due to second order effects, because indirect actions due to restrained thermal expansion and gradient of the column and related to other structural elements are added to the stresses in service state. Moreover, due to elevated thermal gradient in columns exposed to one side the mean temperature and the maximum temperature in the section differ of 40÷60%. For this reason also if the collapse occurs with average temperatures of 300°C, some regions of the cross section could be characterized by a temperature also greater than 600°C.

6.4 Regression

Input data, mean temperatures, and other significant quantities were stored in a database. The database was used to build a regression model using the method proposed by Gardoni et al. 2002. This consolidated procedure allows to create a probabilistic regression model based on existing deterministic model (EC3) that take into account several parameters and characterize critical temperature as a random variable. The probabilistic model is created using the Bayesian updating. Two relationships that express the collapse temperature of beams and columns, respectively, were obtained. The collapse mechanism C1s was excluded because is characterized by a very low probability of occurrence. To create a good

regression model for the critical temperature in the initial part of the study it was taken into account the 21 fire and thermomechanical parameters. After the regression creation it was conducted a step deletion process in order to simplify the formulation. This procedure allowed to delete several parameters in particular most of those concerning the fire analysis.

Regarding the formulation for the beams, it depends on ventilation factor (o_v) and specific fire load (q_f), which mainly affect the maximum temperature and the duration of fire, respectively, on height of column (h), beams load level (μ_L) and cross section area (A_{beam}) and the load level of the structure (μ_0), which affect the stresses redistribution capacity. The proposed regression for the critical temperature improves the estimation of Eurocode adjusting mean value and reducing variance and, above all, implicitly allows taking into account of indirect actions due to restrained thermal expansions.

As concern columns, the regression model adjust mean and reduce the variance. In this case the critical temperature depends from parameters that influence the stresses, resistance, and heating capacity. Regarding parameters that influence stresses they are the load level of beams (μ_L), load level measured on the top of the columns (μ_N) and the length of the beams (L). Since the input parameters of the regression are calculated in a simplified way the real load level at the foot of columns depends from μ_N and from the load transferred by the beams ($\mu_L \cdot L$). Moreover, the length of column influences the bending moment in the column-beam joint. Regarding resistance there are two parameters: plastic modulus of the column ($W_{pl,col}$) and the Area of the column (A_{col}). While the first influence the capacity of column to absorb the bending moment that come from beams, the second one take into account the capacity of absorb normal stresses. Finally, the heating parameter is the section factor A_m/V that take into account the massivity of the section so its own heating capacity.

The regression model of the beams take into account fire model parameters, whereas the regression model of the columns take into account the section factor, that is correlated to the heating capacity of the structural element. This means that while the beam's critical temperature is correlated to the fire scenarios, the critical temperature of the column depends only from the heating capacity of the structural element. Moreover, note that the number of parameters relative the other structural elements in both regression highlight the influence of the structural framework on critical temperatures.

The regression presented could be applied to estimate critical temperature of beams and columns taking in account the structural framework and natural fire scenarios.

6.5 Further Developments

Analysed substructures are moment resisting frames, so a further development could be the creation of the regression for concentric brace frames or eccentric brace frame structure.

The developed probabilistic model should be used instead of the FEM model in a reliability analysis in order to develop fragility curves for the structural typology.

Another very interesting aspect to investigate is the third dimension. The developed probabilistic model was calibrated on a set of 2D nonlinear FEM model results. This means that regression model can be used to evaluate the critical temperature of structural members subjected to Axial load and a non-combined bending action (N, M_x or N, M_y). Further analysis allows to recalibration of the regression model on 3D frame and let us to take into account combined actions (N, M_x, M_y)

Note that since the critical temperature doesn't depend from insulations, this regression could be applied also to fire protected structures. Nevertheless, further study should be focused on protected steel structures in order to confirm assumptions or taking into account properties uncertainty of protection materials .

References

Eurocode EN1991-1-2, 2002. Actions on structures - Part 1-2: General actions - Actions on structures exposed to fire.

Eurocode EN 1993-1-2, 2005. Eurocode 3: Design of steelstructures - Part 1-2: General rules - Structural fire design.

International Organization for Standardization. 1999. Fire-Resistance Tests, Elements of Building Construction, Part 1: General Requirements. International Organization for Standardization.

T. R. Kay, B. R. Kirby, R. R. Preston. 1996 Calculation of the heating rate of an unprotected steel member in a standard fire resistance test. Fire Safety Journal, 26(4):327–350.

G. Li P. Wang. 2013. Advanced Analysis and Design for Fire Safety of Steel Structures Zhejiang University Press, Hangzhou and Springer-Verlag Berlin Heidelberg

S. Tavelli, R. Rota, M. Derudi, 2014. A Critical Comparison Between CFD and Zone Models for the Consequence Analysis of Fires in Congested Environments. Chemical Engineerint Transactions , AIDIC Italian association of Chemical Engineering. ISBN 978-88-95608-27-ISSN 2283-9216.

A. Kolmogorov, 1956. Foundations of the Theory of Probability. Chelsea Publishing, New York.

D. S. Lemons, 2002. An Introduction to Stochastic Processes in Physics. The Johns Hopkins University Press.

H. D. Patterson. 1954. The errors of lattice sampling. Journal of the Royal Statistical Society B 1954;16:140-9

Kirkpatrick S., Gelatt C. D., and Vecchi M. P., 1983. Optimization by Simulated Annealing, Science, vol. 1, n. 220, pp. 671-680.

M. Vorechovský, D. Novák., 2009. Correlation control in small-sample Monte Carlo type simulations I: A simulated annealing approach, Probabilistic Engineering Mechanics

G. Heskestad. 1984. Engineering Relations for Fire Plumes. Fire Safety Journal, 7 25-32

SFPE Handbook of Fire Protection Engineering, Third Edition (2002). Philip J. DiNenno, P.E. (Hughes Associates, Inc.), Dougal Drysdale, PhD. (University of Edinburgh), Craig L. Beyler, PhD. (Hughes Associates, Inc.), W. Douglas Walton, P.E. (National Institute of Standards and Technology), Richard L. P.

Custer (Arup Fire USA), John R. Hall, Jr., PhD. (National Fire Protection Association), John M. Watts, Jr., PhD. (The Fire Safety Institute).

T. R. Kay, B. R. Kirby, and R. R. Preston. 1996 Calculation of the heating rate of an unprotected steel member in a standard fire resistance test. Fire Safety Journal, 26(4):327–350.

M. Manes, D. Rush. 2018. A Critical Evaluation of BS PD 7974-7 Structural Fire Response Data Based on USA Fire Statistics. Fire Technology, Volume 55, Issue 4, pp 1243-1293.

Ang, A. H.-S., Tang, W.-H., 2007. Probability Concepts in Engineering: Emphasis on Applications to Civil and Environmental Engineering. John Wiley, New York, NY.

Andreini, M., Gardoni, P., Pagliara, S., Sassu, M., 2016. Probabilistic Models for Erosion Parameters and Reliability Analysis of Earth Dams and Levees. ASCE-ASME J. Risk Uncertain. Eng. Syst. Part A Civ. Eng. 2. https://doi.org/10.1061/AJRUA6.0000878.

Box, G.E.P., Cox, D.R., 1964. An analysis of transformations. J. R. Stat. Soc. Ser. B 26, 211–252. https://doi.org/10.2307/2984418

Box, G.E.P., Tiao, G.C., 1992. Bayesian Inference in Statistical Analysis. John Wiley & Sons.

Gardoni, P., Der Kiureghian, A., Mosalam, K.M., 2002a. Probabilistic Capacity Models and Fragility Estimates for Reinforced Concrete Columns based on Experimental Observations. J. Eng. Mech. 128, 1024–1038. https://doi.org/10.1061/(ASCE)0733-9399(2002)128:10(1024)

Gardoni, P., Der Kiureghian, A., Mosalam, K.M., 2002b. Probabilistic Models and Fragility Estimates for Bridge Components and Systems Probabilistic Models and Fragility Estimates for Bridge Components and Systems. Berkeley, CA.

Kirkpatrick, S., Gelatt, C.D., Vecchi, M.P., 1983. Optimization by Simulated Annealing. Science (80-.). 220, 671–680.

Richards, F.S.G., 1961. A Method of Maximum-likelihood Estimation. J. R. Stat. Soc. Ser. B 23, 469–475.

Vořechovský, M., Novák, D., 2009. Correlation control in small-sample Monte Carlo type simulations I : A simulated annealing approach. Probabilistic Eng. Mech. 24, 452–462. https://doi.org/10.1016/j.probengmech.2009.01.004

Yang, Z., 2006. A modified family of power transformations. Econ. Lett. 92, 14–19. https://doi.org/10.1016/j.econlet.2006.01.011

R. Van Coile, T. Gernay, N. E. Khorasani, D. J. Hopkin. 2018. Evaluating uncertainty in steel-composite structure response under fire - Application of the ME-MDRM. The 10th International Conference on Structures in Fire, At Ulster University, Belfast, UK.

E. Mikkola, T. Hakkarainen, A. Matala, 2012. Fire safety of EPS ETICS in residential multi-storey buildings. Research report.

R. Suwondo, M.Gillie, L. Cunningham, C. Bailey. 2018. Effect of earthquake damage onthe behaviour of composite steelframes in fire. Advances in structural Engineering. Doi: 10.1177/1369433218761138

A. Stephani, R. Van Coile, N. E. Khorasani, T. Gernay, D. Hopkin. 2018. Probabilistic model for steel yield strength retention factor at elevated temperatures. Beton-und stahlbetonbau International Probabilistic Workshop 2018

N. E. Khorasani, P. Gardoni, M. Garlock. 2015. Probabilistic Fire Analysis: Material Models and Evaluation of Steel Structural Members. Journal of Structural Engineering, 141(12)

C. R. Rao, H. Toutenburg. 1999. Linear Models and Generalizations: Least Squares and Alternatives. Second edition. Springer. ISBN: 0-387-98848-3.

F.S.G. Richards. 1961. A method of maximum-likelihood estimation. Journal of the Royal Statistical Society. Series B Vol. 23, No. 2 , pp. 469-475

J.M. Frannsen , V.K.R. Kondor, J. Mason (2000). SAFIR User Manual. University of Liege, Belgium.

Franssen, J. M., & Gernay, T. (2017). Modeling structures in fire with SAFIR®: Theoretical background and capabilities. Journal of Structural Fire Engineering, 8(3), 300-323.

JM Franssen, T Gernay. 2017. Modeling structures in fire with SAFIR®: theoretical background and capabilities. Journal of Structural Fire Engineering 8 (3), 300-323

A. Bilotta, A. Compagnone, L. Esposito, E. Nigro. 2019. Numerical analyses of the structural behaviour of steel and FRP reinforced slabs in fire. Application of Structural Fire Engineering (ASFE). International Conference, Singapore.

A. Compagnone, A. Bilotta, E. Nigro. 2018. Methods to assess the bearing capacity of concrete-filled hollow section columns in fire. 10th International Conference on Structures in Fire FireSERT, Ulster University, Belfast, UK, June 6-8, 2018.

A. Compagnone, A. Bilotta, E. Nigro. 2017. Fire resistance evaluation through fragility curves. IFireSS 2017 – 2nd International Fire Safety Symposium. Naples, Italy, June 7-9, 2017.

Gernay, T., & Gamba, A. 2018. Progressive collapse triggered by fire induced column loss: Detrimental effect of thermal forces. Engineering Structures, 172, 483-496

Franssen J. M. , Zaharia R. 2005. Design of steel structures subjected to fire. Les Editions de l'Universitè de Liège